The Mitochondrial Fission Regulator Drp-1 (Dynamin-related protein-1) as a Novel Therapeutic Target to Prevent Atherosclerosis

INAUGURALDISSERTATION

zur Erlangung des Grades eines Doktors der Humanbiologie

des Fachbereichs Medizin

der Justus-Liebig-Universität Gießen

Vorgelegt von

Gustavo Enrique Crespo Avilan

aus

Maracaibo, Zulia, Venezuela

Gießen 2023

Aus dem Institut für Biochemie
des Fachbereichs Medizin der Justus-Liebig-Universität Gießen*

* Teile der Experimentellen Arbeit zu dieser Dissertation wurden am National Heart Research Institute, National Heart Centre in Singapur durchgeführt (Mentor: Prof. Derek J. Hausenloy).

Gutachter: Prof. Dr. Klaus T. Preissner

Gutachter: PD Dr. Damir Erkapic

Tag der Disputation: 26.09.2023

I. Table of contents

II. List of figures

III. List of tables

IV. List of abbreviations

α-Sma	= α-smooth muscle actin
Apoe-/-	= Apolipoprotein E Knockout
Arg1	= Arginase 1
ATP	= Adenosine triphosphate
CAD	= Coronary artery disease
CD206	= Macrophage mannose receptor-2
CD31/PECAM-1	= Platelet endothelial cell adhesion molecule-1
CSF	= Colony-stimulating factor
CVD	= Cardiovascular disease
DMSO	= Dimethyl sulfoxide
DNA	= Deoxyribonucleic acid
Drp1	= Dynamin-related protein 1
ELISA	= enzyme-linked immunosorbent assay
ETC	= Electron transport chain
FCCP	= Carbonyl cyanide 4-(trifluoromethoxy)phenylhydrazone
FET	= Forward electron transport
FMI	= Forward migration index
GAPDH	= Glyceraldehyde-3-phosphate dehydrogenase
GED	= GTPase effector domain
GM-CSF	= Granulocyte-macrophage colony-stimulating factor
GPD	= Glycerol phosphate shuttle
GPD2	= Glycerol 3-phosphate dehydrogenase
HFD	= High-Fat-Diet
HIF-1α	= Hypoxia-inducible factor 1a
ICAM-1	= Intercellular Adhesion Molecule 1
IDH	= Isocitrate dehydrogenase
iNOS	= Inducible nitric oxide synthase
LDH	= Lactate dehydrogenase
LDL	= Low-density lipoproteins
LPS	= Lipopolysaccharides
M-CSF	= Macrophage colony-stimulating factor
MAC-2	= Galectin-3; M3/38
MCP-1	= Monocyte chemoattractant protein-1
Mdivi-1	= Mitochondrial division inhibitor-1
Mff	= Mitochondrial fission factor
Mfn1/2	= Mitofusin 1/2

MiD49/51	= Mitochondrial dynamics protein 49/51
MMP	= Matrix metalloproteinase
MRC	= Maximal respiratory capacity
mtDNA	= Mitochondrial DNA
NF-kappa B	= Nuclear factor-kappa B
OCR	= Oxygen consumption rate
Opa1	= Optic atrophy type one
OXPHOS	= Oxidative phosphorylation
PAD	= Peripheral arterial disease
PBMC	= Peripheral blood mononuclear cell
PBS	= Phosphate buffered saline
PCR	= Polymerase chain reaction
PFA	= Paraformaldehyde
PKC	= Protein kinase C
PMA	= Phorbol 12-myristate 13-acetate
PVDF	= Methanol-activated polyvinylidene difluoride
RBC	= Red blood cells
RNA	= Ribonucleic acid
ROS	= Reactive oxygen species
SDH	= Succinate dehydrogenase
SOD	= Superoxide dismutase
SRC	= Spare respiratory capacity
TCA	= Tricarboxylic acid
TEMED	= N,N,N',N'-tetramethyl-ethane-1,2-diamine
TGF	= Transforming growth factors
TLR	= Toll-like receptor
TNF-α	= Tumor necrosis factor - alpha
TUNEL	= Terminal deoxynucleotidyl transferase (TdT) dUTP Nick-End labeling
VCAM-1	= Vascular cell-adhesion molecule 1
VEGF	= Vascular endothelial growth factor
VLA-4	= Very late antigen 4
VSMCs	= Vascular smooth muscle cells

V. Summary

Coronary artery disease (CAD) and peripheral arterial disease (PAD) are among the leading causes of death and disability worldwide. New treatments are needed to prevent post-angioplasty and stent restenosis in CAD and PAD patients. Accumulated findings have shown that mitochondrial dysfunction is involved in the pathophysiology mechanism underlying several cardiovascular conditions, however, in the scenario of vascular remodelling after injury, the role of mitochondrial dynamics is not completely understood.

Here, the inhibition of the mitochondrial fission regulator Drp-1 (Dynamin-related protein-1) by mitochondrial division inhibitor-1 (Mdivi-1) was investigated on neo-intimal hyperplasia (NIH) and plaque inflammation and progression, using *Apoe-/-* mice fed with high-fat diet and subjected to carotid-wire injury to induce NIH. The influence of Mdivi-1 treatment was also investigated on inflammatory gene and protein expression in THP-1 monocytes (T-M) and THP-1-derived Macrophages (T-DM) stimulated *in vitro* with LPS+IFN-y. The influence of Mdivi-1 on cell migration was investigated in T-M cells and human monocytes in response to M-CSF and MCP-1 using transmigration and 3D chemotaxis assays. Finally, the influence of Mdivi-1 on mitochondrial respiratory function (using Seahorse XF Analyzer) and mitochondrial morphology (by confocal microscopy) in T-M and T-DM was evaluated.

The treatment with Mdivi-1 reduced NIH by 37% in mice subjected to carotid-wire injury when compared to control mice, which was associated with a reduction in numbers of vascular smooth muscle cells and macrophages, as well as a decrease in TNF-α and ICAM-1 within the plaques. In T-M and T-DM, LPS+IFN-y stimulation induced up-regulation and production of pro-inflammatory mediators, while Mdivi-1 attenuated these changes. Monocyte chemotaxis responses to M-CSF and MCP-1 were reduced in the presence of Mdivi-1 as well. Finally, administration of Mdivi-1 reduced mitochondrial oxygen consumption rates in T-M and T-DM, and prevented M1-like cell polarization, with no changes in mitochondria morphology.

In conclusion, Mdivi-1 treatment to target the mitochondria fission regulator Drp-1 did reduce NIH, monocyte/macrophage recruitment, and inflammation following endothelial injury via modulation of the cellular oxidative metabolism. Taking these translational data together, Mdivi-1 may be positioned as a potential therapy to prevent vascular restenosis following angioplasty and stenting in CAD and PAD patients.

VI. Zusammenfassung

Die koronare Herzkrankheit (KHK) und die periphere arterielle Verschluss-krankheit (pAVK) gehören weltweit zu den häufigsten Ursachen für Tod und Behinderung. Kumulierte Befunde haben gezeigt, dass mitochondriale Dysfunktion zu den pathophysiologischen Mechanismen beiträgt, die solchen kardiovaskulären Erkran-kungen zugrunde liegen. Der Einfluss der mitochondrialen Dynamik, reguliert u.a. durch den mitochondrialen Teilungsregulator Drp-1 (Dynamin-related protein-1) beim Gefäßumbau nach einer Verletzung, ist allerdings nicht vollständig geklärt.

In dieser Arbeit wurde die Wirkung des mitochondrialen Teilungsinhibitor-1 (Mdivi-1), der die Funktion von Drp-1 blockiert, in der neointimalen Hyperplasie (NIH) und der Plaque-Entzündung und -Progression untersucht. Hierzu wurden Apoe-/--Mäuse, die mit einer fettreichen Diät gefüttert und einer Karotis-Draht-Verletzung unterzogen wurden, verwendet.

Die Behandlung mit Mdivi-1 verringerte die NIH bei Mäusen, die einer Carotis-Drahtverletzung ausgesetzt waren, um 37% im Vergleich zu Kontrollmäusen, und dieses Ergebnis war mit einer Verringerung der Zahl der glatten Gefäßmuskelzellen und der Makrophagen sowie mit einer Abnahme u.a. von TNF-α und ICAM-1 innerhalb der Plaques verbunden. Bei THP-1 Monozyten (T-M) und THP-1-abgeleiteten Makro-phagen (T-DM) führte die Stimulation mit LPS+IFN-y zu einer Hochregulierung und Produktion von pro-inflammatorischen Mediatoren, während die Behandlung mit Mdivi-1 diese Veränderungen im Vergleich zur Kontrolle signifikant abschwächte. Darüber hinaus waren die Chemotaxis-Reaktionen von Monozyten auf M-CSF und MCP-1 in Gegenwart von Mdivi-1 im Vergleich zur Kontrolle reduziert. Schließlich verringerte die Verabreichung von Mdivi-1 die mitochondriale Sauerstoffverbrauchsrate (Seahorse XF Analysator) in T-M und T-DM und verhinderte eine M1-ähnliche Zellpolarisation, ohne die Morphologie der Mitochondrien zu verändern (konfokale Mikroskopie).

Insgesamt zeigte sich, dass Mdivi-1 die NIH, die Rekrutierung von Monozyten / Makrophagen und die Entzündung nach einer Endothelverletzung durch Modulation des oxidativen Stoffwechsels der Zellen signifikant reduzierte. Aufgrund dieser trans-lationalen Daten wird postuliert, dass der Drp-1-Inhibitor Mdivi-1 als potenzieller Antagonist zur Verhinderung von Gefäßverengungen nach Angioplastie und Stenting bei Patienten mit KHK und pAVK eingesetzt werden könnte

1 Introduction

1.1 Cardiovascular disease

Cardiovascular disease (CVD) remains the leading cause of mortality in the western world, accounting for almost half of all deaths in Europe (45%) (Movsisyan, Vinciguerra, Medina-Inojosa, & Lopez-Jimenez, 2020) and claims around 18.6 million lives every year worldwide (Pinto et al., 2021). CVD refers to all the diseases of the circulatory system and heart, but mainly includes coronary artery disease (CAD), peripheral vascular disease (PAD), and cerebrovascular diseases (Olvera Lopez, Ballard, & Jan, 2022). Atherosclerosis is the major underlying cause of CVD that contributes to the onset and progression of CAD and PAD, by reducing blood flow to the heart and lower limb muscles and causing angina and intermittent claudication, respectively (Frostegard, 2013). Therefore, a greater understanding of the pathophysiology underlying atherosclerosis is needed in order to discover novel treatment targets for improving outcomes in patients with CVD.

1.2 Atherosclerosis

Atherosclerosis is a chronic inflammatory disease of the large and medium-sized arteries that is initiated in early childhood and has a long asymptomatic phase of development in which early vascular changes are minor. Over time, atherosclerosis progresses and manifests clinically in middle and late adulthood (Hansson & Libby, 2006; Ross, 1999).

1.2.1 Atherosclerosis development

1.2.1.1 Lesion initiation

The disruption of the physiological process involved in vascular homeostasis regulation results in endothelial dysfunction (Favero, Paganelli, Buffoli, Rodella, & Rezzani, 2014), which creates a predisposition to vasoconstriction, lipid infiltration, platelet activation, leukocyte adhesion, and oxidative stress (Verma, Buchanan, & Anderson, 2003). There are many triggers of endothelial dysfunction, including lipid products, inflammation & injury, oxidative stress, or associated risk factors such as smoking, diabetes, obesity, unhealthy diet, and pollution among others (S. Xu et al., 2021).

The endothelial dysfunction leads to the infiltration of low-density lipoproteins (LDL) into the arterial tunica intima where they become oxidized (oxLDL) (Libby, Ridker, & Maseri, 2002). This oxLDL promotes endothelial cell expression of adhesion molecules, as well as secretion of pro-inflammatory mediators such as monocyte chemotactic protein-1 (MCP-1) (X.

H. Yu, Zheng, & Tang, 2015), which facilitates the infiltration of immune cells including monocytes and lymphocytes into the artery wall (Singh, Anshita, & Ravichandiran, 2021; Weber, Zernecke, & Libby, 2008). (**Figure 1.1**)

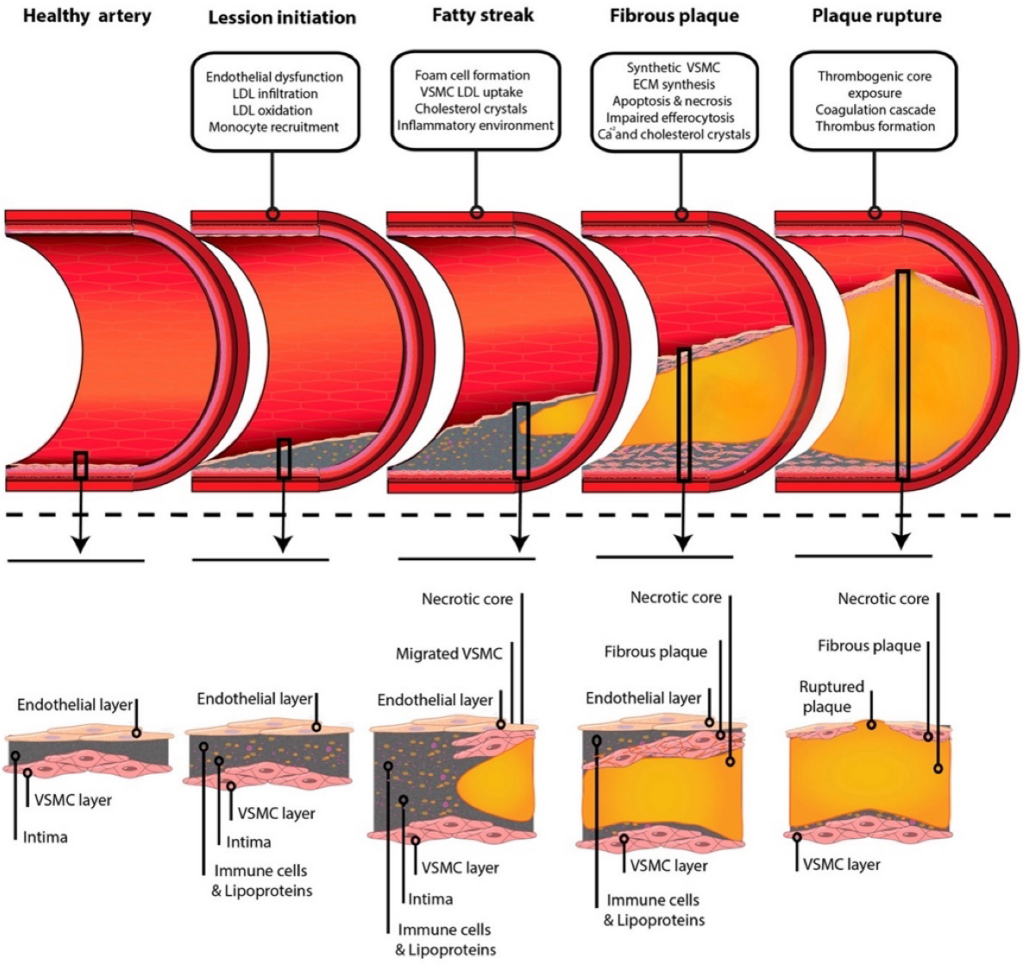

Figure 1.1 Progression of an atherosclerosis lesion. Schematic representation of atheroma plaque formation from a healthy artery to plaque rupture highlighting the key events that contribute to its development in each stage (Jebari-Benslaiman et al., 2022)

1.2.1.2 Fatty streak

Infiltrated monocytes from the blood stream undergo a differentiation process to macrophages under the influence of the macrophage colony-stimulating factor (M-CSF) (Deng et al., 2019). As a part of their immune response to remove the cholesterol deposit, these macrophages take up modified lipoproteins including oxLDL through their scavenger receptors and release reactive oxygen species (ROS). In parallel, the cholesterol accumulation in the subendothelial space also results in the formation of cholesterol crystals that contribute to the development of the fatty streak (Suhalim et al., 2012). The higher intake of oxLDL by macrophages results in their differentiation into foam cells (Hansson & Libby, 2006; Yvan-

Charvet et al., 2007). Additionally, the vascular smooth muscle cells (VSMCs) within the media layer get attracted to migrate to the neointima region as well where they also internalize oxLDL, contributing to the formation of the foam cell pool. Both types of foam cells undergo an apoptosis process, resulting in cellular debris formation that together with the cholesterol serve as a signal to enhance the inflammatory response and lead to the formation of a lipid-rich necrotic core (Libby et al., 2002). The accumulation of oxLDL, foam cells, and debris further promotes the migration of VSMCs into the neointimal layer, leading to the maturation of fatty streaks into more advanced plaques (Fok, 2012). (**Figure 1.1**). In this early phase of atherogenesis, the inflamed endothelium as permeability barrier between the flowing blood and the growing plaque area beneath remains largely intact.

1.2.1.3 Fibrous plaque

The fibrous cap is a subendothelial layer formed between the lumen of the vessel and the necrotic core, which encloses cholesterol, lipids, VSMCs that have migrated to the luminal side as well as the extracellular matrix (ECM). The function of the fibrous cap is to act as a structural provision to prevent the exposure of pro-thrombotic material of the core to the vessel lumen, avoiding a thrombosis event (Chamie, Wang, Bezerra, Rollins, & Costa, 2011). During fibrous plaque formation, VSMCs change their phenotype from contractile to a synthetic one, increasing the production of ECM components. At this step, the phagocytic capacity of the cells is limited due to impaired efferocytosis, and they undergo processes of necrosis and apoptosis with the associated release of intracellular oxidative and inflammatory components favouring the cholesterol crystal accumulation and plaque calcification (Jebari-Benslaiman et al., 2022). (**Figure 1.1**).

1.2.1.4 Plaque rupture

At the site of the affected blood vessel, containing the plaque with thick fibrous caps, the effective vessel lumen has considerably narrowed with time, such that the fluid shear forces are extremely high. Although this pro-atherogenic plaque area is considerably stable, due to the constant exposure of increasing shear forces it eventually becomes prone to rupture. This is known as a vulnerable plaque, which is characterized by a large necrotic core, thinner fibrous cap, and increased inflammation. The reduction in the fibrous cap's thickness is a consequence of the VSMC death, which leads to a reduction of EMC and to an increase in the metalloproteinases (MMP) secretion (Jebari-Benslaiman et al., 2022). After rupture, the subendothelial space is exposed to the vessel lumen, immediately activating the coagulation

cascade, leading to thrombin formation and to fibrin polymerization. The fibrin together with the platelets cover the lesion, forming the thrombus (Libby et al., 2002). At this point, depending on the vascular location of the blockage, severe and often fatal clinical complications occur, such as myocardial infarction (MI) and stroke (Finn, Nakano, Narula, Kolodgie, & Virmani, 2010; Kaandorp, Lamb, Bax, van der Wall, & de Roos, 2005). (**Figure 1.1**)

1.2.2 Immune response in atherosclerosis

The events that initiate the inflammatory response in the artery during atherosclerosis, are not fully understood. However, as mentioned above, increased amounts of pro-atherogenic lipids are found on the arterial wall, endothelial dysfunction and modified lipids result in the formation of several immunogens that are responsible for endothelial injury. The activated vascular cells of the arterial wall are responsible for the early vascular changes, specifically the inflammatory cell recruitment mediated by cytokines, chemokines, and adhesion molecules.

1.2.2.1 LDL

LDL particles are responsible for initiating the inflammatory response during lesion formation. Generally, modified lipoproteins increase endothelial damage, leukocyte recruitment, and inflammation. Besides oxidation, LDL can undergo other modifications, such as de-sialylation that leads to autoantibody production, resulting in the formation of LDL-containing immune complexes (Malekmohammad, Bezsonov, & Rafieian-Kopaei, 2021). These immune complexes are known to induce secretion of pro-inflammatory cytokines and promote macrophage apoptosis and have been detected in the blood of atherosclerotic patients (Orekhov et al., 2020). Additionally, the de-sialylated LDL can induce lipid accumulation, ECM synthesis, chronic inflammation, and cell proliferation (Malekmohammad et al., 2021). Moreover, some studies have shown that malondialdehyde (MDA), an oxidative stress epitope of oxLDL (Yang et al., 2014), can act as a Damage-associated molecular pattern (DAMP) and modulate lesional inflammation in the process of atherogenesis (Papac-Milicevic, Busch, & Binder, 2016)

1.2.2.2 Immune cells recruitment

In response to fluid shear stress and accumulated cholesterol the inflamed endothelial layer expresses cell adhesion molecules such as vascular cell-adhesion molecule 1 (VCAM-1), intercellular cell-adhesion molecule 1 (ICAM-1), P-selectin, and E-selectin (Ley, Miller, &

Hedrick, 2011). Leukocytes, including T-cells, B-cells, NK-cells, and monocytes undergo the extravasation cascade: capture, rolling, arrest, intravascular crawling, and paracellular/transcellular trans-endothelial migration (Salminen et al., 2020). These steps in cell-cell interactions are mediated by such adhesion molecules via contacts with cell membrane receptors such as very late antigen 4 (VLA-4) or lymphocyte function-associated antigen 1 (LFA-1), interacting both with VCAM-1 or ICAM-1, respectively (Yusuf-Makagiansar, Anderson, Yakovleva, Murray, & Siahaan, 2002).

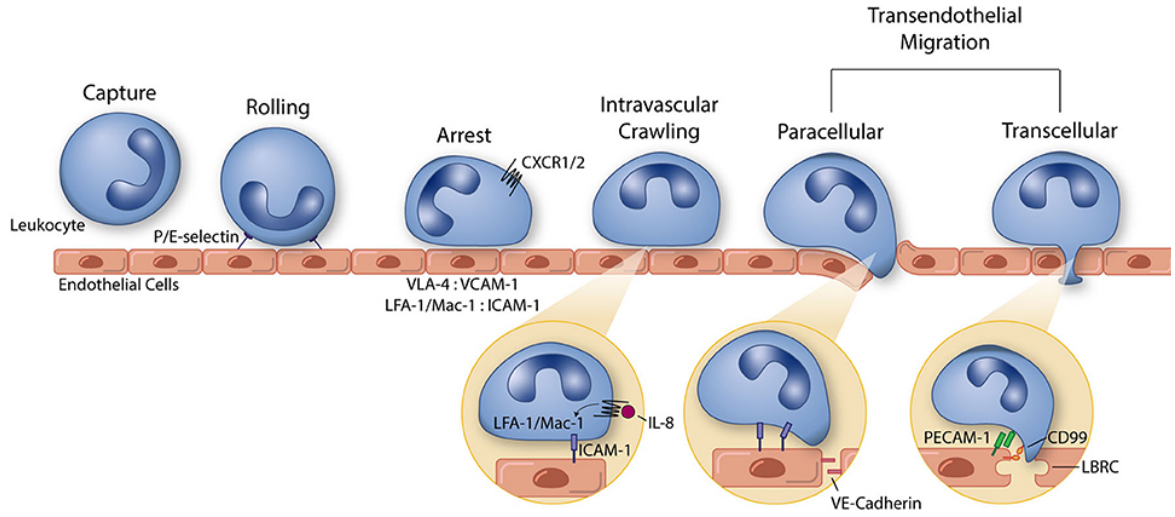

Figure 1.2 The leukocyte extravasation cascade: capture, rolling, arrest, intravascular crawling, and both paracellular and transcellular transendothelial migration. Both, P and E selectin bind leukocytes to achieved the capture and rolling phases of extravasation. LFA-1/Mac-1: ICAM-1 and VLA-4: VCAM-1 interactions, halt leukocytes on the apical endothelial cell surface during arrest. Integrin activation is aided by chemokine signaling (IL-8 and its receptors CXCR1/2 pictured here). In addition to leukocyte arrest and intravascular crawling, LFA-1/Mac-1: ICAM-1 interactions function to signal VE-cadherin junctional turnover and opening of the endothelial cell-cell junctions. Additionally, PECAM-1 and CD99 homophilic interactions between leukocytes and endothelial cells function to drive membrane mobilization from the lateral border recycling compartment (LBRC) to increase membrane surface area around the transmigrating leukocyte. (Salminen et al., 2020)

During leukocyte migration, the cells respond to the chemokines in the environment that also promote their infiltration to the intimal space (**Figure 1.2**). Also, platelets facilitate monocyte recruitment to the inflamed endothelium by interacting with the adhesion protein von Willebrand Factor (vWF) (Postea et al., 2012).

The leukocyte trafficking cascade is a complex process that has mainly been described in well-controlled *in vitro* studies, with the use of platforms incorporating vascular endothelial cells and physiological environmental conditions (e.g., chemokines) allowing the study of cell migration and the discovery of new drug targets for preventing (trans-) migration.

1.2.2.3 Cytokines and Chemokines

Cytokines are signaling proteins with pleiotropic effects, in charge of the regulation of the innate and adaptative immune response by paracrine, autocrine or juxtacrine processes. Commonly, they are grouped into different classes, including interferons (IFN), tumor necrosis factors (TNF), colony-stimulating factors (CSF), transforming growth factors (TGF), interleukins (IL), and chemokines (Ait-Oufella, Taleb, Mallat, & Tedgui, 2011). Several cytokines are capable to act synergistically to amplify their immunological function and have both pro- and anti-inflammatory functions, therefore promoting or preventing atherogenesis (Liongue, Sertori, & Ward, 2016).

1.2.2.4 Monocytes and Macrophages

It was well-accepted for a long time that circulating monocytes are the only precursors of tissue macrophages. However, recent studies have challenged this concept, showing that many tissue-resident macrophages are originated from yolk sac-derived erythro-myeloid progenitors which developed into self-maintaining and greatly specialized populations of macrophages (Gomez Perdiguero et al., 2015; Kierdorf, Prinz, Geissmann, & Gomez Perdiguero, 2015). Despite their origin, circulating monocyte-derived macrophages and native tissue-resident macrophages express similar gene expression patterns in response to anti-inflammatory stimulation (Honold & Nahrendorf, 2018). Both sources of macrophages are the earliest recruited leukocytes in the nascent atherosclerosis lesion (Camici, Rimoldi, Gaemperli, & Libby, 2012). These monocytic cells are known to be the most abundant cell population among immune cells in the atherosclerotic plaques (Hansson & Libby, 2006). The bone marrow is responsible for producing new blood cell components, including monocytes. In humans, circulating monocytes are known to be heterogenic, and classified by their expression of surface receptors CD14 and CD16. Monocytes expressing high levels of CD14 and very low levels of CD16 ($CD14^{hi}CD16^{-}$) are called “classical” monocytes (M1-like), which are capable of producing many inflammatory cytokines and represent 80% of the total cell population. The other subtype is defined as a “intermediate” monocytes, characterized by their surface expression of low CD14 and expression of CD16 ($CD14^{+}CD16^{+}$), and lastly, the “non-classical” (alternative) monocytes ($CD14^{++}CD16^{+}$) which are involved in the early responses to pathogens and tissue repair (Costantini et al., 2018; Kapellos et al., 2019). In mice, monocytes have been also classified, based on their expression of Ly6C, CX3CR1, and CD43. Being classical, these cells express $Ly6C^{hi}CX_3CR_1^{lo}$ whereas non-classical (alternative)

contain $Ly6C^{lo}CX_3CR_1{}^{hi}CD43^{hi}$; the third population of intermediate monocytes in mice is characterized by intermediate expression of Ly6C (Olingy et al., 2017).

Similar to monocytes, macrophages are also classified into two main groups, called M1-like (pro-inflammatory macrophages – equivalent to the classically activated monocytes) and M2-like (anti-inflammatory macrophages). Both cell populations are involved in atherogenesis (Barrett, 2020), thereby releasing different types of cytokines and therefore modulating the inflammatory response (**Figure 1.3**).

In vitro, M1-like macrophage polarization can be achieved by incubation with LPS or IFN-γ (or both together) (Martinez, Sica, Mantovani, & Locati, 2008). After LPS stimulation via Toll-like receptor activation, macrophages are able to release high quantities of pro-inflammatory cytokines, including IL-1β, IL-6, IL-12, TNF-α, and commonly low levels of anti-inflammatory cytokines such as IL-10. However, it has been shown that after sustained pro-inflammatory stimulation, macrophage expression of IL-10 is increased. This elevation is mediated by a delayed autocrine/paracrine loop of type I interferons to ensure timely attenuation of inflammation, acting as a compensatory response (Ernst et al., 2019). M1-like macrophages actively contribute to the growing and persistent pro-inflammatory environment at the site of plaque formation, contributing to the progression of atherosclerosis.

On the other hand, the M2-like macrophage phenotype can be induced *in vitro* by stimulating macrophages with IL-4, IL-10, and IL-13 (Chuang, Hung, Cangelose, & Leonard, 2016). Upon activation, these cells release increased levels of anti-inflammatory cytokines, including IL-10 and CCL-1 (Asai, Nakamura, Kobayashi, Herndon, & Suzuki, 2012), thereby protecting against atherosclerosis. Additionally, these M2-like macrophages are able to secrete pro-fibrotic factors such as TGF-β, resulting in tissue repair and remodeling (Luong et al., 2018) which helps to increase plaque stability and prevent plaque-rupture with the consequent thrombosis. In terms of markers, M1-like macrophages have been associated with an increased level of inducible nitric oxide synthase (iNOS) as well as the pro-inflammatory cytokines mentioned above. In the case of M2-like macrophages, they express high levels of arginase 1 (Arg1) and mannose receptor (CD206) together with the mentioned anti-inflammatory cytokines (Hirosawa et al., 2018).

The process of cell polarization is reversible due to the plasticity of these cells, allowing them to quickly switch from one phenotype to another in response to the soluble mediators present in their environment (N. Wang, Liang, & Zen, 2014). During atherosclerosis, the microenvironment composition is defined by the cholesterol levels and their oxidation, cytokines, chemokines, immune cell infiltration, growth factors, and cell death (Adamson &

Leitinger, 2011; J. Gao et al., 2021; Yurdagul, Finney, Woolard, & Orr, 2016). As described before, atherogenesis consists of different stages in which the lesional microenvironment is changing such that the polarization status of these immune cells will be modified as well during the course of the disease (Tabas & Bornfeldt, 2016).

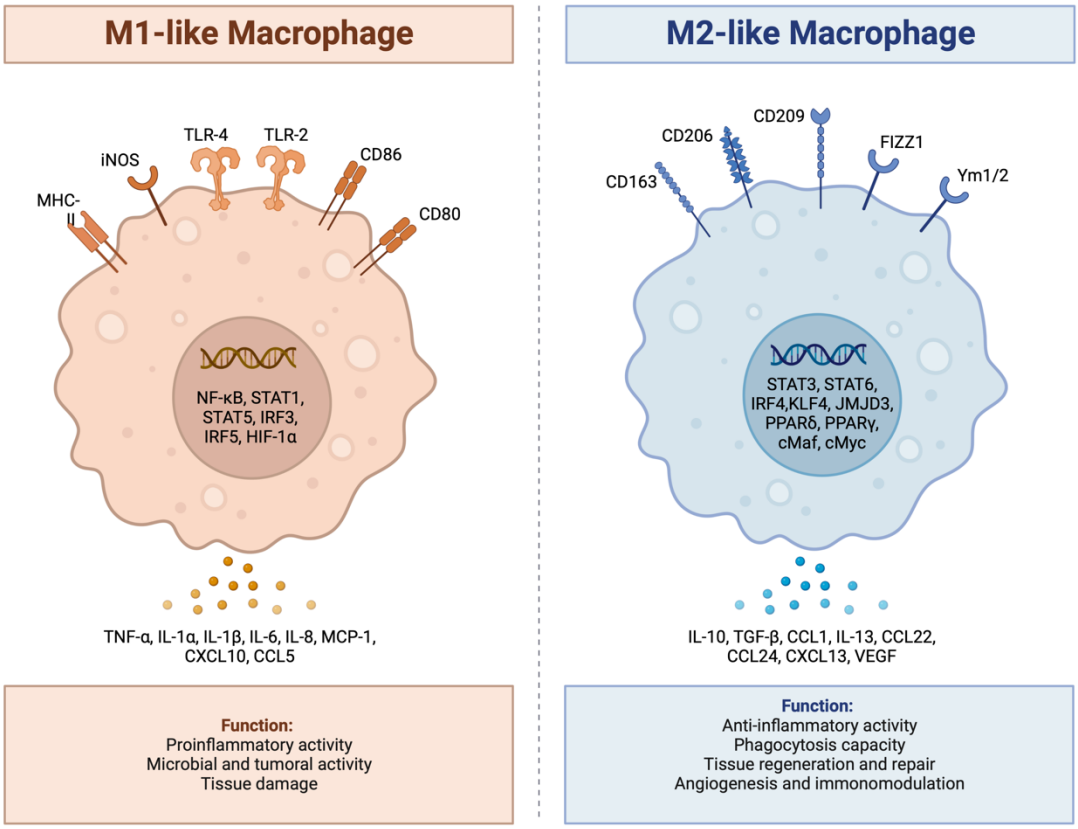

Figure 1.3 Macrophage polarization during atherosclerosis. Schematic representation of the M1-like and M2-like macrophages, indicating key cytokines, cell surface markers as well as signaling pathways involved in the cell polarization process.

1.3 Immuno-metabolism and Inflammation

Immuno-metabolism is a term used to describe changes in immune cells' intracellular metabolic, that either enable or modify their physiological activity (O'Neill, Kishton, & Rathmell, 2016). In the past ten years, cutting-edge technology has been developed to measure metabolism, which led to significant growth in interest in the immuno-metabolism area.

Leukocyte metabolism is a crucial component for a well-organized immune response of these cells. Extensive research has indicated that macrophage metabolism is involved in much more than only cellular energy production. Instead, it is a dynamic mechanism that directly and specifically contributes to the activation of inflammatory signals and other macrophage effector functions (Noe & Mitchell, 2019; O'Neill & Pearce, 2016).

1.3.1 M1-type polarization and metabolism

Macrophages have a basal metabolic state that relies mainly on oxidative phosphorylation (OXPHOS), which is powered by the tricarboxylic acid (TCA) cycle, to provide their energy requirements. Following M1-like polarization (i.e using IFN-γ and LPS as stimulants), murine macrophages have a sharp rise in their energy requirements, which leads to an increase in the glucose flow to satisfy these demands. Transcription factors, including nuclear factor-kB (NF-kB) and hypoxia-inducible factor 1a (HIF-1α), are activated after cell polarization, to carry out modifications in inflammatory gene expression as well as participate in metabolic re-programming (Kawai & Akira, 2006; Newton & Dixit, 2012). Additionally, is known that M1-like macrophages switch their metabolism during polarization to favour aerobic glycolysis over OXPHOS (Nelson & O'Connell, 2020; Van den Bossche, Baardman, & de Winther, 2015; Viola, Munari, Sanchez-Rodriguez, Scolaro, & Castegna, 2019).

The increase in glucose flux in these cells enables the energy generation to meet cellular requirements in a faster way, however, this process (aerobic glycolysis) is less effective at producing ATP when compared to OXPHOS. At the same time, some glycolysis-derived intermediates feed the pentose phosphate pathway (**Figure 1.4**), which provides NADPH for ROS formation and nitric oxide and aids in the maintenance of the cell's redox state (Nelson & O'Connell, 2020; Viola et al., 2019). Lastly, aerobic glycolysis also causes pyruvate to be converted to lactate, which maintains the glycolytic flux in activated macrophages (L. Liu et al., 2016; O'Neill et al., 2016).

Murine macrophages polarized to an M1-like phenotype are known to have a defective tricarboxylic acid (TCA) cycle, which is compromised at two different sites, leading to an accumulation of TCA intermediates. The first site corresponds to the isocitrate dehydrogenase (IDH) level, which leads to build-up citrate. The accumulated citrate is then transformed into itaconate (an intermediate metabolite with antimicrobial properties) or used to drive fatty acid synthesis and NO production, therefore supporting the M1-like polarization status (O'Neill et al., 2016). (**Figure 1.4**).

The second defective site of the TCA is at the succinate dehydrogenase (SDH) level, with the consequent accumulation of succinate (Nelson & O'Connell, 2020) that results in the stabilization of the transcription factor HIF1α, which supports the production of ROS and IL-1β.

1.3.2 M2-type polarization and metabolism

In the case of cells stimulated with IL-4 and IL-13, resulting in M2-like or alternative macrophages, they display a metabolic phenotype that is closer to the non-polarized macrophages (M0), based on extracellular flux analysis. Studies have shown that M2-like macrophages use glutamine and glucose as fuel for the TCA cycle and oxidise fatty acids (*via* β-oxidation) to fuel OXPHOS (Huang et al., 2014) .

During the polarization into M2-like macrophages, the interferon regulatory factor 4 (IRF4) appears to be the transcription factor responsible for the response to IL-4 stimulation and helps to reduce inflammation, can support wound repair and angiogenesis, and plays a key role during the metabolic reprogramming of M1-like macrophages (Huang et al., 2016). Another important protein in alternative macrophage differentiation is the energetic sensor AMP-activated protein kinase (AMPK). When anti-inflammatory cytokines are released from macrophages, AMPK is highly stimulated, leading to an increased β-oxidation flux to fuel OXPHOS (Huang et al., 2014; Sag, Carling, Stout, & Suttles, 2008). Additionally, a metabolic product of glucose and glutamine, the coenzyme UDP-GlcNAc, is generated during M2-like polarization and it glycosylates receptors, including the mannose receptors CD206 and CD301 (Nelson & O'Connell, 2020) (**Figure 1.4**).

In summary, the metabolic pathways differ between M1-like or M2-like cells after respective polarization. Some of these differences take place in the cell mitochondria matrix and changes in this organelle have been associated with the metabolic status as well (Silva Ramos, Larsson, & Mourier, 2016).

1.4 Mitochondrial dynamics

Commonly addressed as “the powerhouse of cells”, mitochondria are double membrane-dynamic organelles that can move to different regions within a cell and experience morphological changes by two opposite processes, mitochondrial fusion and fission (Roy, Reddy, Iijima, & Sesaki, 2015), to maintain normal cellular functions such as energy production, Ca^{2+} homeostasis, cellular differentiation/division, and DNA stability (McBride, Neuspiel, & Wasiak, 2006).

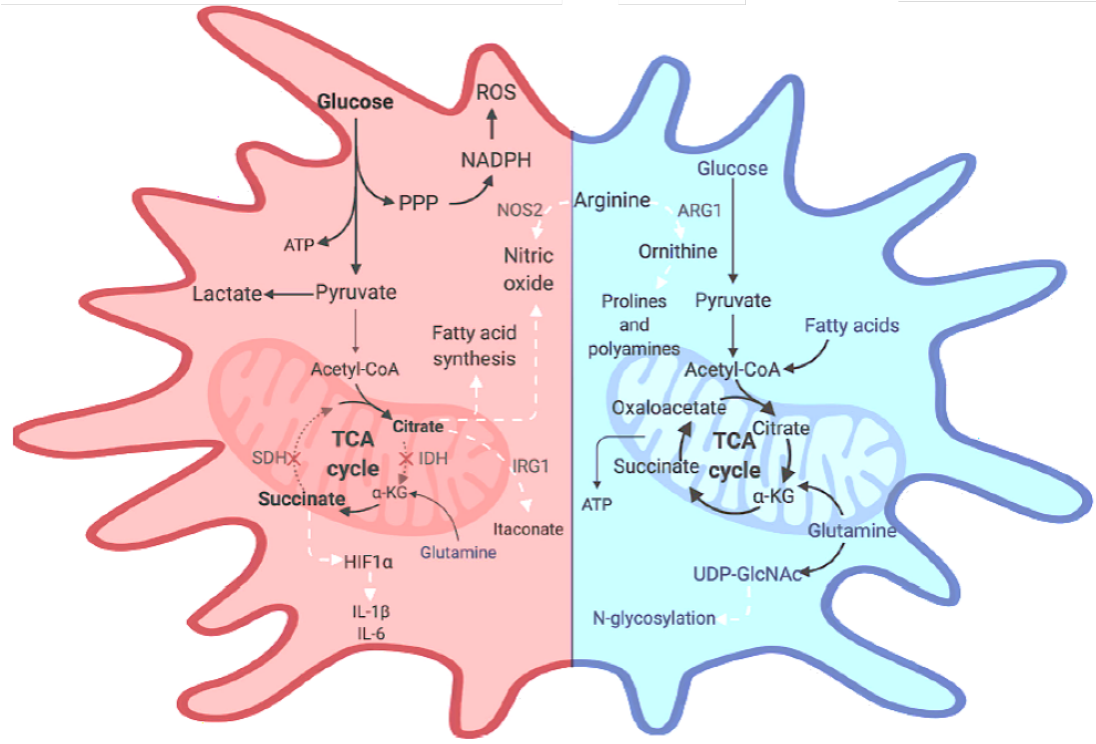

Figure.1.4 Polarized macrophages have differential metabolic programming. M1-like macrophages (Red color) have enhanced glucose uptake to fuel aerobic glycolysis, resulting in increased lactate and ATP production. The defective isocitrate dehydrogenase (IDH) at succinate dehydrogenase (SDH), results in the accumulation of citrate and succinate. HIF1α activity is promoted, leading to glycolysis and inflammatory cytokine production. M2-like macrophages (blue color) utilize glutamine, glucose, and fatty acids to fuel the TCA cycle and OXPHOS. Glutamine uptake drives UDP-GlcNAc production, that drives N-glycosylation of cell surface receptor. In M2-like cells, arginine is metabolized to ornithine promoting tissue repair through production of prolines and polyamines. White arrows indicate metabolic intermediates driving M1-like or M2-like activities. a-KG, alpha-ketoglutarate; ARG1, arginase; HIF1a, hypoxia-inducible factor 1a; IDH, isocitrate dehydrogenase; IRG1, immune-responsive gene 1; NOS2, nitric oxide synthase; PPP, pentose phosphate pathway; ROS, reactive oxygen species; SDH, succinate dehydrogenase. Adapted from: (Nelson & O'Connell, 2020).

Modifications in the morphology of mitochondria can happen due to the existence of evolutionary conserved mitochondrial dynamic proteins. Defects in the fusion or fission machinery are frequently lethal as observed in mice embryos and are associated with human illnesses (Waterham et al., 2007). For instance, extensive mitochondrial fragmentation has been reported in neurodegenerative diseases (such as Parkinson's Disease and Alzheimer's Disease) and in cardiovascular diseases (such as acute myocardial infarction or heart failure) (Maneechote, Palee, Chattipakorn, & Chattipakorn, 2017; Maneechote et al., 2021; Ong et al., 2010; Serasinghe & Chipuk, 2017).

1.4.1 Mitochondrial Fusion

Mitochondrial fusion is initiated by the fusion proteins Mitofusin 1 (Mfn1), Mitofusin 2 (Mfn2), and Optic atrophy type one (Opa1), and accompanied by the mixing of the mitochondrial contents within the matrix. This process is essential for signal transmission, preservation of mitochondrial membrane potential, and mitochondrial DNA (mtDNA) stability (Legros, Lombes, Frachon, & Rojo, 2002; Tondera et al., 2009). Fusion is a crucial element in improving the efficiency of mitochondrial respiration. As a result of the increased energy demand, ATP production is stimulated by mitochondrial fusion, which contributes to the increase in mitochondrial respiration (oxidative capacity) (Westermann, 2012; Yao et al., 2019) (**Figure 1.5**). Stress-induced mitochondrial hyperfusion will increase ATP generation and decreases autophagy and appears to be a pro-survival response to stressors such as starvation and UV irradiation (Westermann, 2012; Youle & van der Bliek, 2012). Any defects in Mfn1, Opa1, and Mfn2 weaken mitochondrial stability and lead to poor cellular respiration (H. Chen, Chomyn, & Chan, 2005).

1.4.1.1 Mitochondrial outer membrane fusion

Located at the external mitochondrial membrane, the mammalian Mfn1 and Mfn2 are responsible for the outer mitochondria membrane (OMM) fusion. These proteins can form stable homodimers as well as heterodimers in a nucleotide-dependent manner via GTPase domains (Cao et al., 2017; Y. J. Li et al., 2019). In mice, the loss of both Mfn1 and Mfn2 proteins leads to embryonic lethality, pointing to their importance during the development (Filadi, Pendin, & Pizzo, 2018). The embryonic lethality of double Mfn KO proteins may be attributed to the pleiotropic qualities of Mfn2. Other distinct functions besides controlling the mitochondrial morphology have been attributed to this protein as well, such as ER-mitochondria connections, energy metabolism as well as insulin signaling, mitophagy and apoptosis (S. Han et al., 2021; Traaseth, Elfering, Solien, Haynes, & Giulivi, 2004; R. Yu, Lendahl, Nister, & Zhao, 2020).

1.4.1.2 Mitochondrial inner membrane fusion

OPA-1 is an inner mitochondria membrane (IMM) protein predominantly located at cristae junctions. As for Mitofusins, Opa1 is a member of the dynamin GTPase family and is an element of the mitochondrial fusion machinery. Opa1 oligomer tethering causes IMM fusion, allowing the mixing of mitochondrial matrix contents (Ge et al., 2020). Different mRNA variants (at least eight) have been identified from the OPA1 gene, responsible for the

generation of the long and short isoforms. The membrane-anchored long forms of OPA1 (L-OPA1) undergo proteolytic cleavage, resulting in soluble short forms of OPA1 (S-OPA1) (R. Yu et al., 2020). Fusion of the inner and outer membrane does not take place simultaneously, and the loss of mitochondria membrane potential results in the inhibition of Opa1-mediated IMM fusion, stopping the mixing of matrix contents without compromising the OMM fusion (Malka et al., 2005). The knockdown of Opa1 has been reported to induce mitochondrial fragmentation (Liao et al., 2017), and its overexpression induces mitochondrial elongation (Kyriakoudi, Drousiotou, & Petrou, 2021). Opa1 at cristae junctions is crucial for maintaining cristae integrity, minimizing the risk of apoptosis by stopping the release of cytochrome c (Varanita et al., 2015)

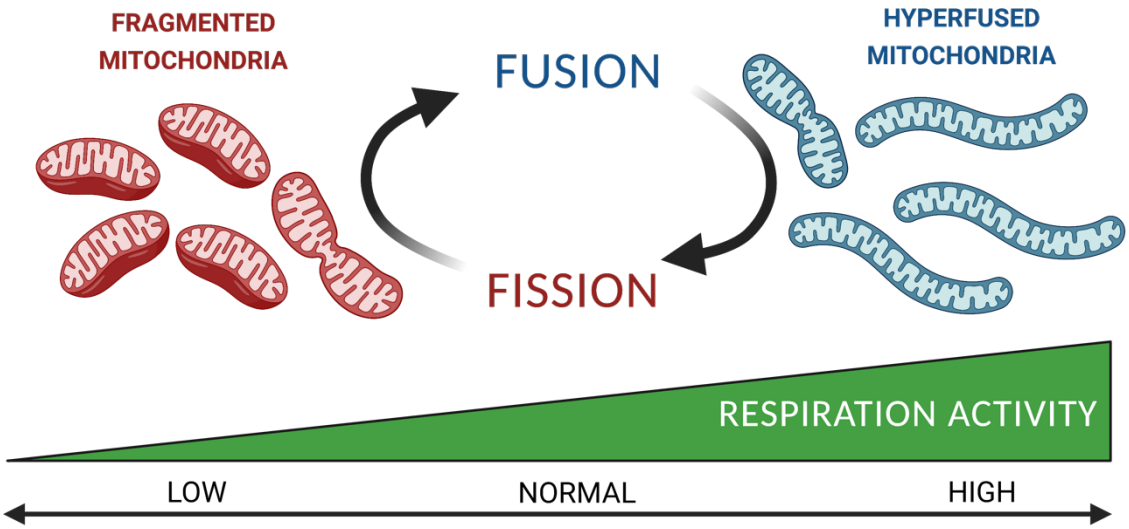

Figure.1.5 Mitochondrial metabolic status is associated with organelle morphology. High respiratory activity is linked to elongated mitochondria, while fragmented mitochondria is associates with a lower level of mitochondria respiration.

1.4.2 Mitochondrial Fission

Fission is essential for mitochondrial transmission during cellular division, as mitochondria cannot be created *de novo* and is vital for many other cellular functions, including differentiation, mitochondrial transport, mitophagy, and apoptosis (Samangouei et al., 2018). The dynamin-related protein 1 (Drp1) is the main protein involved in mitochondrial fission, and its function is dependent on the ER, OMM proteins as well as actin filaments (Hatch, Gurel, & Higgs, 2014; Ji et al., 2017). The process of fission leads to fragmented mitochondria, which have been associated with reduced mitochondrial respiratory capacity (Gasier, Dohl, Suliman, Piantadosi, & Yu, 2020) (**Figure 1.5**).

1.4.2.1 Dynamic related protein 1

Drp1 (80 kDa) is a member of the dynamin protein family and predominantly located in the cytosol. Drp1 forms higher-order structures by aggregating into spirals around vesicles, promoted through GTP hydrolysis, to induce the constriction of the mitochondria, resulting in the membrane scission of the parent organelle (Elgass, Pakay, Ryan, & Palmer, 2013). Drp1 is composed of four domains, a C-terminal GTPase effector domain (GED), a variable domain, a helical middle domain, and the highly conserved N-terminal GTPase domain. (**Figure 1.6**). Due to the absence of a lipid-interacting pleckstrin homology domain, this protein only binds to the mitochondria membrane by interacting with its receptors/adapters at the OMM (Macdonald et al., 2016). These are: mitochondrial fission factor (Mff), fission 1 (Fis1), and the two mitochondrial dynamics protein 49 and 51 (MiD49 and MiD51). These proteins help Drp1 to polymerise and form rings around the mitochondria tubules for proper fission to occur (Samangouei et al., 2018).

It is known that Mff can recruit Drp1 independently of hFis1 at the OMM and it is believed to be the major adapter protein for ubiquitously expressed Drp1 (Kraus & Ryan, 2017). Additionally, the relative levels of Mff and MiD51/49 and the balance between Mff and MiD51/49 during their interactions with Drp1, are considered vital determinants of balanced mitochondrial dynamics in cells (Jin, Wei, Zhi, Wang, & Meng, 2021; R. Yu et al., 2017). However, the role of Fis1 as a fission protein in mammalian cells has been discussed controversially, as its KO has only a light effect on Drp1 recruitment and mitochondrial morphology, but instead, it appears to be involved in the mitophagy, a mitochondria-specific form of autophagy (Jin et al., 2021; Q. Shen et al., 2014).

1.4.2.2 Drp1 Regulation

Different posttranslational modifications can regulate Drp1 functions, including SUMOylation, palmitoylation, ubiquitination, S-nitrosylation, O-GlcNAcylation, and phosphorylation as the most studied one (**Figure 1.6**). All of them interfere with Drp1 stability, activation, protein-protein interactions, translocation between cytosol and OMM, and GTPase activity (Hu, Huang, & Li, 2017). Phosphorylation is the posttranslational modification of Drp-1 that is heavily associated with inflammation in the endothelium and in monocytic cells (Forrester et al., 2020; Kapetanovic et al., 2020; Y. L. Shen et al., 2018).

Phosphorylation of Drp1 can lead to activation or inhibition of its function, depending on the site/domain of the protein that is affected. From all the phosphorylation sites expressed by Drp1 (**Figure 1.6**), two of them are the ones linked to the main changes seen under

inflammatory conditions. These are Ser616 and Ser637 as has been reported in myeloid-derived cells (J. Park et al., 2013). The phosphorylation of Ser616 is known to be mediated by Protein kinase C (PKC)-δ, by Rho-associated protein kinase (ROCK), ERK1/2, cyclin-dependent kinase 1 (CDK1), or calmodulin-dependent protein kinase II (CaMKII). Among them the CDK phosphorylation pathway has been mostly studied (Adaniya, J, Cypress, Kusakari, & Jhun, 2019; Jin et al., 2021). On the other hand, phosphorylation at Ser637 is mediated by calcineurin, protein kinase D (PKD), protein kinase A (PKA), or ROCK1.

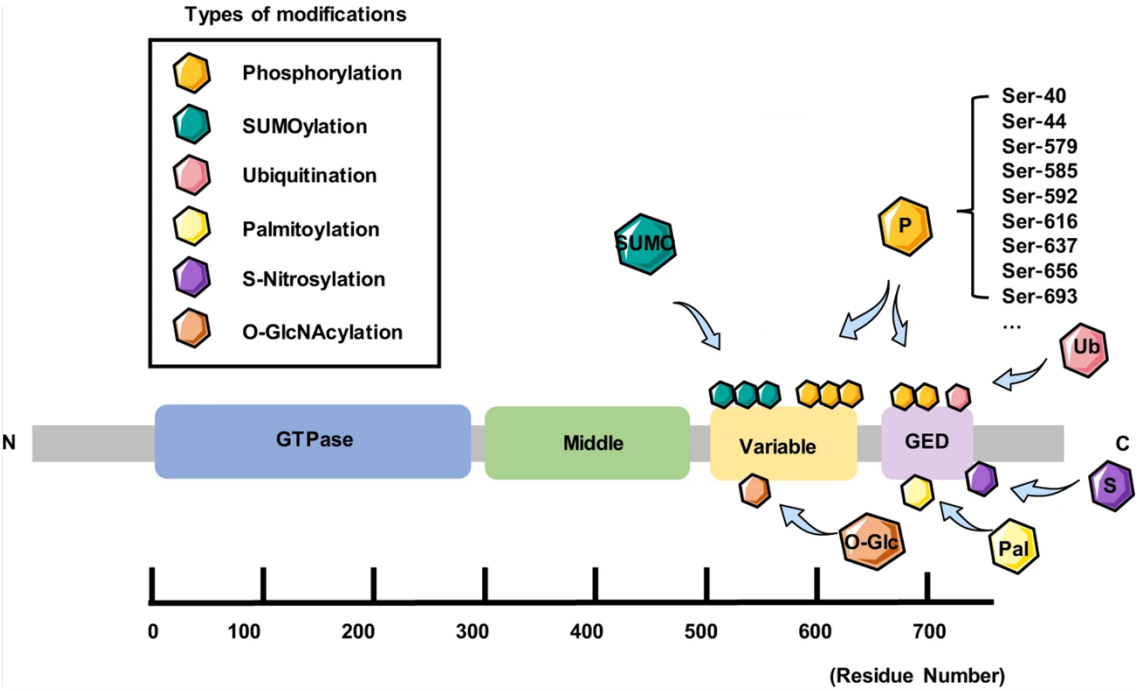

Figure.1.6 Posttranslational modifications and structure-based domain architecture of human Drp1. Adapted from: (Jin et al., 2021)

Commonly, after phosphorylation at Ser637, there is a decrease in the GTPase hydrolysis activity of Drp1. However, the exact function triggered after Ser637 modification has been controversially discussed and depends on the cell type, Drp1 receptors, or by which pathway the phosphorylation is induced, thereby leading to different responses (Serasinghe & Chipuk, 2017). For instance, in the context of hepatic ischemia/reperfusion, Ser637-dephosphorylation by calcineurin results in the translocation of Drp1 to mitochondria (X. Yu, Jia, Yu, & Du, 2019). Conversely, PKA- induced Ser637-phosphorylation will prevent the interaction between the GTP-binding domain and the GED domain, resulting in a diminished mitochondrial fission activity (Chang & Blackstone, 2007). However, ROCK1-mediated Ser637 (Ser600 in mice) phosphorylation can induce mitochondrial fission in murine podocytes by Drp1 activation (Forte et al., 2021; W. Wang et al., 2012). Therefore, is clear that

the modification of the same phosphorylation (Ser637) site by different kinases may result in different biological responses.

1.4.3 Mitochondria and atherosclerosis

The events taking place during the initial phase of atherosclerosis, such as endothelial dysfunction, changes in blood lipid profile, oxidative stress, and the inflammation of both vessel-resident and circulating immune cells, seem to be strongly related to mitochondrial dysfunction of the participating cells, indicative of mitochondria as the vital factor in the pathogenesis of atherosclerosis (Shemiakova et al., 2020) .

As mentioned, the mitochondria respiration chain is the principal source of energy production. Under physiological conditions, the chain uses over 98% of the total electron transport capacity to produce ATP, and only 1-2% are released and used to mainly produce intracellular ROS, which is required for other cellular functions (Peng et al., 2019). In contrast, under pathophysiological conditions, the overproduction of ROS is increased in the form of nicotinamide adenine dinucleotide phosphate oxidase, xanthine oxidase, and lipoxygenase, mainly due to malfunctioning of complexes I and III of the respiratory chain (Yeh, Kuo, Sung, & Yeh, 2018), which results in a state of oxidative stress. A situation then occurs that is aggravated by the inability of the antioxidants (glutathione, carotenoids, catalase, and glutathione peroxidase) to remove the excess of ROS produced (Peng et al., 2019), leading to a loss of redox balance.

Oxidative stress has been pointed to as an early driving force of atherosclerosis development, thereby contributing to inflammation and lipid modification. In this regard, the process of mitophagy appears to be defective during atherosclerosis. As damaged mitochondria are not removed under such conditions, they contribute to ROS accumulation, cell death and stress which results in the formation of necrotic core and plaque destabilization (Madamanchi & Runge, 2007). Additionally, mitochondrial ROS accumulation causes damage of mitochondrial DNA (mtDNA). The damage of mtDNA has been documented in human atherosclerosis fibrous cap and core area, as well as in high fat-fed Apoe-/- mice, resulting in altered VSMC proliferation and increased apoptosis (E. P. K. Yu et al., 2017). Also, mutations in the mtDNA induced by ROS, have been reported to decrease the synthesis of respiratory chain complexes and weakens mitochondrial respiration in monocytes and macrophages as well as induces alterations in mitochondrial membrane potential and reduces ATP production in VSMCs and endothelial cells (Madamanchi & Runge, 2007; Shemiakova et al., 2021). Defective mitochondria have been reported in VSMCs isolated from human atherosclerotic

plaques, which displayed a reduced ATP synthesis and mutations on mtDNA promoting their proliferation (Peng et al., 2019).

Macrophages from atherosclerotic lesions of the Western diet-fed Ldlr-/- mice were shown to develop increased mtDNA damage, which results in enhanced mitochondrial oxidative stress (Y. Wang, Wang, Rabinovitch, & Tabas, 2014). Moreover, studies in macrophages have shown that mitochondrial ROS beyond physiological levels can induce polarization to an M1-like phenotype, and the reduction of ROS levels by NAC treatment prevented this polarization (Zhou et al., 2018). Also, mitochondrial oxidative stress in monocytes and macrophages has been associated with inflammation during atherosclerosis development, mediated by activation of the NF-κB signalling pathway (Y. Wang et al., 2014). Such activation results in the production of pro-inflammatory cytokines, adhesion molecules, and growth factors, involved during atherosclerosis development.

Therefore, mitochondria occupy a central position in the pathogenesis of atherosclerosis and mediate utmost relevant aspects of disease development and progression. This fact makes them a promising potential therapeutic target.

1.4.3.1 Drp1 as a treatment target for atherosclerosis.

Extensive mitochondrial fragmentation is a central player in the pathogenesis of a variety of disorders, including cancer, obesity, neurodegenerative diseases (such as Parkinson's Disease and Alzheimer's Disease), and cardiovascular diseases (such as acute myocardial infarction and heart failure) (Maneechote et al., 2017; Maneechote et al., 2021; Ong et al., 2010; Serasinghe & Chipuk, 2017). In support of this, targeting mitochondrial fission by inhibiting the mitochondrial fission protein, Drp1, has been reported to be beneficial under certain disease conditions.

In the context of atherosclerosis, Drp1 was found to be enriched in calcified human carotid arteries and aortic valves, and its inhibition with mitochondrial division inhibitor 1 (Mdivi-1) attenuates human and mouse smooth muscle cell calcification under oxidative stress (Rogers et al., 2017). Additionally, another study showed that atherosclerotic lesions formation in diabetic-Apoe-/- mice was suppressed following treatment with metformin which reduced mitochondrial fragmentation, ROS production, and inflammation (Q. Wang et al., 2017). In line with the latest findings, it was recently found that Mdivi-1 reduced macrophage burden, oxidative stress, and advanced calcified atherosclerotic plaque in aortic roots of diabetic ApoE-deficient mice (Rogers et al., 2021). Lastly, a study inducing genetic ablation of Drp1 in

macrophages attenuated intimal thickening and macrophage accumulation in a femoral arterial wire injury model (Umezu et al., 2020).

Thus, Mdivi-1 has been shown to provide therapeutic effects in different cardiovascular and neurological disease models (Kalkhoran. et al., 2020), although its role in vascular injury and tissue remodeling has not been fully explored. This is the focus of the present work.

2. Aim of the study

Atherosclerosis contributes to the onset and progression of CAD and PAD by reducing blood flow to the heart and the lower limb muscles, thereby causing angina and intermittent claudication, respectively. The treatment of choice for many patients, symptomatic for CAD and PAD, is revascularisation by angioplasty and stenting. However, due to post-angioplasty tunica intima hyperplasia and infiltration of inflammatory cells, these patients are at risk of developing restenosis, a complication that requires repeated angioplasty and may increase the risk of CAD- and PAD-related complications. As such, new treatments are needed to prevent post-angioplasty restenosis to reduce atheroma progression/inflammation in patients with CAD and PAD in order to improve health outcome. Given that mitochondrial fragmentation is a central player in the pathogenesis of this disease, in this work a novel candidate target, Drp1, was tested for its role in atherosclerosis.

Hypothesis: Pharmacological inhibition of mitochondrial fission with Mdivi-1 to target Drp1 will prevent atherosclerosis development by reducing monocyte activation and migration (**Figure 2.1**)

General aim 1: To investigate the effect of mitochondrial fission inhibition *in vivo* in atherosclerosis development.

Specific aim 1.1: To investigate the effect of Mdivi-1 in atherosclerotic plaque development in a model of vascular restenosis.

Specific aim 1.2: To evaluate the effect of Mdivi-1 on atherosclerotic plaque cell complexity.

Specific aim 1.3: To study the anti-inflammatory effect of Mdivi-1 on atherosclerotic plaque development.

Specific aim 1.4: To assess the efficacy of Mdivi-1 in preventing plaque-apoptosis

General aim 2: To investigate the effect of Drp1 inhibition on pro-inflammatory monocyte and macrophage activation.

Specific aim 2.1: To investigate the effects of pharmacological inhibition of Drp1 on pro-inflammatory monocytes.

Specific aim 2.2: To investigate the effects of Mdivi-1 on pro-inflammatory monocyte migration.

Specific aim 2.3: To investigate the effects of pharmacological inhibition of Drp1 on pro-inflammatory macrophages.

General aim 3: To investigate the mechanisms through which Drp1 inhibition reduces monocyte activation and migration.

Specific aim 3.1: To investigate the changes in mitochondrial morphology which occur with pro-inflammatory and anti-inflammatory activation of monocytes.

Specific aim 3.2: To investigate the changes in mitochondrial metabolism which occur with pro-inflammatory and anti-inflammatory activation of monocytes and macrophages.

Specific aim 3.3: To investigate the effects of pharmacological inhibition of Drp1 on mitochondrial morphology and metabolism.

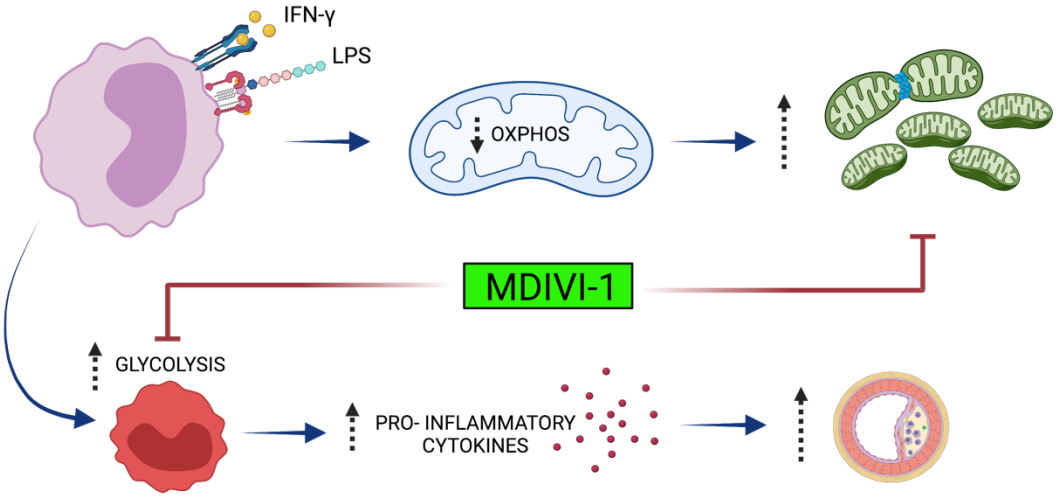

Figure.2.1 Overall hypothesis of the study

3. Material and methods

3.1.1 Reagents

Product Name	Company	Country
1.7ml centrifuge tubes	Axygen	Singapore
15ml centrifuge tubes	Falcon	Singapore
2-mercaptoethanol (50mM)	GIBCO	Singapore
2-mercaptoethanol (50mM)	GIBCO	Singapore
2.0 ml centrifuge tubes	VWR	Singapore
4X Laemmli sample buffer	Bio-Rad	Singapore
50 ml centrifuge tubes	Falcon	Singapore
6-well TC-treated plates	CORNING	USA
6-well TC-treated plates	CORNING	USA
6.5 mm Transwell® with 8.0 µm Pore Polycarbonate Membrane Insert	Corning	Singapore
96-well PCR plates	Applied Biosystems	Singapore
Agarose, Biotechnology Grade	First BASE Laboratories	Malaysia
Anti- COX-IV	Cell Signaling Technology	USA
Anti-CD14 microbeads	Miltenyi Biotec	Germany
Anti-Drp1 antibodies	Cell Signaling Technology	USA
ART Pipette filtered Tips	ThermoFisher Scientific	Singapore
CD31-antibody	Santa Cruz Biotechnology	USA
Chloroform	Sigma-Aldrich	Singapore
Counter Chamber slides	Life Technologies	Singapore
Cryovials	Nalgene	Singapore
Cy3-conjugated antibody	Jackson ImmunoResearch	Germany
Cytokine antibody array	Abcam	Singapore
Dimethyl sulfoxide	Sigma-Aldrich	Germany
DMLB fluorescent microscope	Leica	Germany
DMSO	SIGMA	Germany
DNA Gel Loading Dye (6X)	ThermoFisher Scientific	Singapore
DNase I, RNase-free	Thermo Scientific	Singapore
DPBS	Lonza	Singapore

e-Myco™ Mycoplasma PCR detection kit	iNtRON Biotechnology	South Korea
Elastica-van Gieson	Merck	Singapore
FBS	GIBCO	Singapore
Ficoll-Paque Plus	GE Healthcare	Germany
Ficoll-Paque Plus	GE Healthcare	Germany
Filter units - 0.22µM	VWR	Singapore
FITC–conjugated antibody	Jackson ImmunoResearch	Germany
Gel blotting paper	Bio-Rad	USA
GelRed® Nucleic Acid Gel Stain	biotium	USA
GeneRuler DNA ladder mix	ThermoFisher Scientific	Singapore
Glass-bottom dishes	ThermoFisher Scientific	Singapore
Halt TM protease and phosphatase inhibitor cocktail	ThermoFisher Scientific	Singapore
Hoechst 33342	ThermoFisher Scientific	Singapore
Human Macrophage Colony-Stimulating Factor, (MCS-F)	Miltenyi Biotec	Singapore
Hybond-P PVDF Membran	Bio-Rad	USA
ICAM-1 antibody	eBioscience	USA
IFN-γ	Miltenyi Biotec	Singapore
IL-4	Miltenyi Biotec	Singapore
IL-6 ELISA	ThermoFisher Scientific	Singapore
iScript cDNA Synthesis kit	BIO-RAD	Singapore
L-glutamine solution (100X)	GIBCO	Singapore
LDH-release detection kit	Roche	Germany
LPS	InvivoGen	USA
MAC-2-antibody	Cedarlane	Germany
Mdivi-1	Tocris Bioscience	USA
MicroAmp™ Optical Adhesive Film	Applied Biosystems	Singapore
Monocytes Isolation Kit II	Miltenyi Biotec	Germany
NaCl (0.9%)	B-Braun	Germany

Osmotic pump (model 1004)	Alzet	USA
Parafilm paper	Sigma	Singapore
Paraformaldehyde	Roth	Germany
PCR tubes	Axygen	Singapore
Penicillin-Streptomycin (100X)	GIBCO	Singapore
Phosphate buffered solution	Fisher Scientific	USA
Pierce™ BCA Protein Assay Kit	ThermoFisher Scientific	Singapore
PMA	Sigma-Aldrich	Singapore
Poly-D-lysine	Sigma-Aldrich	Singapore
Poly-Prep Slides	Sigma-Aldrich	Germany
Precision FAST 2x qPCR MasterMix with SYBR green and low ROX	PrimerDesign	UK
Ribolock RNase Inhibitor	Thermo Scientific	Singapore
RiboRuler high range RNA ladder	ThermoFisher Scientific	Singapore
RIPA buffer	ThermoFisher Scientific	Singapore
RNA gel Loading dye	ThermoFisher Scientific	Singapore
RNeasy minikit	Qiagen	Singapore
Rompun	Bayer	Germany
RPMI 1640 media	GIBCO	Singapore
Seahorse Cell Mito Stress Test kit	Seahorse biosciences	Singapore
Seahorse XF Calibrant solution	Seahorse biosciences	Singapore
Seahorse XF media	Seahorse biosciences	Singapore
SMA-antibody	Dako	Germany
Sutures (0/5, 0/7)	B-Braun	Germany
THP-1 cell line	ATCC	USA
TNF-α (Quantikine®) ELISA	R&D Systems	Singapore
TNF-alpha antibody	Abcam	UK
TNF-α	Miltenyi Biotec	Singapore
Tris-Acetate-EDTA (TAE) Buffer, pH 8.0	First BASE Laboratories	Malaysia
T*RIzol® Reagent*	Invitrogen	Singapore

Trypan blue 0.4%	Life Technologies	Singapore
TrypLE Express	GIBCO	Singapore
TUNEL-FITC apoptosis detection kit.	Vazyme Biotech	China
Ultra-pure water (pyrogen free)	Lonza	Singapore
UltrapureTM DNase/RNase-Free Distilled water	Invitrogen	Singapore
UltrapureTM DNase/RNase-Free Distilled water	Invitrogen	Singapore
Vetalar	Boehringer Ingelheim	Germany
Western Type Diet	Altromin International	Germany
XFe96 Extracellular Flux Assay Kit	Seahorse biosciences	Singapore
μ-Slide Chemotaxis	ibidi	Germany

3.1.2 Equipment

Name	Company	Country
BD^{TM} LSR II	BD Bioscience	Singapore
ChemiDoc MP+ Imaging System	BIO-RAD	Singapore
ChemiDoc XRS+ Imaging System	BIO-RAD	Singapore
CoolCell	Corning CORNING	USA
CoolRack® XT PCR96	Biocision	UK
Countess II FL Automated Cell Counter	Life Technologies	Singapore
DMi8 M Microscope	Leica	Germany
DMLB fluorescent microscope	Leica	Germany
Dry gGlass bead sterilizer	Cole-Parmer?	Germany
Fluorescence microscope BX51	Olympus	Singapore
Freezer (-20°C)	Sanyo	Japan
Freezer (-80°C)	Thermo Fisher Scientific	Singapore
Fridge (4°C)	Panasonic	Japan
Liquid Nitrogen	CryoExpress	Singapore

Liquid Nitrogen tank	Thermo Fisher Scientific	Singapore
Magnetic stirrer	Corning	USASingapore
Microplate centrifuge, PCR Plate Spinner	VWR	Singapore
Microplate reader SpectraMax	Molecular DEvices	USA
Microplate Reader-Tecan	Life Sciences	USA
NanoDrop1000 spectrophotometer	Thermo Fisher Scientific	Singapore
PowerPac™ Basic Power Supply	BIO-RAD	Singapore
Refrigerated microcentrifuge	Eppendorf	Germany
Seahorse XFe96	Agilent Technologies	Singapore
ST16R Refrigerated Centrifuge	Thermo Fisher Scientific	Singapore
Stereomicroscope	Leica	USA
Sterile pippettes for cell culture	Gilbson	Singapore
Therma cycler	Applied biosystem	Singapore
Tissue culture humidified incubator	Thermo scientific	Singapore
Vacum suction pump	VWR	USA
Veriti 96-Well Programmable Thermocycler.	Applied Biosystems	Singapore
ViiA 7 Real-Time PCR System	Applied Biosystem	Singapore
Vortex Mixer	Scientific Industries	USA
Water bath	Grant Instruments	UK
Wide Mini-Sub cell GT system	BIO-RAD	Singapore
Zeiss LSM710 confocal microscope	Carl Zeiss	Germany

3.2. Methods

3.2.1. *Apoe-/-* wire injury atherosclerosis model

The recovery wire injury-induced atherosclerosis *in vivo* model was used to assess plaque size and complexity after left carotid artery endothelial denudation in apolipoprotein E Knockout (*Apoe*$^{-/-}$) mice (**Figure 3.1**) (Schumacher et al., 2021; Yakala et al., 2019). All animal procedures were approved by the Singapore Institutional Animal Care Committee. Animals were handled in accordance with good animal practice as defined by the relevant animal welfare bodies.

3.2.1.1 Animal maintenance and diet

Male *Apoe-/-* mice (C57BL/6J background, n=6 per group) were obtained from Charles River Laboratory (Italy). Animals were maintained on 12 h dark/light cycle and placed on an atherogenic high-fat diet (HFD) containing 21% fat, 0.15% cholesterol, and 19.5% casein (Western Type diet, Altromin) for one week prior to the surgical procedure and continued on the diet until up to two weeks after the artery injury when atherosclerotic plaque analysis was performed.

3.2.1.2 Surgical preparation and anaesthetics

Mice 10 to 12-week-old, from the Apoe-/- colony, were injected with an intraperitoneal bolus of an anaesthetic cocktail containing: ketamine hydrochloride 100 mg/kg (Vetalar, Boehringer Ingelheim) and xylazine 10 mg/kg (Rompun, Bayer). Once anaesthesia was confirmed by lack of reflexes and whisker movement, a small amount of sterile eye ointment in the eye was applied to minimize drying. Hair in the ventral neck region was removed using a small electrical clipper. Loose hair was then removed with a moistened sterile gauze, and the surgical site was disinfected using betadine surgical scrub. The mice were then placed on a surgical platform and the legs and arms were secured using surgical tape.

Under a stereomicroscope, the carotid artery was exposed by a 1cm skin incision in the median region of the neck area, on top of the trachea. The two fat bodies were separated to guarantee the adequate visualization of the tracheal region and retractors were placed to hold the muscle layer. A blunt-dissection of the thing muscle layer covering the carotid artery was perform when it was present and by using sharp curved forceps, it was separated from the vagus nerve and jugular vein. At this point the bifurcation area with external and internal carotid artery was visible and 0.9% sodium chloride solution was added to avoid tissue dryness.

3.2.1.3 Surgical procedure

Stopping blood flow - A 0/5 silk suture open loop was positioned under the carotid artery, proximal to the aortic arch, then a 7/0 silk suture open loop was inserted around the internal carotid artery and lastly, another two 0/7 silk sutures open loops were placed around the external carotid artery: one loop near to the bifurcation point and the other loop was placed as distal as possible. Next, the surgical platform position was changed to ensure the proper orientation of the mouse head towards the operator to facilitate the correct guide-wire insertion during the endothelial denudation step. Blood flow cessation through the common carotid

artery was achieved by holding and pulling the ends of the 5/0 silk suture with hemostat forceps and immediately proceeded to close two suture loops, one located on the internal carotid artery and the other positioned on the distal area from the external carotid artery.

Arteriotomy – wire injury - A small incision was performed distal to the external carotid artery between the two loops, using a small scissor. The flexible 0.36-mm guidewire was disinfected with 70% alcohol and moisten with 0.9% NaCl and inserted into the external carotid artery via the transverse arteriotomy to induce the endothelial denudation by passing the guidewire along the vessel while rotating three times, always maintaining the same amplitude of rotational movement in all mice.

Restoring the blood flow - After removing the guidewire, the proximal loop located on the external carotid artery was closed tightly and subsequently the blood flow was restored in the carotid artery by removing the sutures positioned around the common artery and the other one placed around the internal carotid artery. Restoration of blood flow was visually evidenced by the red colour in the artery.

Suture and recovery – The retractors were removed and the muscle layer together with the two fat bodies were returned to their physiological position. The skin was closed by applying 2 -3metallic clips in to the incision around the neck area. Finally, mice were laid down on their left side under infrared light and monitored until they woke up.

3.2.1.4 Carotid artery isolation.

Once the end-time point of the experiment has been reached (14 days after injury), mice were anesthetized with an intraperitoneal injection of 100 mg/kg ketamine hydrochloride by bodyweight and 10 mg/kg xylazine by bodyweight. When proper anesthetization was confirmed by absence of pedal and palpebral reflexes, the skin was disinfected with betadine and the thoracic cavity was opened, and the right auricle of the heart was removed. Mice were perfused via the left ventricle with 20-25 ml phosphate buffered solution (PBS) to remove blood and then perfused with 15-20 ml of 4% Paraformaldehyde (PFA) solution to fix the tissue. Fixation was indicated by mice when they exhibited vigorous muscle contractions and become rigid.

After fixation, the carotid artery was explanted with minimal manipulation, as proximal to the aortic arch, using curved forceps and small scissors, then was dehydrated, and embedded in a paraffin block placing it upright on bifurcation position.

3.2.1.5 Osmotic mini-pump implantation.

The *Apoe−/−* mice were continuously treated during the experiment with the mitochondrial fission inhibitor Mdivi-1 (1.2 mg/kg/d), or it's vehicle DMSO (0.5%), via Alzet® osmotic minipumps, subcutaneously implanted 1 day before the surgery.

Osmotic mini-pump filling – All the handling of mini-pumps was performed in a sterile laminar flow hood to prevent contamination. First, the filling tube was attached to a 1 mL syringe and the Mdivi-1 or the vehicle were and draw up. Then, the filling tube was inserted through the orifice located at the top of the mini-pump, until it could not go further and was slowly filled up with the compound or vehicle noticing the dark shadow inside the pump which indicated the fluid level. The filling process was stopped when a small drop of fluid raised out of the mini-pump body. Lastly, the filling tube was carefully removed, and the flow regulator was inserted into the body of the pump, always being sure that was seated tightly against the pump body, at this point the osmotic mini-pumps were ready for implantation in the animals.

Subcutaneous implantation – Before the surgical procedure started, adequate depth of anaesthesia was ensured by testing pedal withdrawal and palpebral reflexes and eyes were protected from drying out by applying ophthalmic ointment. Hair on the back was removed for mini-pump subcutaneous implantation slightly posterior to the scapulae. The dedicated space was disinfected with 70% ethanol and all the tips of the instruments were placed in glass bead sterilizer. With surgical scissor, a 0.8-1 cm incision was made around 2 cm close to the tail. The subcutaneous tissue was then spread and a pocket for the mini-pump was created from the back upwards to the scapula on the right side of the mouse. The mini-pump was inserted into the incision and gently positioned into the pocket oriented toward the front of the mouse. Once the pump was inserted, the incision was closed with wound clips. Next, the animals were kept on a warming stage until they recovered and after were returned to their housing. Analgesics (buprenorphine, 0.05 mg/kg) and antibiotics (enrofloxacin 85 mg/kg) were provided to reduce post-surgical pain and avoid post-surgical infection.

3.2.2. Histology and Immunohistochemistry

The embedded carotid arteries in paraffin blocks were subjected to a serial 5-μm transverse sectioning, within a distance of 0 to 320 μm starting from the bifurcation and collect them all on poly-L-lysine coated histological slides (Poly-Prep Slides, Sigma-Aldrich). In total 9 sections per mouse (50 μm apart) were collected and stained using Elastica-van Gieson

(Merck) to highlight the vessel laminas as previous described (Yakala et al., 2019). After the microscope pictures from all vessels were collected, a planimetry measurement was performed for the areas of interest (lumen, internal and external lamina) using the specialized software Diskus (Hilgers). Lastly, the 9 sections collected from each mouse were averaged to represent the neointima formation and media of the vessels.

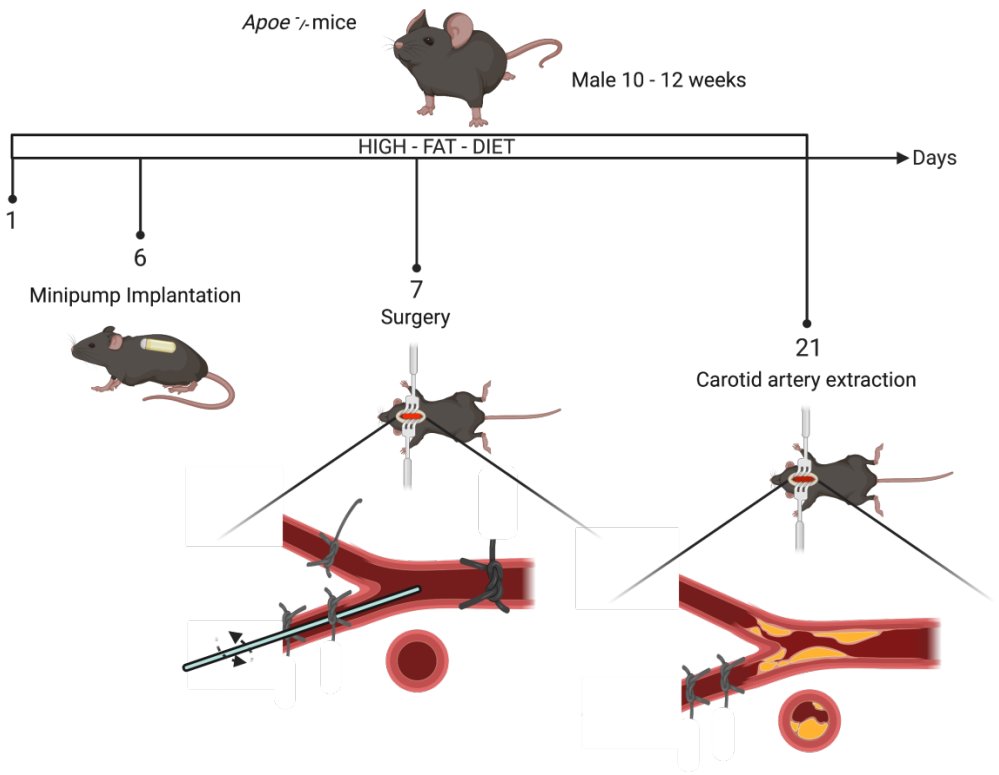

Figure 3.1 Wire injury - surgery procedure in Apo-/- mice. Male 10 – 12 weeks old were fed with HDF for 21 days. One day before surgery the minipump filled with Mdivi-1 or vehicle was implanted subcutaneously in the mice and at day 7, endothelial denudation of the common carotid artery was performed with a guidewire. At the end of 3 weeks, carotid arteries were extracted for analyses.

Immunohistochemistry analyses were carried out on paraffin sections to first assess plaque complexity by detection of macrophages, smooth muscle cells, and endothelial cells in the neointima. Secondly, ICAM-1 and TNF-α were assessed to evaluate inflammation and lastly, TUNEL assay was performed to study apoptosis. First, the sections were deparaffinized (2 x 5 min Xylol, 2 x 5 min 100% alcohol, 1 x 5 min 96% and 1 x 5 min 70% alcohol) and were placed on PBS for 5 min at room temperature (RT). Next, the sections were subjected to an antigen retrieval protocol by treating them with citrate buffer (10 mM Sodium citrate, 0.05% Tween 20, pH 6.0), washed again with PBS. Potential non-specific binding of the antibodies was blocked using optimized blocking method with sera. Primary antibodies specific to the tissue targets and isotype controls were added for 24 h at 4°C. Following the incubation, the

primary antibodies were removed by washing the sections with PBS for 5 – 20 min at RT and visualized by incubation with a secondary antibody reactive to the species of the primary antibody at the optimized dilution in PBS for 1 h at room temperature protected from light. Then, unbound secondary antibody was washed out with PBS and then sections were then subjected to immunofluorescence imaging.

Negative controls, lacking the primary antibody, were included to determine the non-specific binding of the secondary antibodies. The exclusion of both primary and secondary antibodies was initially used to determine cellular auto-fluorescence from the tissue. Macrophages were visualized by immunofluorescence staining of MAC-2 (Galectin-3; M3/38; Cedarlane), smooth muscle cells (SMC) were marked with SMA (smooth muscle actin; 1A4; Dako), and endothelial cells were identified targeting the cluster of differentiation 31 (CD31) (M-20; Santa Cruz Biotechnology) (Shagdarsuren et al., 2008; Shagdarsuren et al., 2009). The inflammatory markers TNF-α (abcam) and ICAM-1 (eBioscience) in the plaque were also assessed by immunofluorescence. For apoptosis, the TUNEL FITC apoptosis detection kit (Vazyme Biotech Co., Ltd, China) was used. As second antibodies, Fluorescein isothiocyanate (FITC)–conjugated (Jackson ImmunoResearch) or Cyanice Cy^{TM}3 (Cy3) -conjugated (Jackson Immuno Research) were used. Leica DMLB fluorescent microscope and CCD camera were used to image the tissue sections using green fluorescence excitation at 488 nm or red fluorescence excitation at 543 nm.

3.2.3. Cell culture

All cell culture techniques were carried out under sterile conditions in a laminar flow hood operating with sterile equipment.

3.2.3.1 THP-1 cells.

THP-1 cells are derived from the peripheral blood of a 1-year-old male with acute monocytic leukemia. They are widely used as a suitable model of human blood monocytes due to their phenotypic characteristics since they express many distinct monocytic markers, which are maintained over the time during cell culture (Tsuchiya et al., 1980). THP-1 cells, originally obtained from the American Type Culture Collection (ATCC), were cultured in RPMI 1640 media supplemented with 10% inactivated Fetal Bovine Serum (FBS), 1% L-glutamine, 1% Penicillin-Streptomycin, and 0.05 mM 2-mercaptoethanol at 37°C and 5% CO_2 in a humidified tissue culture incubator (Thermo Fisher scientific). Culture media and supplements were obtained from GIBCO. Media was changed approximately every 48 h keeping the cell

concentration below $1x10^6$ cell/mL and cells were used until passage 20. This was to prevent use of cells undergoing genetic drift and other variations (Calles, Svensson, Lindskog, & Haggstrom, 2006).

3.2.3.2 THP-1 derived macrophages differentiation.

Differentiation of THP-1 cells to macrophages-like cells was achieved by treating them with phorbol 12-myristate 13-acetate (PMA, Sigma-Aldrich), a widely used reagent to study the function and biology of human macrophages (Chanput, Mes, & Wichers, 2014; Meijer et al., 2015). As the conditions used for differentiation, particularly the concentration of PMA and the duration of treatment, vary widely (Auwerx, 1991; Daigneault, Preston, Marriott, Whyte, & Dockrell, 2010; Kohro et al., 2004; E. K. Park et al., 2007), different conditions were assayed to establish the differentiation protocol, by culturing $1x10^6$ cell/mL THP-1 cells in six well plates (Costar) and stimulated with two different concentrations of PMA, 10 ng/mL and 25 ng/mL for incubation periods of 48 h and 72 h. Lastly, to complete the differentiation, cells were subjected to a resting period for 24h incubation in PMA free culture media (Chanput, Mes, Savelkoul, & Wichers, 2013). Cell culture supernatants were collected, centrifuged at 13,000g for 10 min, aliquoted in 2 mL centrifuge tubes (VWR), and store at -20°C for cytotoxicity assays. Optimised results were achieved using the 10 ng/mL for 48 h followed by 24 h of resting period as reported (Yakala et al., 2019).

3.2.3.3 Experimental conditions for polarization on THP-1 monocytes and THP-1-derived macrophages

A well-known platform to study the inflammatory response is the use of THP-1 cells stimulated *in vitro* with different treatments to achieve M1-like or M2-like phenotypes (Jakopin & Corsini, 2019; Loeffler et al., 2020; Yakala et al., 2019). In this study, different conditions were used (**Table 3.1**) to achieve the right cell polarization status of the cells.

LPS and cytokines were reconstituted following manufactures protocols in ultra-pure-pyrogen free water (Lonza) or PBS (Gibco). Aliquots of 10 – 50 µl were made and and kept at -80°C during the course of the experiments. Cells were treated in culture media with the above-mentioned concentrations for 6 h or 24 h, to study changes in gene expression, protein levels, metabolic profile, and mitochondria morphology modifications. In the case of groups treated with Mdivi-1 (TOCRIS), this agent was added to the cell culture alone or together with M1-like or M2-like stimulus, in a final concentration of 10 or 50 µM. The mentioned concentrations used for Mdivi-1 were based on previous studies (Bordt et al., 2017; Ruiz, Alberdi, & Matute,

2018; Smith & Gallo, 2017; F. Xu et al., 2016).The vehicle for Mdivi-1 was DMSO (Sigma), used at a final concentration of 0.1-0.5% in the *in vitro* experiments.

Table 3.1 Cell treatments used in THP-1 monocytes and macrophages to induce polarization towards M1-like or M2-like phenotype.

Polarization Phenotype	Agent / Cytokine	Concentration (ng/ml)	Company
M1-like	LPS + IFN-γ	100 + 20	InvivoGen / Miltenyi Biotec
	TNF-α	50	Miltenyi Biotec
M2-like	IL-4	20	Miltenyi Biotec

3.2.4. Subculture of cells and cell viability.

At 70-90% confluence, medium was removed from the culture flasks and cells were washed twice with PBS. TrypLE Express solution (Gibco) was applied (3 ml/T-25 and 7 ml/T-75 flask) to the cells (THP-1 derived macrophages) and incubated 3-5 min at 37°C. The flask was tapped gently to dislodge cells and monitored, every 1-2 min, under a light microscope. Once cells had detached, TrypLE activity was inhibited by the addition of the same volume of supplemented (serum-containing) cell culture medium. The cell suspension was transferred to sterile tubes and centrifuged for 5-7 min at 200 x g. After removing the supernatant, the cells were resuspended in 1 ml of pre-warmed culture medium. Next, cell count was determined by mixing 10 µl cell suspension with 10 µl of trypan blue 0.4% (Life Technologies) (1:1 ratio). Cell density was determined automatically by adding 10 µl of this mixture to the grid of new counter chamber slides (Life Technologies) and inserted in Countess II FL Automated Cell Counter (Life Technologies). Viable cells were then further diluted to working densities and used in the experimental procedures, subcultured, or cryopreserved. To determine cell viability, cells were loaded with 0.04% trypan blue (Invitrogen) and cell viability was immediately analyzed the mentioned cell counter equipment, and the number of viable (unstained) and nonviable (blue stained) cells was recorded. For the THP-1 cell subculture, the same procedure was followed with the omission of the detachment step.

3.2.5. Cryopreservation of cells.

To create cell line stocks, cells were removed from the culture flasks as in section 3.2.6., at low passage (usually P2 – P5). Cells were counted and resuspended within the range of 2-4 x 10^6 cells/ml on freezing media (90% FBS and 10% DMSO, filtered by 0.22 μm). One mL of cell suspension was aliquoted per cryovial (NALGENE) and store at -80°C in a Cryo freezing container (Corning CoolCell) overnight in order to gradually lower the temperature by approximately 1°C/min and ensure cell preservation. Finally, frozen cell suspension vials were then transferred to liquid nitrogen storage.

3.2.6. Thawing cryopreserved cells

To thaw frozen stocks of cells, vials were removed from liquid nitrogen and instantly placed in a 37°C water bath. As soon as no more ice crystals were present, the cryovial was wiped with 70% ethanol and the cell suspension was pipetted up and down to disperse the cells, and the whole content was gently transferred to a 15 mL centrifuge tube (Falcon) previously filled with pre-warmed - CO_2 calibrated -supplemented media. When cells were suspended in the fresh media, were centrifuged 200 g for 7 min. The supernatant was aspirated and cell pellet was once again resuspended in fresh supplemented media and seeded into T-75 flasks (10 – 12 mL). Following thawing of cryopreserved cells they were used for experiments after three passages in culture.

3.2.7 Fetal bovine serum heat inactivation

Deep frozen bovine serum was allowed to thaw in a water bath at 37°C, swirling the bottles every 10 - 15 min to disperse the released salts and proteins uniformly. To start the heating process in order to inactivate complement (Aleo & Padh, 1985; Pinyopummintr & Bavister, 1994; Triglia & Linscott, 1980)., the temperature was controlled to 56°C ensuring enough water volume to submerge the entire contents of the FBS bottle media. A control bottle filled with water was placed in the water bath to monitor the temperature, this bottle was identical to the FBS bottle subjected to heat inactivation. Then, a calibrated thermometer was suspended inside the control bottle without touching the sides or bottom allowing the temperature to be monitored. A timer was set to 30 min when the temperature in the control bottle reached the mentioned temperature. During the incubation period, the FBS bottle was swirled every 5 – 7 min to ensure the serum remained uniform throughout heating. Completed the 30 min, the heated inactivated serum was removed from the water bath and gently swirled once again and allowed it to cool. When the room temperature was reached, the whole volume

of serum was filtered by 0.22 µm using a filter unit (VWR) and subsequently aliquoted into labelled 50 ml centrifuge tubes (Falcon). Caps of the tubes were covered with parafilm paper (Sigma-Aldrich), and stored at -20°C.

3.2.8 Mycoplasma PCR detection

Mycoplasma denotes the smallest (0.2-2 µm in diameter) and simplest free-living parasitic organism known (Hay, Macy, & Chen, 1989). This bacteria is known to be a common contaminant (30% - 87%) (McGarrity, Vanaman, & Sarama, 1984) of mammalian cell cultures. Due to its size, it does not produce visible changes in cell culture media characteristic of contamination and it does not destroy host cells, but mycoplasma can influence cell growth, morphology, metabolism, DNA, RNA, protein synthesis and functional activity of the host cell, decreasing cell viability (Rottem & Yogev, 2000) and ultimately invalidating experiments. Therefore, mycoplasma testing is an essential quality control procedure needed to assure reliable experiments.

The e-Myco™ Mycoplasma PCR detection kit (iNtRON Biotechnology) was used in the present study. This kit uses PCR to specifically obtain amplification of a conserved, mycoplasma-specific ribosomal RNA gene region (16S rRNA) by implementing optimized primers which allows for sensitive and specific detection of different mycoplasma species. PCR-amplified DNA fragments are verified by electrophoresis to confirm the presence or absence of mycoplasma infection.

The mycoplasma PCR test was performed regularly using the boiling extract method by collecting $5x10^4$ cells from the cell cultures and centrifuged 300 g for 5min. The supernatant was discarded, and the cell pellet was washed twice with 1 mL of PBS. The tube was spin down in a micro-centrifuge for 20 sec, and the supernatant was decanted.

The washed pellet was resuspended in 100 µl of PBS and heated at 95°C for 10 min. Next, samples were mix by quick vortexing (10 sec) and centrifuged for 2 min at 10,000g (RT). Ten µl of the resulted supernatant was used as PCR template and transferred to a fresh e-Myco™ Mycoplasma PCR detection kit tube (that contains all components for PCR except the template), and resuspended by adding 10 µl of sterile water for a final reaction volume of 20 µl. Both, positive (recombinant DNA with partial 16S sequence of *M.hyorhinis*,) and negative (water) controls test reaction tubes were included. Tubes were placed into a thermal cycler (Applied Biosystem) and subjected to PCR (**Figure 3.2**). The obtained PCR products were analysed by gel electrophoresis, following the protocol described at section 3.2.9.7.2. (**Figure 3.3**)

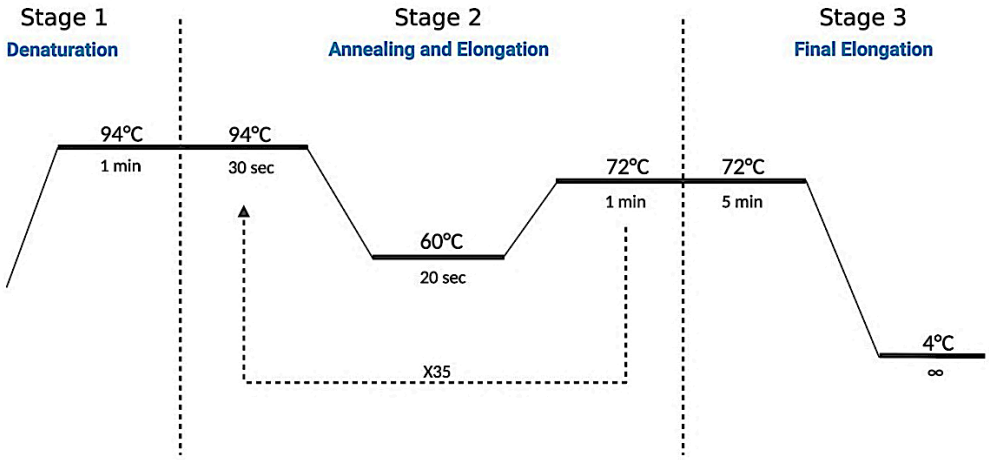

Figure 3.2. e-Myco™ Mycoplasma PCR detection steps. During PCR, denaturation of the template DNA separates the double strands, exposing the nucleotides. The annealing of primers with the complementary template DNA nucleotide sequence, by formation of hydrogen bonds, permits the amplification of the region of interest. Cell culture samples were used for the PCR reactions.

3.2.9 Molecular investigation of gene expression by semi-quantitative real-time reverse transcription polymerase chain reaction.

Reverse transcription polymerase chain reaction (RT-PCR) is an upgrade of the common PCR reaction, in which specific sequences of DNA are amplified using a thermocycler. Primers anneal to the matching sequence when the target gene is present in the sample being analyzed and the amplification takes place in an exponential manner as cycles are repeated to produce millions of copies of the target DNA to be synthesized (Arnheim & Erlich, 1992). Real-time RT-PCR (qRT-PCR) measures the amplification cycle by cycle in real-time. Quantifying PCR products, while the reaction is in the exponential phase of amplification and where there is an exact doubling of the products every cycle, is a more precise procedure. During qRT-PCR the fluorescence produced during each of the cycles of the reaction is measured by a fluorogenic dye double-stranded DNA (SYBR Green), or by the separation of a fluorescent molecule from its adjacent signal quenching molecule (TaqMan®). The intensification of the florescent signal and the cycle that the specified threshold is reached reflect the amount of the DNA target, allowing their quantification (Kubista et al., 2006).

3.2.9.1 RNA extraction

Total cellular RNA was extracted from cells (THP-1 and THP-1-derived macrophages) by adding T*RIzol*® Reagent (Invitrogen) to the tubes, containing the cell pellet, to induce disruption and solubilization of cellular components after repeated pipetting, followed by

vortexing until the cells were fully lysed. Chloroform (Sigma-Aldrich) was added in a 1:5 ratio (Chloroform:T*RIzol*®), vortexed immediately and mixed samples were centrifuged at 21,000 g for 15 min at 4°C to separate protein, DNA and RNA in different layers. The upper aqueous layer containing RNA was transferred into a sterile 1.7 mL centrifuge tube (Axygen) and the same amount of 2-propanol (Sigma-Aldrich) was added to the tube (1:1 ratio) and mixed by pipetting. The mixture was subjected to RNA purification using RNeasy minikit (Qiagen). Briefly, RNA mixture was loaded onto the RNeasy mini spin column, centrifuged at 8,000g for 2 min at RT, followed by washing with 700 µl of RW1 buffer and 500 µl of RPE buffer (twice). Next, the column was placed in a sterile 1.7 mL centrifuge tube, 32 µl of UltrapureTM DNase/RNase-Free Distilled water (Invitrogen) was added and the column was incubated for 1 min at RT and centrifuged at 8,000g for 1 min to elute the total RNA. Tubes were placed on ice and immediately quantify.

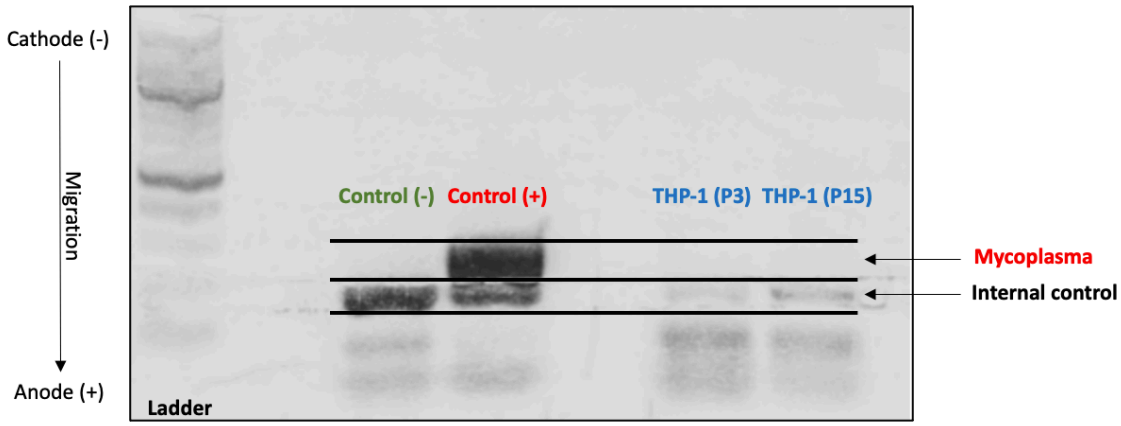

Figure 3.3 Mycoplasma detection e-Myco™ Mycoplasma PCR detection kit.
DNA samples derived from THP-1 cells at passage 3 (P3) and passage 15 (P15) were loaded into two adjacent wells for Mycoplasma detection, determined by the presence/ absence of DNA products.; Mycoplasma control product (270bp) and internal control product (160bp). DNA bands: lane 1) DNA ladder, 2) empty 3) negative control, 4) positive control, 5) empty, 6) THP-1 (P3), 7) THP-1 (P15). Reactions that are mycoplasma positive produces two DNA bands (as per lane 3). A mycoplasma negative reaction only produces product of 160pb (as per line 3, 6 and 7).

3.2.9.2 RNA Quantification and purity

ThermoFisher Scientific NanoDrop1000 was implemented to determine the quantity and purity of the RNA samples extracted from cells (THP-1 and THP-1-derived macrophages. This instrument is a full spectrum spectrophotometer (200-750 nm) which employs a patented sample retention technology holding the sample in place by utilising surface tension, guaranteeing accuracy and reproducibility during the measures. The aqueous sample forms a column between the two fibre optic-containing pedestals and light is passed through the

specimen and the absorbance is measured at different wavelengths (260 and 280 nm) to determine the concentration and purity according to Beer-Lambert law (Gallagher, 2017). A sample/blank volume of 1 µL was loaded onto the lower pedestal with fibre optic cable (receiving fibre) and the upper pedestal with a second fibre optic cable (the source fibre) was lowered and brought into contact with the sample, forming a gap between the fibre optic ends, allowing the spectrophotometric measure as described above. Samples were wiped clear from the pedestals between each analysis and UltrapureTM DNase/RNase-Free Distilled water (Invitrogen) was used as a blank control measurement to calibrate the NanoDrop. Nucleic acid concentrations were automatically calculated and expressed in ng/µL by instrument software and purity was indicated by the ratio of the absorbance at 260 nm/280 nm and 260 nm/230 nm within a range of ~2.0±0.4 and 1.8-2.2 respectively, indicating good purity (Gallagher, 2017).

3.2.9.3 DNase digestion

The isolated RNA may contain small amounts of contaminating genomic DNA which should be removed from the preparation to achieve a high quality RNA for subsequent analysis like RT-qPCR (Green & Sambrook, 2019). For this reason, DNase digestion of the RNA preparations was carried out using RNase-free DNase I (Thermo-Scientific). Briefly, 1 µg of RNA was added in a final reaction volume of 10 µL together with 1 µL 10X reaction buffer with $MgCl_2$, 1 µL DNase I -RNase-free, 1U/µL RiboLock RNase Inhibitor (Thermo-Scientific) and DEPC-treated water. The preparation was incubated 30 min at 37°C, and then 1 µL 50 mM EDTA was added to the preparation and immediately incubated for 10 min at 65°C. After the incubation, the RNA samples were transferred to ice and subjected to an integrity RNA test.

3.2.9.4 RNA Integrity.

Total RNA integrity is known to affect down-stream analysis such as qRT-PCR as well as the quantitative results in mRNA expression profiling. (Taylor & Mrkusich, 2014). Therefore, a classical quality control of RNA was performed to minimize non-specific sample variations using agarose gel electrophoresis, with the aim to visualize two sharp bands denoting 28S and 18S rRNA components in the gel (Imbeaud et al., 2005).

RNA samples (1 µg) were mixed with RNA gel Loading dye (ThermoFisher Scientific), incubated for 10 min at 70°C, chilled on ice, and then subjected to 1.2% agarose gel electrophoresis. The first line of each row was loaded with a RiboRuler high-range RNA ladder (ThermoFisher Scientific). The gel preparation, running protocol, and the imaging system used are described in section 3.2.9.7.2.

3.2.9.5 Complementary DNA (cDNA) synthesis

Reverse transcription and subsequent conversion to cDNA was performed for accurate and precise quantification of RNA targets. iScript cDNA synthesis kit (BIO-RAD) was used for cDNA synthesis, which contains a blend of oligo(dT) and random hexamer primers that anneal to the RNA template at multiple locations and produce targets <1 kb in length. The RNA was diluted in UltrapureTM DNase/RNase-Free Distilled water (Invitrogen) to a final concentration of 1 μg in a PCR tube (Axygen) together with the iScript Reverse Transcriptase and the iScript reaction mix in a final reaction volume of 20 μL. The samples were then loaded into a thermocycler (Applied biosystem) and incubated according to the protocol in **Table 3.2**.

A negative control reaction (no RT control) was utilized to investigate genomic DNA contamination for each cell type or experimental procedure. In this reaction, all components were added except for the iScript Reverse Transcriptase. The lack of amplification in these samples in the subsequent qRT-PCR analysis indicated no contamination by genomic DNA.

Table 3.2 cDNA Synthesis Kit Reaction Protocol.

Step	Time	Temperature
Priming	5 min	25°C
Reverse Transcription	20 min	46°C
RT inactivation	1 min	95°C
Optimal step	Hold	4°C

PCR mixtures were prepared fresh on the day of the experiment, using iScript cDNA Synthesis kit. RNA sample mixture was subjected to 4 reaction steps: 1) Priming, 2) Reverse Transcription, 3) RT inactivation and 4) Optimal step, to form the complementary DNA for downstream analysis.

3.2.9.6 qRT-PCR using SYBR Green

PrecisionFAST 2x qPCR MasterMix with SYBR green and low ROX (PrimerDesign) was used for real-time PCR. The SYBR green intercalates with double-stranded DNA, absorbs blue light at a wavelength of 497 nm and emits a green fluorescence light at 520 nm. The cycle at which the fluorescence intensity increases above the threshold is proportional to the initial abundance of the target sequence (Bustin & Mueller, 2005). ROX is an inert additive to the mix, not interfering with the PCR reaction (passive reference dye), that provides a constant fluorescent signal for sample normalization. PrecisionFAST is designed for rapid cycling protocols that significantly reduce the running times. A mutation in the active site of the Taq Polymerase used provides higher affinity for DNA and faster processing. Also, the buffer is

designed for optimum sensitivity and to decrease formation of primer dimers, which are common artefact found when using fast processing enzymes. For each gene target 1 µL of the sample (10 ng/µL) or controls (no RT controls and no template controls) were carefully pipetted in triplicates using sterile filtered tips (ART) into 96-well plates PCR plates (Applied Biosystems) placed in a Cool-Rack (Biocision) on ice. This was followed by 3 µL of UltrapureTM DNase/RNase-Free Distilled water (Invitrogen), 5 µL of PrecisionFAST 2x qPCR MasterMix with SYBR green and low ROX, and 0.5 µL from both forward and reverse primers (10 µM), to form a final PCR reaction volume of 10 µL. Plates were covered with a MicroAmp^{TM} optical adhesive film (Applied Biosystems), transferred to a PCR plate spinner (VWR) and centrifuged for 30 sec at RT to ensure that all solutions were collected at the bottom of the wells. Plates were then analysed using the ViiA 7 Real-Time PCR System (Applied Biosystem) using the protocol shown in **Table 3.3**

Table 3.3. qRT-PCR Reaction Protocol.

Step	Time	Temperature
Hold Stage	2 min	95°C
PCR Stage (50 cycles)	5 sec	95°C
	5 sec	62 - 64°C
	10 sec*	72°C
Melt Curve Stage	15 sec	95°C
	1 min	60°C
	15 sec*	95°C

PCR mixtures were prepared fresh on the day of the experiment, using PrecisionFAST 2x qPCR MasterMix with SYBR green and low ROX. cDNA samples mixture were subjected to 3 reaction steps: 1) Hold Stage, 2) PCR Stage, 3) Melt Curve Stage. (*) Data collection on.

3.2.9.7 Validation of primer targets

The products that were amplified during real-time RT-PCR analysis require further validation to ensure complete specificity in the assay which is given by a single amplification product for each primer target evaluated during the reaction. To evaluate the specificity, both melt curve analysis and gel electrophoresis were performed in this study (Ruiz-Villalba, van Pelt-Verkuil, Gunst, Ruijter, & van den Hoff, 2017).

3.2.9.7.1 Melting curve analysis.

Melt curve analysis is commonly used to assess whether the intercalating dye such a SYBR green has produced a single–specific product during the qRT-PCR, as this type of dye bind to any double-stranded DNA formed in the reaction. As shown in **Table 3.3**, after the amplicon was produced (PCR Stage), it was subjected to incubation at increasing temperatures and then the changes in fluorescence were determined and plotted automatically by the ViiA™ 7 Software as the rate of variation of fluorescence vs. temperature. A single melt peak was obtained for all of the gene targets evaluated.

3.2.9.7.2 Gel electrophoresis

To confirm the single melt peak obtained during the melting curve and the amplicon size, a gel electrophoresis analysis was performed to visualize the presence of a single band which indicated a single product formation that matched the predicted amplicon size. Horizontal agarose gel electrophoresis was used for separation and visualization of the amplicons according to size. Two µL of DNA gel loading dye (6X) (ThermoFisher Scientific) were mix with 10 µL of real-time RT-PCR product for each target, and loaded into a freshly prepared agarose gel.

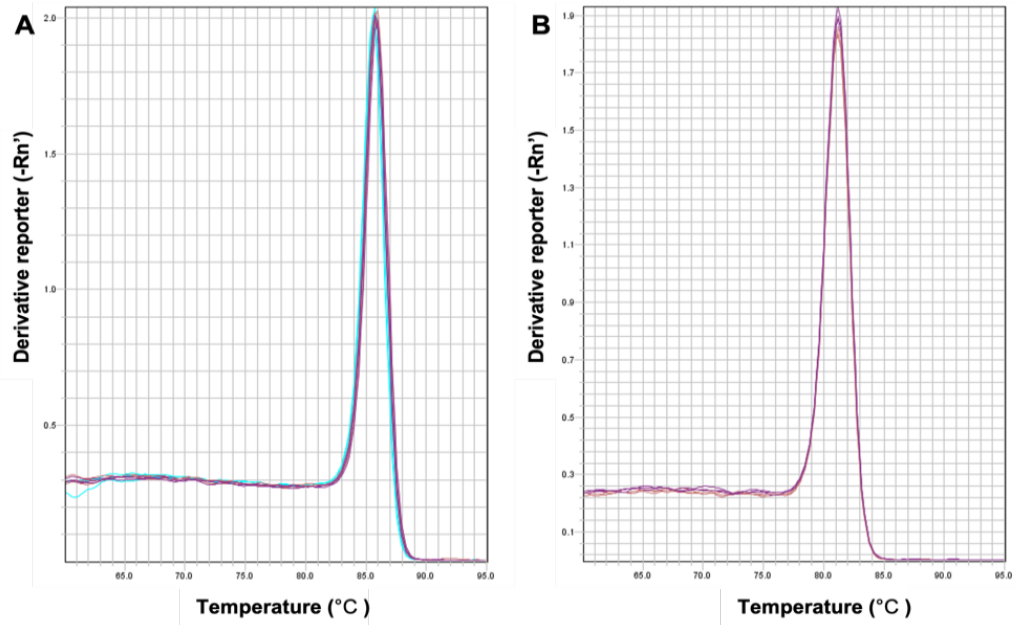

Figure 3.4 Melting curve analysis of target genes after qRT-PCR. DNA samples derived from THP-1 cells were subjected to qRT-PCR process. Representative melting curves for *β-actin* (A) and *MCP-1* (B) showing a single pick, indicative of a single product during the qRT-PCR assay.

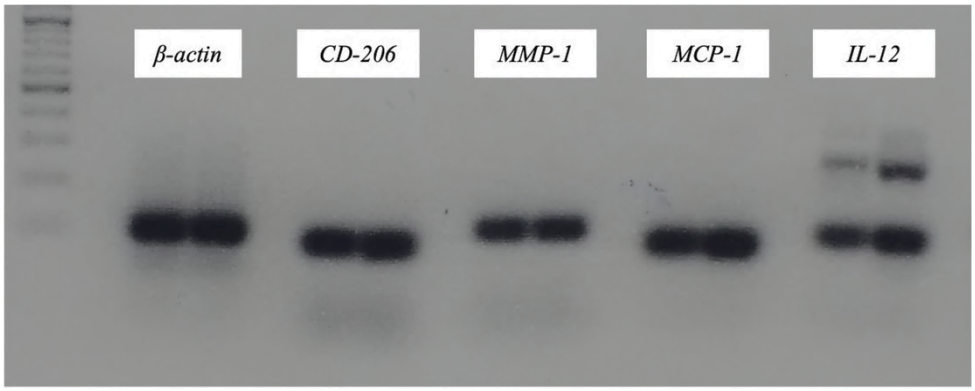

Figure 3.5 Gel electrophoresis analysis of qRT-PCR DNA products. Different DNA derived from THP-1 cells were subjected to qRT-PCR process and product samples were then loaded in duplicates into an agarose gel for an electrophoresis run. All the analyzed target genes showed a single specific DNA product (100-120bp), except *IL-12*, which showed an unspecific amplified product (approx.. 250 bp).

The gel was prepared with 2% agarose Biotechnology grade (First BASE Laboratories) in Tris-Acetate-EDTA (TAE) Buffer, pH 8.0 (First BASE Laboratories) and 1X GelRed® Nucleic Acid Gel Stain (biotium). Once set, gels were placed in the a Wide Mini-Sub cell GT system (BIO-RAD) and immersed in TAE Buffer. The first line of each row was loaded with GeneRuler DNA ladder mix (ThermoFisher Scientific) and after all samples were loaded onto the gels, these were run at 100V for 30-45 min using a PowerPac™ Basic Power Supply (BIO-RAD). Lastly, DNA bands were visualized using the BIO-RAD ChemiDoc XRS+ Imaging System.

3.2.9.8 Relative quantification analysis of qRT-PCR

The analysis of relative gene expression data was performed by the $2^{-\Delta\Delta C_T}$ method (Livak & Schmittgen, 2001)**.** The triplicate Ct values from each target gene studied were averaged to obtain a representative value and account for inter-assay variability. The mean values of all Ct sample targets were primarily normalized to the expression of the reference gene target , β-actin, to determine de delta ΔCt value:

ΔCt = Ct target gene – Ct reference gene

Ct values for target genes in experimental conditions were represented relative to their expression in control conditions (calibrator sample) for the semi-quantitative analysis of mRNA expression. The mean ΔCt from control samples of each repeat of the experiment was taken as the ΔCt calibrator value for which all other individual ΔCt values were normalized, including individual control ΔCt. This permitted for between-experiment variation to be accounted for in control samples. The mentioned quantification was calculated as ΔΔCt:

ΔΔCt = ΔCt treated sample – ΔCt untreated sample

Lastly, to calculate the gene expression values, the 2 to power of negative ΔΔCt was done. This value ($2^{-\Delta\Delta C_T}$) for the calibrator control sample is approximately equal to 1, and data is represented as fold-change from this calibrator control value (Livak & Schmittgen, 2001):

Fold gene expression = 2^-(ΔΔCt)

3.2.10 Cell migration assays

To study the migration process of both THP-1 monocytes and primary human isolated monocytes, two different protocols were assayed, the Boyden chamber assay (or transwell migration assay) and a 3-dimensional (3D) chemotaxis assay as described in detail below.

3.2.10.1 Transmigration assay

Transmigration using automated cell counter: Both THP-1 cells and human monocytes derived from blood isolated by positive selection (section 3.2.12.1), were subjected to a transmigration assay towards chemokine gradient. A 24-well - 6.5 mm Transwell® with 8.0 μm Pore Polycarbonate Membrane Insert (Corning), was used for individual experiments assaying three replicates for each condition per experiment. Cells were centrifuged at 200 g for 10 min and resuspended in starving media (RPMI 1640 with 0.2% FBS) in different amounts (150,000, 250,000 and 500,000 cells/well) being 250,000 cells/well the one that provided the best results and was used for experiments as previous described (Yakala et al., 2019). The bottom of the lower chamber (**Figure 3.6A**) was filled with conditioned media which consists of 0.65 mL of RPMI 1640 medium (GIBCO) supplemented with 0,5% FBS (GIBCO) and the chemoattractant, either human Macrophage Colony-Stimulating Factor (MCS-F) (Miltenyi Biotec) or Monocyte Chemoattractant Protein-1 (MCP-1) (Miltenyi Biotec). The cells (100 μL) were seeded on top of the filter membrane in the transwell insert already placed on the lower chamber (**Figure 3.6A**), ensuring the contact between the membrane top insert and the bottom conditioned media to form the chemotactic gradient. The plates were then placed in a humidified tissue culture incubator at 37°C, 5%CO_2 for 6 h to allow cell migration (**Figure 3.6B**). After incubation, the transwell inserts were carefully removed from the wells, and the conditioned media at the bottom chamber was harvested (**Figure 3.6C**), spun down, resuspended in 35 μL of RPMI 1640 media (GIBCO), and the transmigrated cells were counted (three replicates per samples in each experiment) in a Countess II FL Automated Cell Counter (Life Technologies). For the experiments of chemotaxis inhibition, the inhibitor was added to the starving media, mixed with the cells and immediately seeded on a transwell insert. For

experiments with THP-1-activated monocytes, cells were stimulated with 100 ng/mL of lipopolysaccharide (LPS-EB Ultrapure; InvivoGen) for 4 h as described (Yakala et al., 2019).

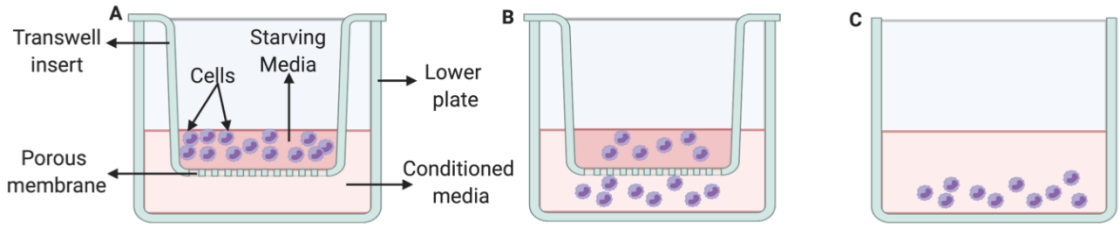

Figure 3.6 Transwell migration assay. Cells are seeded in the membrane of the transwell insert in starving-media and the lower plate is filled with conditioned media (containing chemoattractant) (A). Cells migrate from the transwell insert to the lower plate through the porous membrane (B). Cells present in the bottom of the transwell insert as well as the ones in the lower plate are counted to determine cell migration.

Transmigration assay using software cell counter: After removing the inserts from the lower plate, they were cleaned with a cotton-tipped applicator to carefully remove the media and remaining cells that have not migrated from the top of the membrane without damaging it. Then the cells at the bottom of the membrane were fixed by placing the insert in to a lower chamber previously filled with 700 µL of with 70% ethanol and incubated for 10 min. After the fixation, the remaining ethanol from the top of the membrane was removed with a cotton-tipped applicator, and the transwell membranes were allowed to dry for 15 min. Next, cells nuclei were stained for 10 min by placing the insert in the lower chamber filled with 700 µL of Hoechst 33342 (ThermoFisher-Scientific) solution 1µg/mL in DPBS (Lonza). The Hoechst solution was gently removed from the top of the membrane with a pipette tip or cotton tipped applicator. Very carefully, to avoid washing off fixed cells, the membrane was dipped into DPBS to remove the excess of Hoechst. The transwells were allowed to dry and then the membrane was carefully removed using an scalpel and placed in a glass slide with cover slip and the cells were visualize in a fluorescence microscope (Olympus) using the common DAPI filter. Three images per membrane were taken and the cell number was determined using the analyse particle tool on ImageJ (Papadopulos et al., 2007).

3.2.10.2 3D chemotaxis assay

The migratory behaviour in response to MCP-1 of human peripheral blood monocytes was assessed by 3D time-lapse chemotaxis assay as previously described (Bzymek et al., 2016). Non-pepsinized-rat tail collagen type I (ibidi GmbH) was initially diluted to 2X concentrated (2 mg/mL) with pH neutralizing solution consisting of 20 µL DMEN [10X] (Sigma Aldrich), 6 µL NaOH [1M] (Sigma Aldrich), 49 µL ultrapure sterile H_2O, $NaHCO_3$ [7.5%] (Sigma), 100

µL DMEM [1X] (Sigma Aldrich) and 120 µL of collagen type I [5 mg/mL]. The final pH of the 2X concentrated collagen solution ranged between 7.2 – 7.4.

After isolation, 100 µL of human monocytes cell suspension ($4x10^6$ cells/mL) in DMEM media were mixed with an equal amount of the freshly prepared 2X concentrated collagen solution. Next, using a 3D chemotaxis µ-Slide (Ibidi GmbH) (**Figure 3.7**) , 8 µL of the resulting collagen gel containing cell suspension was applied to the top of the filling port A, and immediately afterwards, air was aspirated from the opposite filling port B until both ports were filled with the gel and the µ-Slide was incubated at 37°C for 30 min to allow polymerization. After incubation, ports C, D (chemoattractant free-side) and ports E, F (chemoattractant side) were filled with 65 µL of the corresponding media.

MCP-1 (100 ng/mL) was use to form the chemoattractant gradient and was assayed in the presence or absence of Mdivi-1 (10 µM, 50 µM). The migratory behaviour of the cells was assessed by monitored performing time-lapse imaging using DMi8 M Microscope (Leica). To this end, the slide was mounted on the microscope stage, incubated for 15 min to allow temperature equilibration and then the time-lapse experiment was started by imaging every 2 min at 37°C for 2 h. On average, 15 – 25 cells were tracked per experiment by using ImageJ software plugin "Manual Tracking" and further analysed were performed with the "Chemotaxis and Migration Tool from ibidi" (Zengel et al., 2011).

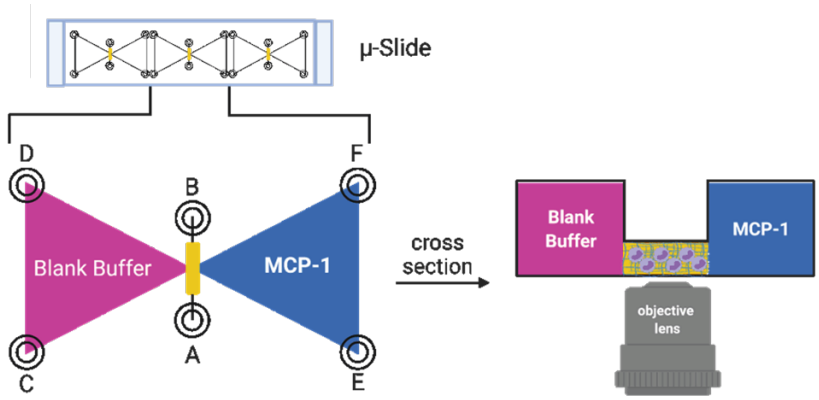

Figure 3.7 Chemotaxis-µ-slide for 3D migration assay. Two large-volume reservoirs (pink and blue) are connected by a small gap (yellow). Cells are placed into this gap (=observation area) an exposed to a linear concentration MCP-1 gradient while their movement is tracked using a microscopy.

The day before seeding the cells and conducting the experiment, all cell culture media, the µ-Slide, and plugs were placed into the incubator for gas equilibration. The medium was placed into a slightly opened vial. This prevented the medium inside the slide, and the slide itself, from allowing air bubbles to form during the incubation time.

3.2.11 Peripheral blood mononuclear cell (PBMC) isolation

The isolation of primary human peripheral blood monocytes was approved by the local ethics committee of National Heart centre of Singapore and LMU Munich University. All experiments were carried out in accordance with the guidelines from both institutions.

PBMC were isolated from peripheral human blood collected in a EDTA vacutainer tubes as described (Lopez et al., 2014). Blood was mixed 1:1 with PBS supplemented with 2% FBS. Diluted blood was centrifuged at 160 g for 20 min with no brakes applied. Plasma supernatant was discarded and cell pellet was resuspended in to a final volume of 30 mL with PBS-2%FBS and subjected to a density gradient centrifugation process using Ficoll-Paque Plus (GE Healthcare) for 30 min at 800 g with no brakes applied. After centrifugation, PBMC cells in the interphase were carefully collected and subsequently washed with prewarmed PBS-2% FBS by centrifugation for 10 min at 600 g and supernatant was discarded via aspiration. If red blood cells (RBC) were present on the obtained cell pellet, they were lysed by an 10min incubation with filter-sterilized RBC lysis buffer: 155 mM NH_4Cl (Sigma-Aldrich), 10 mM $KHCO_3$ (Sigma-Aldrich), 0.1 mM EDTA (ThermoFisher-Scientific) with pH adjusted to 7.3. After the incubation time, cells were washed with PBS- 2% FBS as previous mentioned. The cell pellet was then resuspended in RPMI 1640 medium supplemented with 10% FBS, 1% penicillin/streptomycin, 2 mM L-glutamine and maintained at 37°C in a humidified atmosphere of 5% CO_2 at 1-1.25 x 10^6 cells/mL.

3.2.12. Human monocytes isolation

Human monocytes were isolated from PBMC via magnetic immuno-labelling, by both positive and negative selection. For positive selection, PMBC were incubated with magnetic microbeads coated with monoclonal antibodies against the cluster of differentiation (CD) 14 in monocyte's surface ($CD14^+$) .These labelled cells were retained in the column placed in a strong magnetic field, while the non-monocytic cells (unlabelled) were eluted. In case of cells isolated by negative immuno-labelling, non-monocytic cells, i.e. T cells, NK cells, B cells, dendritic cells, or basophils were indirectly magnetically labelled using a cocktail of biotin-conjugated antibodies (primary labelling reagent) against CD3, CD7, CD16, CD19, CD56, CD123 and Anti-biotin monoclonal antibodies conjugated to microbeads (secondary labelling reagent), which were retained in the column placed on the magnetic field, and the pure unlabelled monocytes were eluted.

3.2.12.1 Monocyte isolation by positive selection

Human monocytes were isolated using positive selection as previously described (Lopez et al., 2014; Lopez-Zambrano, Rodriguez-Montesinos, Crespo-Avilan, Munoz-Vega, & Preissner, 2020). PBMC were centrifuged at 300 g for 10 min and resuspended in 90 µL of MACS buffer (PBS 1X supplemented with 0.5% bovine serum albumin, EDTA 2 mM, filtered by 0.22 µm) per 10^7 cells and mixed with 10 µL of anti-CD14 coated microbeads (Miltenyi Biotec). Cell suspension was then incubated for 15 min at 4°C. After incubation, cells were washed with 10 mL MACS buffer and centrifuged at 300 g for 10 min. The supernatant was discarded and cells were resuspended in 500 µL of MACS buffer and loaded onto a LS-column (Miltenyi Biotec) attached to a strong magnetic field QuadroMACS™ (Miltenyi Biotec). The column was then washed three times with 3 mL of MACS buffer each time and then removed from the magnetic field and placed on top of 15 mL conical tube. Subsequently, 5 mL of MACS buffer was loaded to the column and a plunger was placed on top of the column and pushed carefully to flush out the magnetically $CD14^+$ labelled cells. Eluted cells were then washed with MACS buffer and centrifuged at 300 g for 10 min. The supernatant was discarded and cells were resuspended in RPMI-1640 culture medium with 10% FBS, 1% penicillin/streptomycin, 2 mM L-glutamine. Cell viability and count was performed as described in the previous section and purity was determined by flow cytometry (section 3.2.13). After confirming that cells were suitable for experiments based on their purity, positive isolated monocytes were subjected to a cell transmigration assay.

3.2.12.2 Monocyte isolation by negative selection

Human monocytes were isolated by negative immuno-labelling as previously described (Bernhagen et al., 2007) using the Monocytes Isolation Kit II from Miltenyi Biotec. PBMC were centrifuged at 300 g for 10 min and resuspended in 30 µL of MACS buffer per 10^7 total cells. For primary labelling, FcR blocking reagent and biotin-antibody cocktail were added (10 µL per 10^7 total cells from each reagent) and incubated for 10 min at 4°C. For secondary labelling, 30 µL of buffer and 20 µL of anti-biotin microbeads were added to the cell suspension, mixed, and subjected to a second incubation for 15 min at 4°C. After incubation, cells were washed with 10 mL MACS buffer and centrifuged at 300 g for 10 min, the supernatant was discarded, and cells were resuspended in 500 µL of the same buffer and loaded into the pre-calibrated column already placed in the magnetic field as described. After the corresponding washing steps, the entire effluent was collected and this fraction corresponded to the enriched monocytes, while the non-monocytic cells were retained in the column. The

purity of the isolated monocytes was also assessed by flow cytometry and cells were subsequently used for 3D chemotaxis assays.

3.2.13 Flow cytometry for monocyte purity

Monocytes isolated from blood samples were subjected to purity analysis by their surface expression of CD14 (A. Kelly, Grabiec, & Travis, 2018) as previously described (Lopez et al., 2014). Briefly, 500,000 cells were resuspended in 98 µL of FACS buffer (1% FBS, 2 mM EDTA) and incubated with 2 µL of anti-human CD14-FITC or the corresponding isotype antibody (Miltenyi Biotec) for 10 min at 4°C in the dark. Cells were washed with 1 mL of FACS buffer and centrifuged at 300 g for 10 min. The supernatant was aspirated, and labelled cells were resuspended in 500 µL of FACS and aliquoted in non-pyrogenic 5 mL round-bottom polystyrene tubes (Falcon). Finally, data were acquired on BD^{TM} LSR II using BD FACS-DIVA software version 8.0.1 (BD Bioscience) (**Figure 3.8**). Unstained cells were used as a negative control in the experiments.

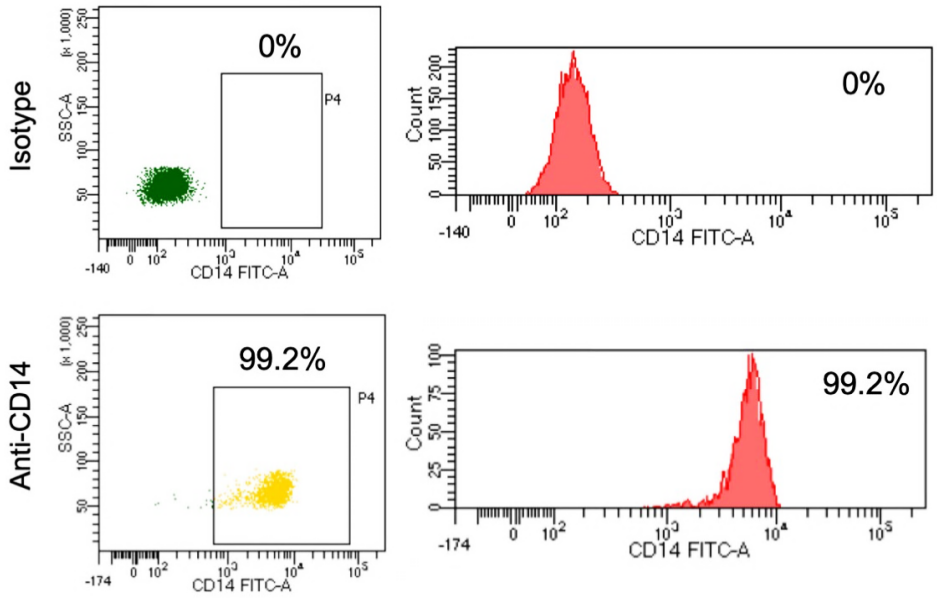

Figure 3.8 Flow cytometry of primary Human monocytes. A representative cell purity analysis by flow cytometry is presented of blood isolated monocytes. Anti-CD14 couple to FITC and its corresponding isotype control were used. Results showed and enriched monocyte (99.2%) population, as per CD14 positive cells.

3.2.14 Seahorse extracellular flux analysis

To evaluate metabolic changes in THP-1 monocytes and THP-1-derived macrophages, the Agilent Technologies Seahorse XFe96 was used according to manufacturer's protocol. This technology allows the measurement of changes in mitochondrial respiration in real-time by

quantifying the "oxygen consumption rate" within cells and is referred to as OCR. The cellular metabolic analyzer works at a physiological temperature of 37°C and is constituted by fiber optic probes that sit in the cartridge sleeve placed above the cellular monolayer, creating a tight chamber-like space, in which the probes can sense small changes allowing the OCR track. The ports on the cartridge are used to load the modulators of mitochondria respiration chain complexes, by either inhibiting or promoting OCR, letting real-time understanding of cellular bioenergetics (Divakaruni, Paradyse, Ferrick, Murphy, & Jastroch, 2014).

Plate coating - Seahorse XFe96 well plates were coated with different reagents, including cell-tak ™ (corning), laminin (sigma), or poly-D-lysine (sigma) to achieve adhesion of THP-1 monocytes. Among them, poly-D-lysine showed better results in terms of monocyte cell adhesion upon visualization under the microscope.

Before the assay, the Seahorse plates were pre-coated with 50 µL poly-D- lysine (1 mg/mL) per well and covered to ensure sterility. After overnight incubation at RT, plates were washed twice with 200 µL of sterile water and were left to dry before the cell seeding. For THP-1-derived macrophages, plate-coating was not needed, as they become adherent after PMA stimulation.

Cell seeding - For THP-1 monocytes a cell suspension (100,000 – 200,000 cells/well) were seeded on the poly-D-lysine precoated plates and spun down for 1 min at 300 g. Next, the cell media was removed and replaced with supplemented seahorse XF media. In the case of experiments with THP-1 macrophages, the THP-1 cell suspension was seeded in the presence of PMA to induce macrophage differentiation, following the protocol described in section 3.2.3.2. All the wells contained cells with the exception of four background temperature correction wells (A1, A12, H1, and H12) which were left blanked with 100 µL media alone as per manufacture instructions (Agilent technologies).

3.2.14.3 Mito-stress assay

The day prior to the assay: The day prior to the assay, the media and sensor cartridge were prepared. An aliquot of at least 20 mL of Seahorse XF Calibrant was added into a 50 mL conical tube and placed in a non-CO2 37°C incubator overnight. Next, the sensor cartridge included on the XFe96 Extracellular Flux Assay Kit was lowered onto a pre-filled utility plate containing 200 µL of sterile water. Lastly, the assembled sensor cartridge and utility plate were placed in a non-CO_2, properly humidified incubator overnight at 37°C.

The day of the assay: THP-1 monocytes and macrophages were stimulated for 6 h with

the corresponding cytokines to induce M1-like and M2-like phenotypes in the presence or absence of Mdivi-1 as described in section 3.2.3.3, together with control cells (DMSO). After stimulation, cells were washed with PSB and 180 µL of freshly prepared XF seahorse assay media was added. The assay media containing HEPES (5,5mM) was supplemented with glucose (5.5 mM), glutamine (2 mM), and sodium pyruvate (1 mM) and pH was adjusted to 7.4. Next, the cell plate was placed in non-CO_2 37°C incubator for 1 h.

Seahorse XF Calibrant solution and assembled sensor cartridge with utility plate incubated overnight, were removed from the non-CO2 incubator. The water was discard from the utility plate and 200 µL of pre-warmed XF calibrant solution was added. The sensor cartridge was lowered again into the utility plate and placed back into the non-CO_2 incubator at 37°C for 1 h.

During this 60 min incubation, the injection ports of the sensor cartridge were loaded with the different mitochondrial respiration modulators contained in the XFe96 Extracellular Flux Assay Kit (Seahorse biosciences). Optimal concentrations for each of these agents were determined, and the final conditions used for the experiments are reflected in **Table 3.4**

Table 3.4. Compound preparation for loading to XF96 sensor cartridges

Mitochondria modulators	Stock [µM]	Loaded volume (µl)	Final well [µM]	Final well (µl)
Port A: **Oligomycin**	10	20	1	200
Port B: **FCCP**	11	20	1	220
Port C: **Rotenone/Antimycin A**	12	20	1	240

Following 1 h incubation, the calibration plate with the loaded sensor cartridge were removed from the non-CO_2 incubator and placed into the instrument tray to start calibration. When finished, the calibration plate was replaced by the cell culture microplate and the measure was started.

For OCR determination, measured parameters were as follows: baseline, 3 cycles; inject port A (oligomycin), 3 cycles; inject port B (FCCP), 3 cycles; inject port C (Rotenone/antimycin A), 3 cycles. Each cycle was composed of mix 3 min, wait 0 min, and

measure 3 min. Three consecutive measurements under each condition were subsequently averaged and used for analysis.

When the measure was finalized, protein determination from each of the plate wells was performed using BCA protein determination assay and the normalization values obtained were used in the subsequent metabolic parameters analysis.

3.2.14.4 Determination of metabolic parameters

When the assay is finished, the result shows the Oxygen Consumption Rate (OCR) data in rate mode (**Figure 3.9**). Analysis was performed as previous described (Divakaruni et al., 2014). It started with the measure of the base level of OCR, and after injection of the ATP synthase inhibitor oligomycin, the OCR rapidly decreased. This effect was reversed by the addition of FCCP, an uncoupling agent that can dissipate the proton gradient and maximize the OCR. And finally, after the injection of a mixture of Rotenone/antimycin A, the OCR drop-down again. Six different parameters were calculated using seahorse wave software, including ATP-linked respiration, proton leak, basal respiration, maximal respiration, and spare respiratory capacity (**Figure 3.9**).

Basal respiration reflects the energetic demand of cells under basal conditions, the oxygen consumed during basal respiration is used to meet ATP synthesis which leads to mitochondrial proton leak. The ATP-linked respiration is shown by the reduction in OCR following the injection of oligomycin, which is a percentage of basal respiration. Proton leak corresponds to the remaining basal respiration not linked to ATP synthesis after oligomycin injection and is used as an indicator of mitochondrial damage. Maximal respiration denotes the maximum capacity that the electron respiratory chain can accomplish and is measured by injection of FCCP. Spare respiration is calculated by the difference between maximal and basal respiration, and it shows how capable are the cells to respond to changes in energy demand, indicating the fitness of the cells. Lastly, Non-mitochondrial respiration is the oxygen consumption taking place in the cell that is linked to cellular enzymes other than mitochondria followed by the injection of rotenone and antimycin A (**Figure 3.9**).

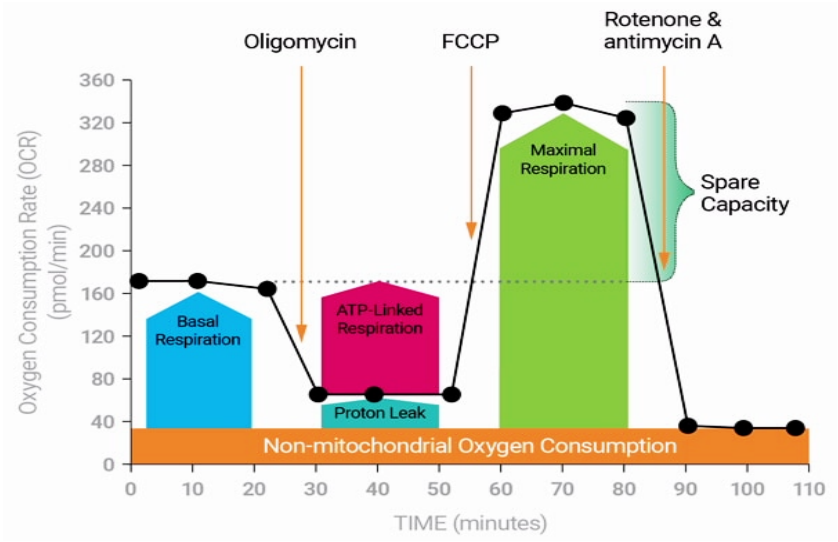

Figure 3.9 Mito Stress Test Assay used to determine the cellular mitochondrial function. Seahorse XF Cell Mito Stress Test profile illustrated the key parameters of mitochondrial function namely basal respiration, ATP production, proton leak, maximal respiration, and spare respiratory capacity.

3.2.15 Western blot analysis

3.2.15.1 Sample lysis and protein quantification

Cell pellets from THP-1 cells under different conditions were lysed using cold 80-100 µL of RIPA buffer (Thermo Fisher Scientific) supplemented with Halt TM protease and phosphatase inhibitor cocktail (ThermoFisher Scientific) in a final concentration of 3X. After lysate formation by pipetting mixing, samples were then subjected to 3 cycles of 5 sec of sonication on ice to ensure complete breakdown of the cell pellet material. From each sample, a 1:4 dilution was made using the same prepared RIPA buffer and then subjected to a Bicinchoninic acid (BCA) protein assay determination (ThermoFisher Scientific), according to the manufacturer's instruction. The standard curve was prepared using the same supplement diluent as the samples.

Samples were adjusted to the same concentration and volume using 4X Laemmli sample buffer (Bio-Rad), 2-mercaptoethanol (Sigma), and lysis buffer, and incubated at 95°C for 5 min in a heat block and immediately transferred to ice for 10 min.

3.2.15.2 SDS-PAGE - Transfer and immunolabelling

Resolving and staking gels were prepared as per **Table 3.5**. All reagents used were purchased from Bio-Rad. Twenty µg per lane of total protein and molecular weight ladder were submitted to a SDS–polyacrylamide gel electrophoresis run as follow: 90V for 20 min to concentrate the samples at the bottom of the well in the stacking gel followed by 110V for 60 – 90 min. After the electrophoretic run was finished, samples were then transferred onto an

methanol-activated polyvinylidene difluoride (PVDF) membranes, using a semi-dry electrophoretic transfer system (Bio-Rad) for 20 – 25 min at 25V with 1A.

Membranes were then blocked with 5% blotting grade milk (Bio-Rad) in TBS-T (50 mM Tris-HCl, 150 mM NaCl, 0.1% Tween 20, pH 7.6) for 4 h at RT. Primary antibodies against Drp1 (total and phosphorylated) and glycerinaldehyd-3-phosphat-dehydrogenase were purchased from Cell Signaling Technology and incubated overnight at 4°C under shaking conditions. All the antibodies were used at 1:1,000 dilution. After overnight incubation, membranes were washed 3X with TBS-T at RT for 10 min, and incubated with secondary antibodies coupled to alkaline phosphatase (Cell Signaling Technology) for 2 h at RT. After washing the membranes, the signal-fire alkaline phosphatase substrate (Cell Signaling Technology) was used for detection according to the manufacturer's instructions. The protein bands were visualized by exposing the membranes to a ChemiDoc TM XRS system (Bio-Rad), and blot bands were quantified using Image Lab software.

Table 3.5. Resolving and Staking gel composition for SDS-PAGE.

Resolving Gel		**Staking Gel**	
Reagent	**Volume**	**Reagent**	**Volume**
H_20	3.29mL	H_20	2.827 mL
Tris-HCl 1,5M pH=8,8	2.5mL	Tris-HCl 1,5M pH=8,8	1.25 mL
SDS 10%	100uL	SDS 10%	50 uL
Acrylamide – bis (30%)	4mL	Acrylamide – bis (30%)	833 uL
TEMED	10uL	TEMED	10 uL
APS (10%)	100uL	APS (10%)	30 uL
Total Vol	**10mL**	**Total Vol**	**5 mL**

3.2.16 Quantitative and semi-quantitative determination of cytokines

THP-1 conditioned medium from monocytes and macrophages were collected and filtered through 0.2 μm filter to remove any residual debris, and quantitative determination of TNF-α (Quantikine®, R&D Systems) and IL-6 (Thermo Fisher Scientific) was assessed by enzyme-linked immune-sorbent assay (ELISA) according to manufacturer's protocols. Absorbance values for individual reactions were determined using Microplate Reader (Molecular Devices) with SoftmaxPro 3.0 data processing software.

For semi-quantitative determination, cytokines, and chemokines in cell culture supernatants (filtered by 0.2 μm) from THP-1 monocytes and macrophages were determined using the human cytokine antibody array (Abcam) with 23 different anti-cytokine/chemokine

antibodies spotted in duplicate on a nitrocellulose membrane according to manufacturer's protocol. For the assay, 1.0 mL of conditioned media of the studied samples were incubated overnight at 4°C under shaking conditions, washed with the corresponding buffer, and signal were detected using ChemiDoc MP imaging system (Bio-Rad). The background membrane was assayed using 1 mL of culture media alone for signal normalization. Lastly, the protein Array Analyzer tool from ImageJ was used for quantification, background correction, and normalization of membrane signals as previously described (Keuper et al., 2017). The expression of cytokines/chemokines data was documented as their change in treated versus untreated (control) cells.

3.2.17 Cell cytotoxicity determination by LDH quantification

First, THP-1 cells were treated with 1% Triton X-100 (maximum LDH release or "high control"), with the different treatments used to induce M1-like and M2-like polarization in the presence or absence of Mdivi-1 (indicated as "experimental values") or cells kept untreated (spontaneous LDH release or "low control"). Secondly, THP-1 conditioned medium was collected and filtered through a 0.2-µm filter to remove any residual debris from the supernatant. Lastly, LDH release in the supernatant was assessed by LDH-release detection kit (Roche Diagnostics) according to the manufacturer's instructions using Microplate Reader (Tecan); values were normalized to the total amount of protein determined by BCA.

3.2.18 Confocal fluorescence microscopy and image analysis

To perform morphometric analysis of the mitochondria, control and stimulated THP-1 monocytes were seeded on poly-D-lysine coated glass-bottom dishes (Thermo). The coating protocol was the same as described in section 3.2.14.2. After seeding, cells were fixed with 4% PFA for 20 min at RT. Cells were washed with 2 ml of PBS to remove the fixation solution and subsequently permeabilized using 0.1% Triton X-100. After permeabilization, cells were blocked using with 5% BSA solution. To stain the mitochondria, an antibody recognizing COX-IV was used (1:250 dilution; Cell Signalling Technology) and incubated overnight at 4°C. The following day, cells were washed twice with PBS twice and stained with a 1:400 dilution of Alexa Fluor 488–conjugated secondary antibodies (Life Technologies) for 1 h at RT and counterstained with DAPI to visualize cell nuclei. After staining, cells were examined under Zeiss LSM710 confocal microscope (Carl Zeiss) and images from the different study groups were taken. For mitochondria morphometric assessment, blinded analysis was

performed by two independent researchers using an ImageJ workflow as previously described (Valente, Maddalena, Robb, Moradi, & Stuart, 2017).

3.2.19 Statistics

Data were analysed by ANOVA analysis of variance followed by Bonferroni's multiple comparisons test, when appropriate and paired and unpaired Student's *t*-test when analyzing two groups to determine the statistical significance of the differences using GraphPad Prism version 9.0 for Mac OS X, GraphPad Software, La Jolla California U.S.A. (www.graphpad.com). Significance values are *P<0.05, **P<0.01, ***P<0.001 and ns for non-significant (p>0.05).

4. RESULTS

4.1 Mdivi-1 treatment in a preclinical wire-induced vascular injury model reduced post-injury neointimal hyperplasia and plaque complexity.

It has been described that Drp1 is expressed in atherosclerotic plaques from human carotid arteries (Rogers et al., 2017) and that mitochondrial dynamics modulate cell metabolism, inflammatory-cell polarization status and chemotaxis (Campello et al., 2006; L. Wang et al., 2015). The aim of the present study was to investigate whether the pharmacological inhibition of mitochondrial fission, using Mdivi-1, could prevent neointima formation in a wire injury model of vascular restenosis.

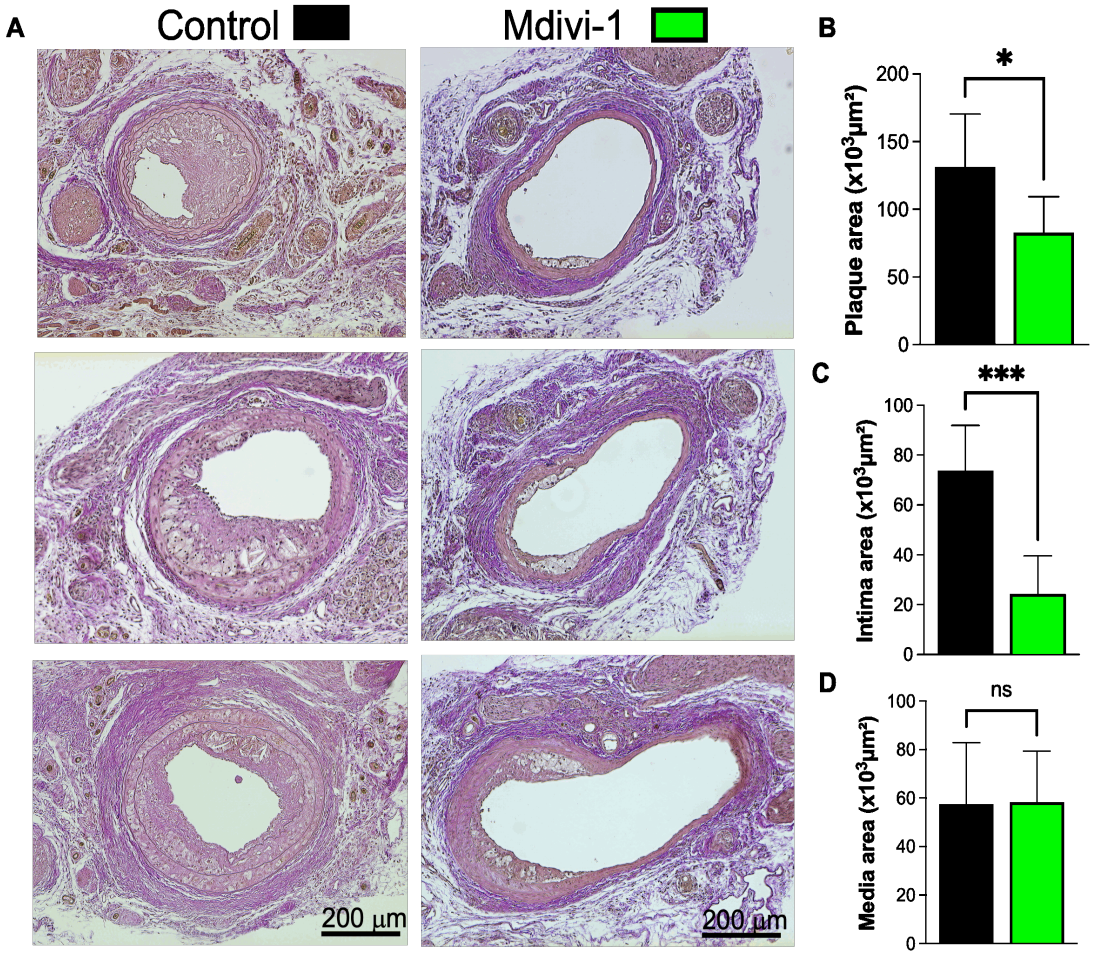

Figure 4.1. **Mdivi-1 treatment inhibited neointimal hyperplasia in a wire-induced vascular injury model**. Male *Apoe*-/- mice were fed a high-fat diet, treated with vehicle (DMSO) or Mdivi-1 and subjected to wire-induced injury of the common carotid artery. (A) Representative photomicrographs of Pentachrome-stained sections 2 weeks after injury in the presence or absence of Mdivi-1 treatment. Compared to control, treatment with Mdivi-1: (B) reduced plaque area; (C) decreased neointima area; (D) had no effect on media area. Groups are abbreviated as $Apoe^{-/-}$ mice (Control); $Apoe^{-/-}$ mice treated with Mdivi-1 (Mdivi-1). Values represent mean±SEM (n=6 mice per group). *P* values (*P<0.05, ***P<0.001) were assessed using Student *t* tests.

The data showed that compared to control, treatment with Mdivi-1 reduced neointimal thickness (Mdivi-1: 24.4±6.2x10^3 μm^2; Control: 73.9±7.4x10^3 μm^2, n=6; *P*=0.0004) and decreased plaque areas (Mdivi-1: 82.7±10.9x10^3 μm^2; Control: 131.5±15.9x10^3 μm^2, n=6; *P*=0.03) (**Figure 4.1A-C**), whereas tunica medial areas remained unchanged in the mouse carotid artery (**Figure 4.1D**).

Knowing that the tunica intimal hyperplasia after the vessel injury is accompanied by an increase of cellularity in the vascular lesion, the next step was to assess the influence of Mdivi-1 treatment on cellular plaque composition in the described *in vivo* model. Following vascular injury, treatment with Mdivi-1 lowered the cell numbers in the plaques in the carotid artery when compared to control (Mdivi-1: 147.1±25.8 cells/plaque; Control: 438.2±45.0 cells/plaque, n=6; *P*=0.0247; **Figure 4.2A**). Additionally, vascular smooth muscle (SMA^+) cell numbers (Mdivi-1: 35.6±5.6 cells/plaque; Control: 54.2±6.3 cells/plaque, n=6; *P*=0.0372; **Figure 4.2B**) as well as macrophage ($MAC\text{-}2^+$) cell numbers (Mdivi-1: 42.5±8.3 cells/plaque; Control: 127.5±16.8 cells/plaque, n=6; *P*=0.0042; **Figure 4.2C**) were significantly decreased in the vascular lesions of Mdivi-1-treated mice compared to control. However, no significant differences in plaque endothelial cell numbers ($CD31^+$) were observed between treatment groups (**Figure 4.2D**).

Together, these data show that *in vivo* administration of Mdivi-1 inhibited post-injury neointimal hyperplasia and reduced plaque cell infiltration by lowering the numbers of VSMCs and macrophages following vascular injury in the mouse carotid artery.

4.2 Mdivi-1 reduced the migration and motility of human monocytes.

Despite the different potential sources of macrophages that can be found in the vessel plaque, monocyte-derived macrophages are considered to be the predominant population in atherosclerosis plaque development (von Ehr, Bode, & Hilgendorf, 2022). Since a reduced number of macrophages were found in plaques-arteries of mice treated with Mdivi-1 compared to control, the next question to be addressed was whether Mdivi-1 was being capable of modulating the migration of monocytes, leading to a decrease in plaque-macrophages. To achieve this, a 3D chemotaxis assay, (i.e. mimicking a physiological setting) and the Boyden chamber assay were applied, using MCP-1 or M-CSF as chemo-attractants.

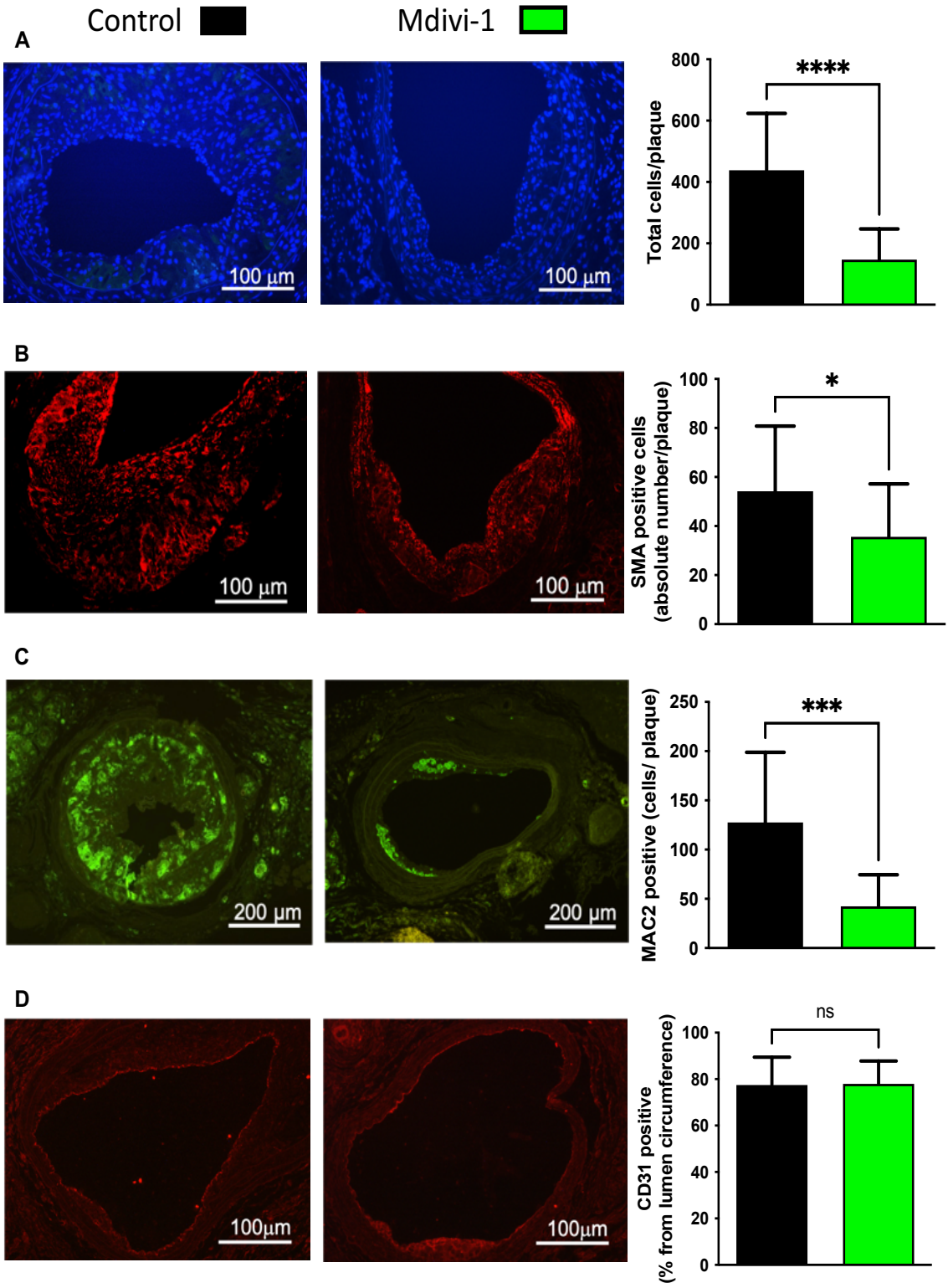

Figure 4.2: Mdivi-1 treatment reduced plaque cellular complexity in a wire-induced vascular injury model
Male *Apoe*$^{-/-}$ mice were fed a high-fat diet, treated with vehicle (DMSO) or Mdivi-1 and subjected to wire-induced injury of the common carotid artery. Compared to control, treatment with Mdivi-1: (**A**) reduced the total number of plaque cells (DAPI); (**B**) decreased the number of plaque smooth muscle cells (SMA^{+}); (**C**) lowered the number of plaque macrophages (MAC2^{+}) per plaque; (**D**) had no effect on the total number of plaque endothelial cells (CD31^{+}). Groups are abbreviated as *Apoe*$^{-/-}$ mice (Control); *Apoe*$^{-/-}$ mice treated with Mdivi-1 (Mdivi-1). Values represent mean±SEM (n=6 per group). *P* values (*P* values *P<0.05, **P<0.01, ***P<0.001, ****P<0.0001) were assessed using Student *t* tests.

The optimal concentration of MCP-1 for these assays was determined by the Boyden chamber assay. Three different concentrations (ng/mL) of the chemokine were used: 50, 75, and 100 (**Figure 4.3A**). The results showed a dose-response effect of MCP-1 on human monocyte migration, being 100 ng/mL the most effective in promoting cell movement toward the chemoattractant (**Figure 4.3A, C, D**). No changes in cell viability were seen with any of the MCP-1 concentrations used (**Figure 4.3B**).

First, migration of primary human monocytes was performed using the Boyden chamber assay. Results revealed a trend in the Mdivi-1 group to reduce cell migration towards the MCP-1 gradient, but no significant differences were found when compared to the control with no changes in cell viability by trypan blue (**Figure 4.4A, B**).

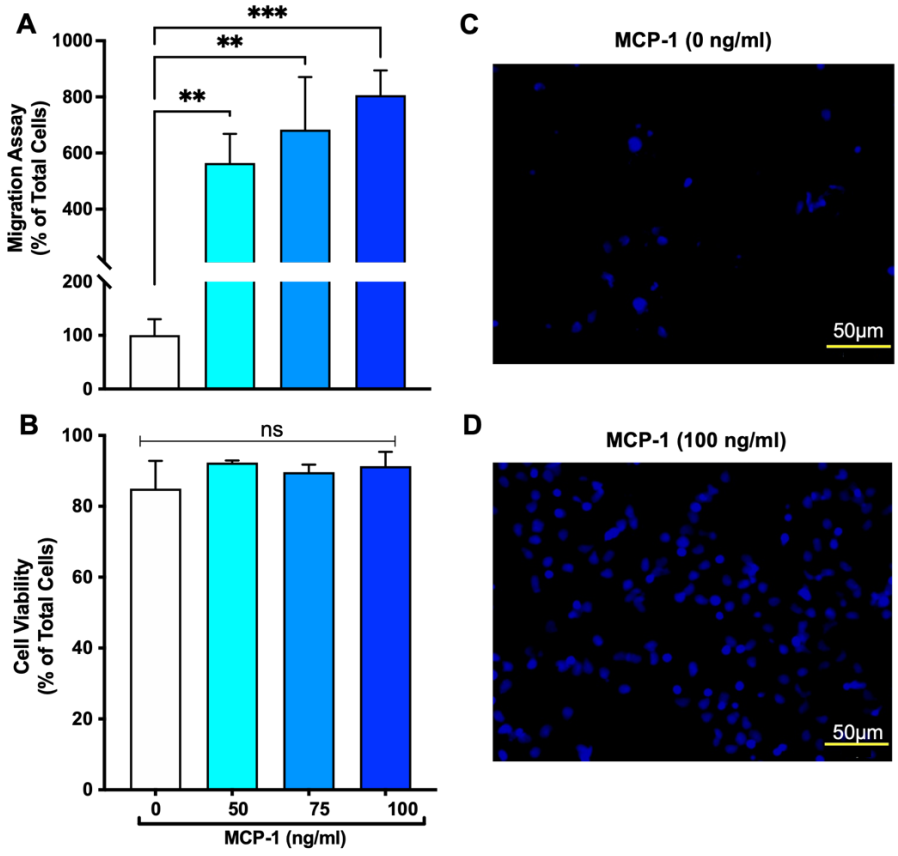

Figure 4.3: Mdivi-1 treatment reduced migration and motility of primary human monocytes in response to MCP-1. Multiple migration tracks of individual human monocytes using 3D chemotaxis assay in response to MCP-1 gradient (100ng/ml). The starting points of the cell tracks were set to the same origin (start point x = 0 and y=0). Compared to control (A), cells respond to MCP-1 gradient showing a homogenous directional migration (B). In the presence of Mdivi-1 (10µM) cells showed a deficiency in sustaining the directionality of the movement (C), whereas 50µM of Mdivi-1 fully abrogated the migration behaviour of monocytes towards MCP-1 gradient (D). Values represent mean±SD. *P* values ***P<0.001, ****P<0.0001, ns= not significant.

Secondly, given the trend to reduce cell migration with Mdivi-1 using the Boyden chamber assay and to further explore the migration behaviour in a more physiological setting,

primary human monocytes were then subjected to a 3D chemotaxis assay. The results showed that cells responded to the MCP-1 gradient showing a homogenous directional migration (**Figure 4.5B**), compared to the buffer control group (**Figure 4.5A**). The treatment with a low concentration of Mdivi-1 (10 μM) reduced the directionality of the cell movement, whereas a high concentration (50 μM) of Mdivi-1 fully abrogated the migration behaviour of monocytes towards the MCP-1 gradient (**Figure 4.5C, D**).

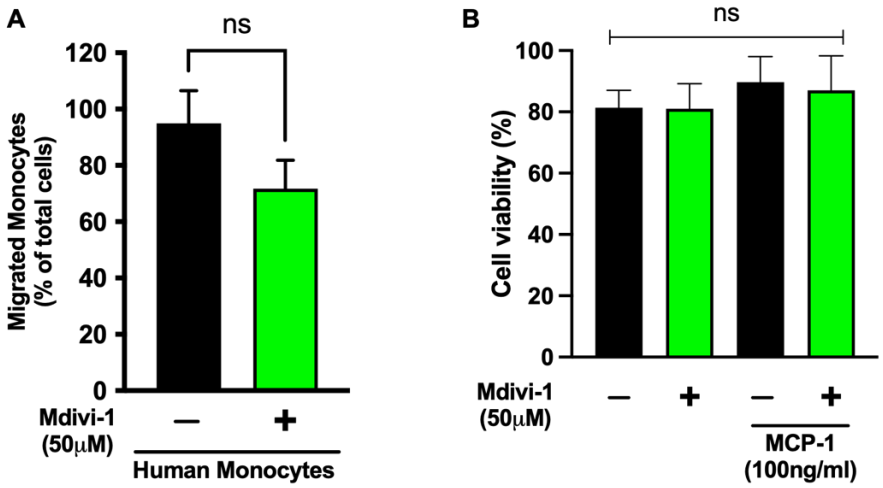

Figure 4.4: Mdivi-1 treatment has trend to inhibit human monocyte migration in response to MCP-1 in a 2D migration assay. Primary human monocytes were subjected to transwell migration assays in the presence or absence of Mdivi-1, a trend of lowering the number of monocytes migrated to the chemoattractant MCP-1 transmigrated was seen (A) and such effect did not result from increased cell death (B). *P* values (*P* values *P<0.05, **P<0.01; ns = not significant) were assessed using Student *t* tests.

To exclude the possibility of random migration and ensure that cell movement complied with the criteria for a directed/chemotactic cell migration, six different parameters were checked. First, the forward migration index (FMI) both, perpendicular (**Figure 4.6A**) and parallel (**Figure 4.6B**) to the chemoattractant was assessed with or without Mdivi-1.

As expected, no differences were found in FMI perpendicular to MCP-1, excluding the possibility of biased migration by non-chemotactic environmental factors. However, FMI parallel to chemoattractant was increased compared to control, and treatment with both concentrations of Mdivi-1 abolished the effect of MCP-1 (**Figure 4.6A, B; Table 4.1**).

Next, the influence of Mdivi-1 on chemotaxis velocity was studied, in which MCP-1 induced a significant increase in cell velocity compared to the control and treatment with Mdivi-1 at 50 μM abrogated these effects, while a concentration of 10 μM had no impact on cell velocity in the presence of the chemoattractant (**Figure 4.6C ; Table 4.1**). Additionally, the effect of Mdivi-1 on both accumulated distance and Euclidean distance was assessed in the

presence of MCP-1. The expected increase in accumulated distance, as well as the Euclidean distance induced by the chemoattractant were significantly attenuated by Mdivi-1 [50 µM] treatment, but not for Mdivi-1 [10 µM] (**Figure 4.6D, 4.6E; Table 4.1**).

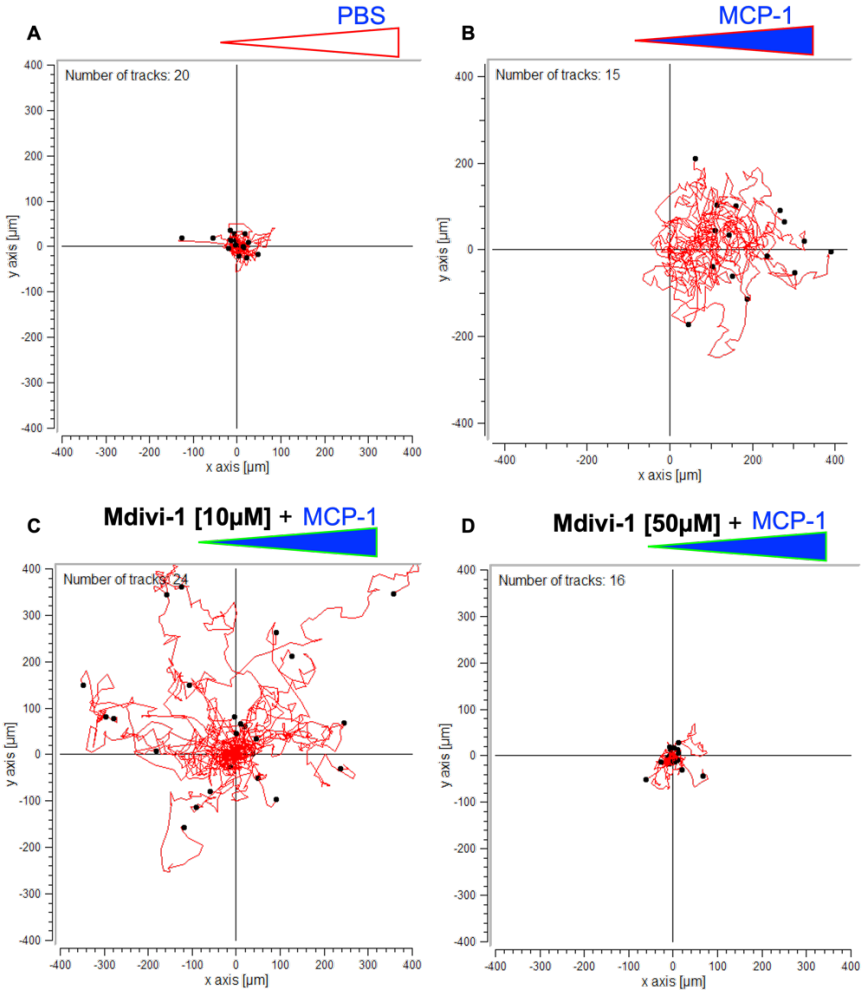

Figure 4.5: Mdivi-1 treatment reduced migration and motility of primary human monocytes in response to MCP-1. Multiple migration tracks of individual human monocytes using 3D chemotaxis assay in response to MCP-1 gradient (100ng/ml). The starting points of the cell tracks were set to the same origin (start point x = 0 and y=0). Compared to control (A), cells respond to MCP-1 gradient showing a homogenous directional migration (B). In the presence of Mdivi-1 (10µM) cells showed a deficiency in sustaining the directionality of the movement (C), whereas 50µM of Mdivi-1 fully abrogated the migration behaviour of monocytes towards MCP-1 gradient (D).

When assessing the Centre of Mass (COM), a displacement towards the MCP-1-treated group compared to the control was noted (**Figure 4.6F**), indicating that these cells primarily travelled in the direction of the chemoattractant. However, in the presence of Mdivi-1, this directional movement was abolished.

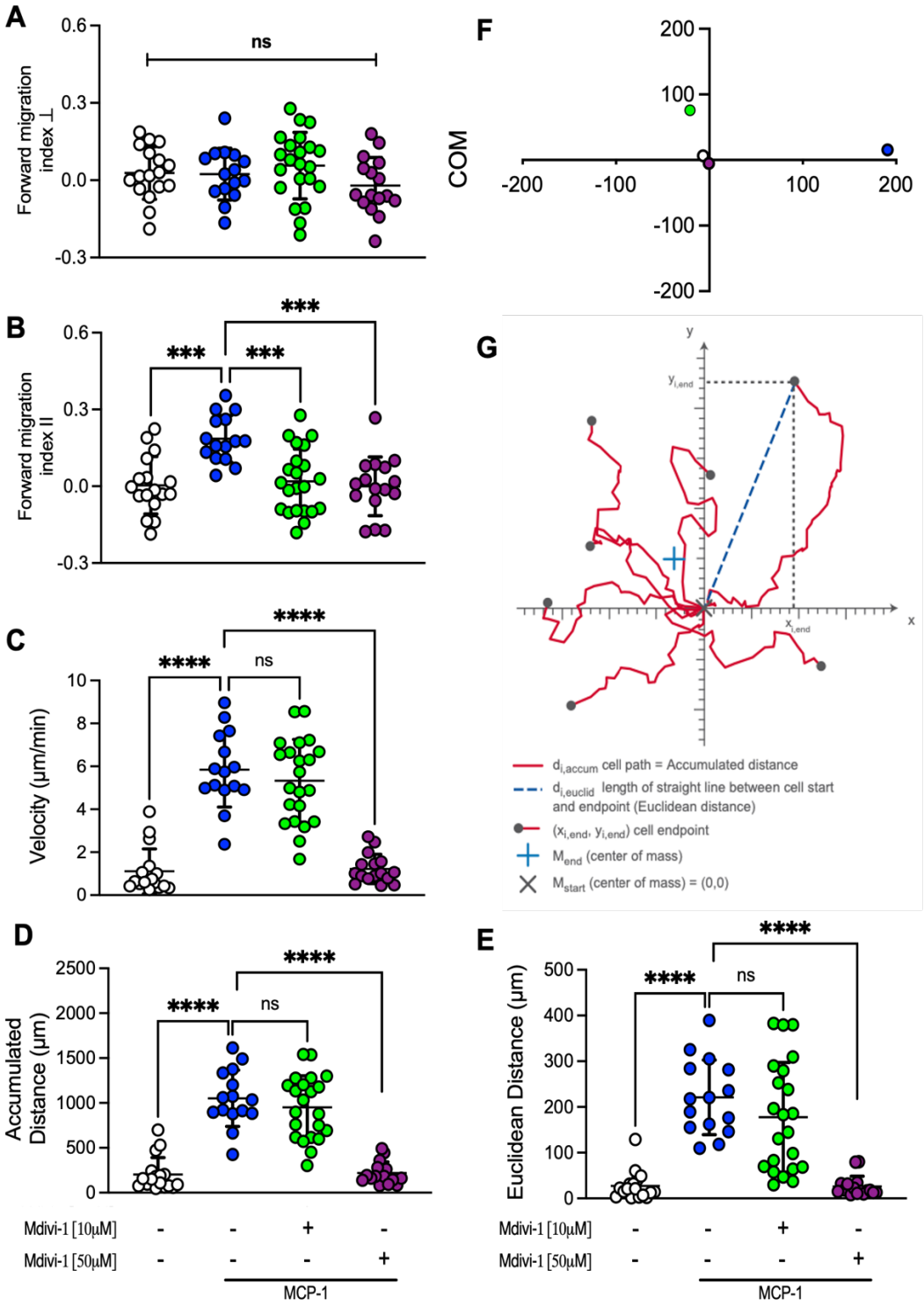

Figure 4.6: Mdivi-1 treatment reduced migration-associated parameter of primary human monocytes in response to MCP-1. (A) Forward migration index perpendicular to chemoattractant showed no effect of MCP-1 or Mdivi-1 on monocyte migration. Compared to control, treatment of human monocytes with Mdivi-1 (50µM) significantly reduced chemotaxis-induced migration induced by MCP-1 as evidenced by (B) Forward migration index parallel to chemoattractant, (C) cell velocity, (D) accumulated distance, (E) Euclidean distance, and (F) centre of mass (H). Diagrammatic representation of a trajectory plot (G) demonstrates methods for quantitating chemotactic and chemokinetic parameters. The diagram was captured from the Ibidi application Guide for Chemotaxis Assays (https://bit.ly/3e7KRJX). Values represent mean±SD. *P* values ***P<0.001, ****P<0.0001, ns= not significant.

These results are consistent with the Rayleigh test p values (Control: p = 0.255, MCP-1: p = $1.41x10^{-6}$, Mdivi-1 [10 µM]: p = 0.191 and Mdivi-1 [50 µM]: p = 0.903), indicating that the distribution of the cell endpoints was only significantly inhomogeneous (i.e., distributed towards the chemoattractant) in the presence of MCP-1 alone.

Lastly, the efficacy of Mdivi-1 was determined in preventing monocyte migration in the presence of M-CSF (20 ng/mL) instead of MCP-1 as a chemoattractant, as this chemokine has been reported to accelerate neointimal formation in the early phase after vascular injury (Shiba et al., 2007) as well as to induce MCP-1 upregulation in endothelial cells and therefore promote monocyte-adhesion and migration (Frangogiannis et al., 2003; Shyy et al., 1993). The results showed that migration of LPS-activated and non-activated THP-1 monocytes towards M-CSF, were significantly decreased in the presence of Mdivi-1 (50 µM) when compared to the control group (**Figure 4.7A,B**). Again, the inhibitory effect was not a result of increased cell death in the Mdivi-1-treated group, as showed by the trypan blue exclusion test (**Figure 7C**).

Table 4.1. Chemotaxis parameters of human monocytes in a 3D chemotaxis assay.

Parameters	Control	MCP-1	MCP-1 + Mdivi-1 [10 µM]	MCP-1 + Mdivi-1 [50 µM]
FMI – Parallel (to MCP-1)	$3.5x10^{-3}$±0.1	$1.85x10^{-1}$±0.09	$1.89x10^{-2}$±0.126	$-3.21x10^{-4}$±0.11
Velocity (µm/mim)	1.11±1.05	5.84±1.74	5.33±1.92	1.22±0.68
Accumulated distance (µm)	202.6±187.3	1052±313.2	951.7±350.9	219.3±122.9
Euclidean distance (µm)	27.35±31.19	221.0±81.77	177.6±119.9	26.11±22.41

Collectively, these data indicate that Mdivi-1 modulates monocyte recruitment and chemotaxis and may limit the cellular transmigration capacity. These results are correlated with the *in vivo* data, in which a reduced macrophage number in the post-injury plaque with Mdivi-1 treatment was found compared to the control.

4.3 Mdivi-1 treatment reduced post-injury inflammatory response *in vivo*

After finding that Mdivi-1 was able to modulate monocyte migration and potentially reduced the number of macrophages found in the plaque after vascular injury, the next step was to assess the efficiency of this molecule in modulating monocytes/macrophage pro-inflammatory response in this setting.

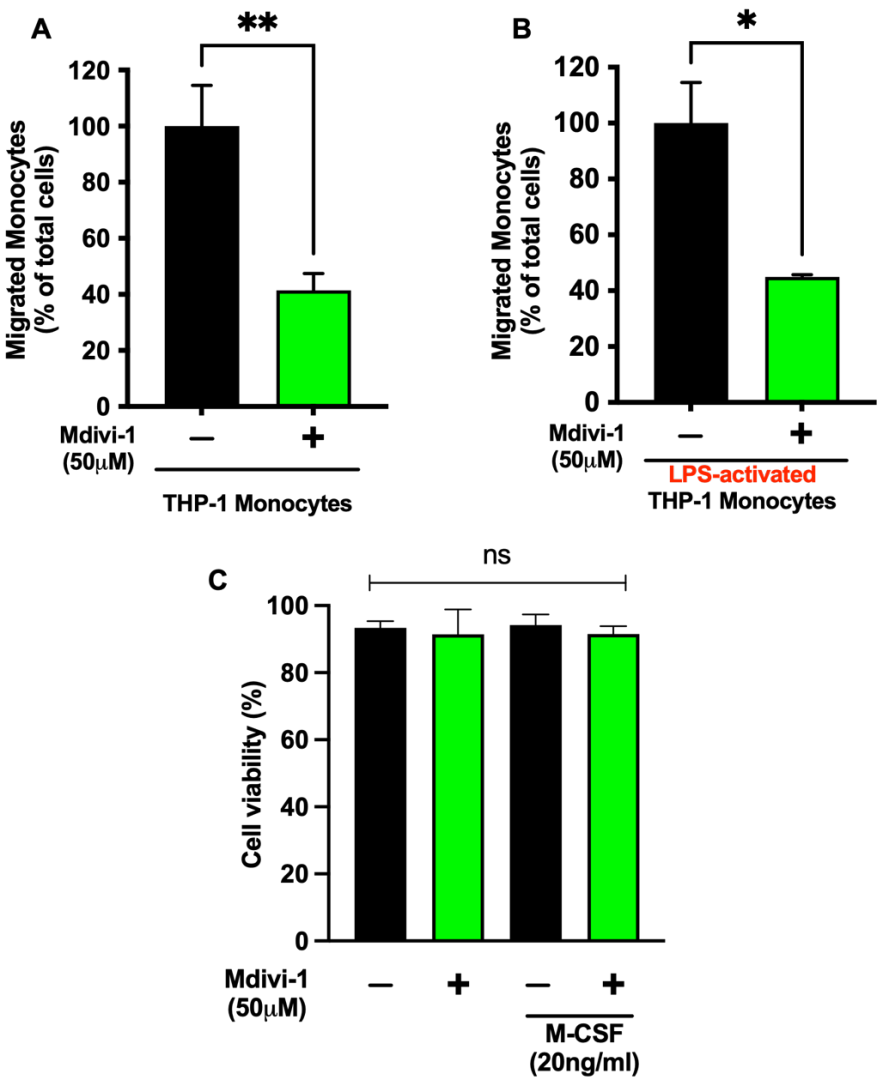

Figure 4.7: Mdivi-1 treatment reduced migration of THP-1 monocytes in response to M-CSF. Non-activated (A) and LPS-activated (B) THP-1 monocytes were subjected to transwell migration assays. In the presence of Mdivi-1, a significantly lower number of monocytes migrated to the chemoattractant M-CSF (macrophage colony-stimulating factor). The lower number of transmigrated monocytes did not result from increased cell death (C). *P* values (*P* values *P<0.05, **P<0.01, ns= not significant) were assessed using Student *t* tests.

The results showed that Mdivi-1 treatment was able to reduce inflammation *in vivo* at the site of injury compared to control, as evidenced by decreased plaque levels of the pro-inflammatory marker, TNF-α (Mdivi-1: 14.5±1.6 arbitrary units/μm^2; Control: 24.4±3.0 arbitrary units/μm^2, n=6; *P*=0.0226; **Figure 4.8A, B**). Additionally, reductions in response to treatment with Mdivi-1 were observed in levels of plaque-associated intercellular adhesion molecule-1 (ICAM-1), when compared to control (Mdivi-1: 20.4±4.0 arbitrary units/μm^2; Control: 34.6±4.1 arbitrary units/μm^2, n=6; *P*=0.0367; **Figure 4.8C, D**). These data show that *in vivo* administration of Mdivi-1 inhibited post-injury neointimal plaque inflammation in the mouse carotid artery.

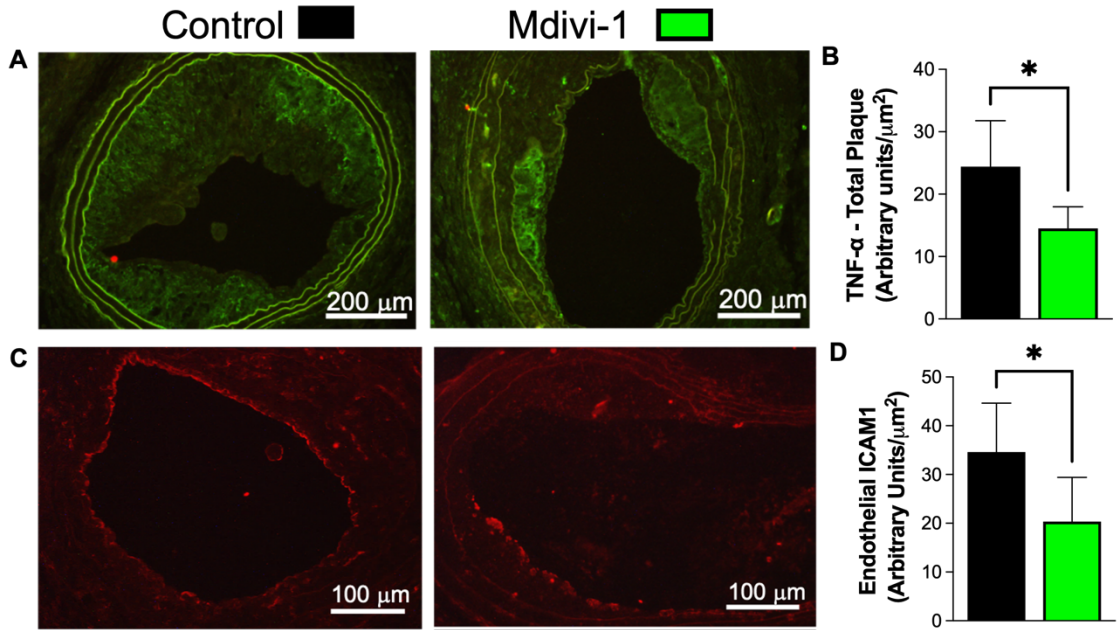

Figure 4.8. **Mdivi-1 treatment reduced plaque inflammation in a wire-induced vascular injury model**. Male *Apoe-/-* mice were fed a high-fat diet, treated with vehicle (DMSO) or Mdivi-1 and subjected to wire-induced injury of the common carotid artery. Representative immunofluorescence sections 2 weeks after injury in the presence or absence of Mdivi-1 treatment. Compared to control, (A,B) treatment with Mdivi-1: lowered levels of vascular inflammatory cytokine TNF (Tumor necrosis factor)-α levels (stained in green); and (C,D) significantly decreased endothelial adhesion molecule ICAM-1 (intercellular adhesion molecule 1) levels (stained in red). Groups are abbreviated as $Apoe^{-/-}$ mice (Control); $Apoe^{-/-}$ mice treated with Mdivi-1 (Mdivi-1). Values represent mean±SEM (n=6 mice per group). *P* values (*P<0.05, ***P<0.001) were assessed using Student *t* tests.

To further expand this anti-inflammatory behaviour seen *in vivo*, the *in vitro* effect of Mdivi-1 on gene expression was evaluated in both THP-1 monocytes and THP-1 derived macrophages under basal and pro-inflammatory settings. For this, the conditions to induce an M1 or M2-like phenotype were established: treatment of IL-4 was used to achieved M2-like phenotype, and for M1-like, treatment with LPS +IFN-γ or TNF-α were tested.

The upregulation of pro-inflammatory markers (MCP-1, IL-1β, MMP-1, ICAM-1 and CXCL-3) after LPS+IFN-γ treatment was greater than the one found after TNF-α stimulation in both THP-1 monocytes and THP-1-Macrophages. (**Figure 4.9A,B**). In the case of IL-14-treated cells, the target gene *CD206* was upregulated, indicating an M2-like phenotype in both cells populations (**Figure 4.9A,B**)

Having established the M1-like and M2-like polarization conditions, Mdivi-1 was tested to determine its effect on the polarization status of the cells. Under basal conditions after Mdivi-1 treatment, both cell populations showed an upregulation of the anti-inflammatory marker *CD206* with no changes in pro-inflammatory target genes (**Figure 4.10A, B**).

Conversely, after polarizing the cells towards an M1-like phenotype, the expression of *MCP*-1, *MMP*-1, and the adhesion molecule *ICAM-1* were significantly reduced in the presence of Mdivi-1 in both, monocytes (**Figure 4.10C**) and macrophages (**Figure 4.10D**). Additionally, LPS+IFN-γ-treated monocytes showed downregulation of IL-1β (Interleukin-1 β) and the chemokine (C-X-C motif) ligand 3 (CXCL3) in the presence of Mdivi-1 (**Figure 4.10C**), but no changes in these target genes were observed in THP-1 derived-macrophages (**Figure 4.10D**).

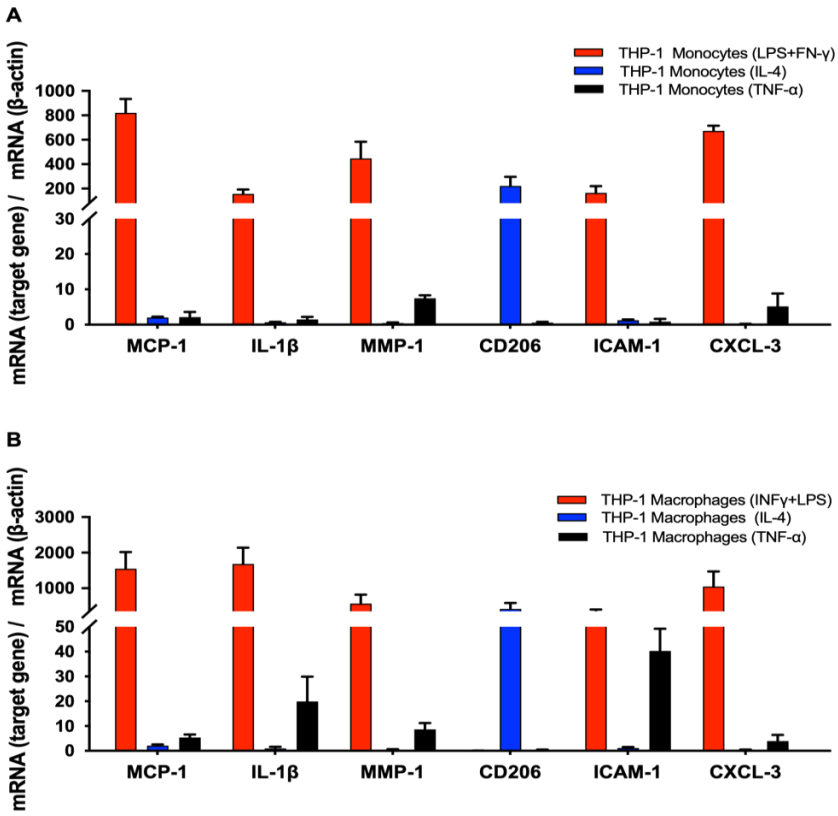

Figure 4.9: M1-like and M2-like profile of THP-1 monocytes and THP-1-derived macrophages. mRNA expression of *MCP-1, IL-1β, MMP-1, CD206, ICAM-1 and CXCL-3* was analysed by real-time PCR in THP-1 Monocytes (A) and THP-1-derived Macrophages (B) after treatment with LPS (100ng/mL)+IFN-γ (20ng/mL), TNF-α (50ng/mL) or IL-4 (20mg/mL) for 24h. Gene expression data are normalised to control cells (untreated) and displayed as fold changes between target gene expression and β-actin mRNA. Values represent mean±SD (n=3 per group in triplicates).

Lastly, a significant upregulation of *CD206* was observed in both cell populations (**Figure 4.10C, D**), indicating a switch from pro-inflammatory to an anti-inflammatory phenotype (M2-like polarization). These data demonstrate that Mdivi-1 can modulate the gene response of monocytes and macrophages when subjected to a pro-inflammatory stimulus.

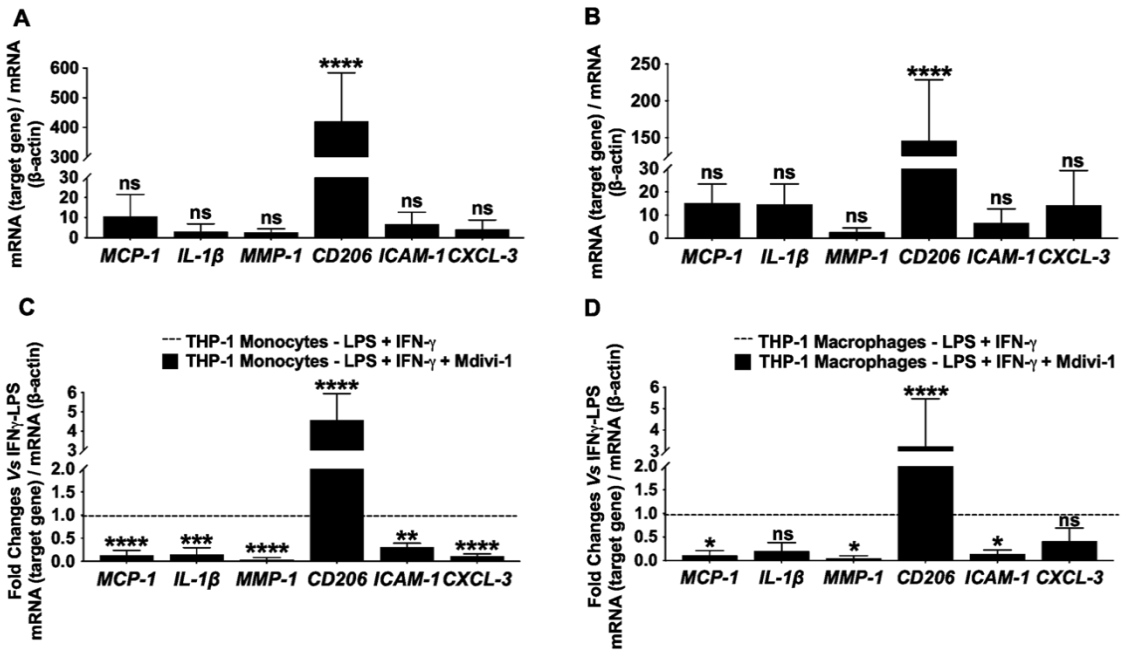

Figure 4.10: Mdivi-1 treatment attenuated pro-inflammatory gene expression THP-1 monocytes and Macrophages. mRNA expression of *MCP-1, IL-1β, MMP-1, CD206, ICAM-1 and CXCL-3* was analysed by real-time PCR in the absence or presence of Mdivi-1 (50μM) for 24 hours in THP-1 Monocytes (A) and THP-1-derived Macrophages (B). Same markers were assessed after treatment with LPS (100ng/mL) and IFN-γ (20ng/mL) (C,D). Gene expression data are normalised to that in the absence of Mdivi1 (dashed line) and displayed as fold changes between target gene expression and β-actin mRNA. Values represent mean±SD (n=3 per group in triplicates); *P<0.05, **P<0.01, ***P<0.001, ****P<0.0001 vs DMSO (A,B) or LPS+IFN-γ treated cells (C,D).

Due to the anti-inflammatory effects seen by Mdivi-1 on gene expression, the next step was to evaluate the LPS+IFN-γ-responsive protein levels in the presence or absence of this molecule. To achieve this, *in vitro* quantitative determinations were performed for the cytokines IL-6 and TNF-α after stimulating the cells for 6 h and 24 h. After M1-like polarization, both monocytes and macrophages released detectable levels of TNF-α (**Figure 4.11A**) and IL-6 (**Figure 4.11B**) compared to their corresponding control (unstimulated cells), in which cytokine levels were below the detection limit of the assay used. An enhanced response to LPS+IFN-γ treatment was observed in macrophages for both assayed cytokines (**Figure 4.11A, B**) compared to monocytes, indicating that THP-1-derived macrophages are more sensitive to pro-inflammatory stimulation.

Additionally, in M1 polarized cells, treatment with Mdivi-1 reduced IL-6 and TNF-α release in both, monocytes (**Figure 4.12A, B**) and macrophages (**Figure 4.12C**, **D**) after 6 h and 24 h of stimulation, implicating that Mdivi-1 can restrain the pro-inflammatory response in both cell populations.

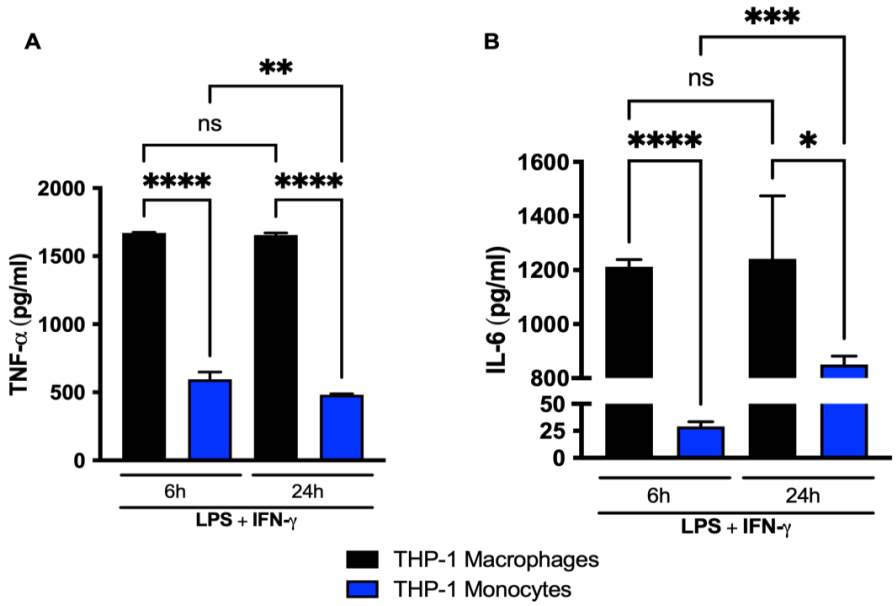

Figure 4.11: **Differential quantitative determinations of cytokines IL-6 and TNF-α in THP-1 monocytes and THP-1 derived macrophages**. ELISA assay was performed after stimulating the cells for 6h and 24h with LPS+IFN-γ. Controls cells (non-stimulated) are not displayed as the concentration of both cytokines was below the limits of detection. Cytokines concentrations are expressed as mean ± SD from three independent experiments. *P* values *P<0.05, **P<0.01, ***P<0.001, ****P<0.0001.

To broaden the panel of pro-inflammatory marker changes in the presence of Mdivi-1 (50 μM), a semi-quantitative determination using a protein profiler was assayed to compare the simultaneous release of 23 targets including both cytokines and chemokines (**Figure 4.13**). In the supernatants of THP-1 monocytes, stimulated *in vitro* for 24 h with buffer/control (**Figure 4.14A,B upper left panel**), Mdivi-1 (**Figure 4.14A,B upper right panel**), LPS+IFN-γ (**Figure 10A,B, lower left panel**), or LPS+IFN-γ+Mdivi-1 (**Figure 4.14A,B, lower right panel**), the readouts from densitometry scans were normalized using the intensity of positive control dots on the membrane corners (**Figure 4.13**) and plotted as relative fold-change of the untreated control (**Figure 4.14C**). The results revealed that the profile of the pro-inflammatory mediators (G-CSF; GRO-α, -β, -γ; IL-6; MCP-1,2; RANTES and TNF-α) released into monocyte cell culture supernatants in response to LPS+IFN-γ stimulation was reduced by Mdivi-1 treatment (**Figure 4.14C,D**).

Also, Mdivi-1 treatment significantly increased the level of IL-8 compared to control, and such changes induced by Mdivi-1 were not seen under inflammatory conditions (**Figure 4.14D**).

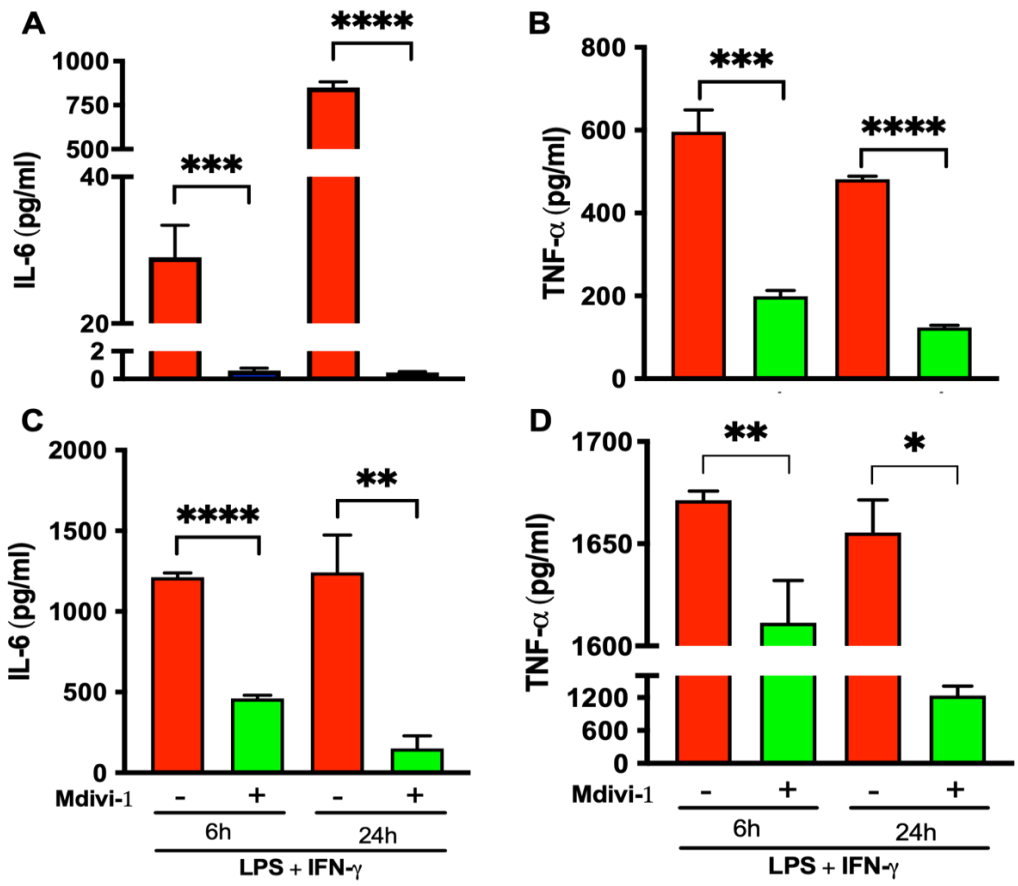

Figure 4.12: Mdivi-1 treatment reduced pro-inflammatory cytokines IL-6 and TNF-α in THP-1 monocytes and macrophages. Differential quantitative determinations of cytokines IL-6 and TNF-α in THP-1 monocytes (A,B) and THP-1 derived macrophages (C,D) by ELISA assay, after stimulating the cells for 6h and 24h with LPS+IFN-γ in the presence or absence of Mdivi-1. Controls cells (non-stimulated) are not displayed as the concentration of both cytokines was below the limits of detection. Cytokines concentrations are expressed as mean ± SD from three independent experiments. *P* values *P<0.05, **P<0.01, ***P<0.001, ****P<0.0001.

The same assay was performed in cell culture supernatants from THP-1-derived macrophages (**Figure 4.15A,B**) subjected to inflammatory stimulation (LPS+IFN-γ) treated or not with Mdivi-1. Similar to the monocyte's response, an anti-inflammatory effect of Mdivi-1 was found, in which the small molecule was able to reduce the pro-inflammatory mediators (G-CSF; GRO-α, -β, -γ; IL-6; MCP-1,2; RANTES and TNF-α) released into macrophage cell culture supernatants in response to LPS+IFN-γ stimulation (**Figure 4.15C,D**). Also, as in the monocytes, macrophage-related IL-8 secretion after Mdivi-1 treatment was increased when compared to control. However, unlike monocytes under inflammatory conditions, the IL-8 level was reduced in the presence of Mdivi-1 in these cells (**Figure 4.15D**).

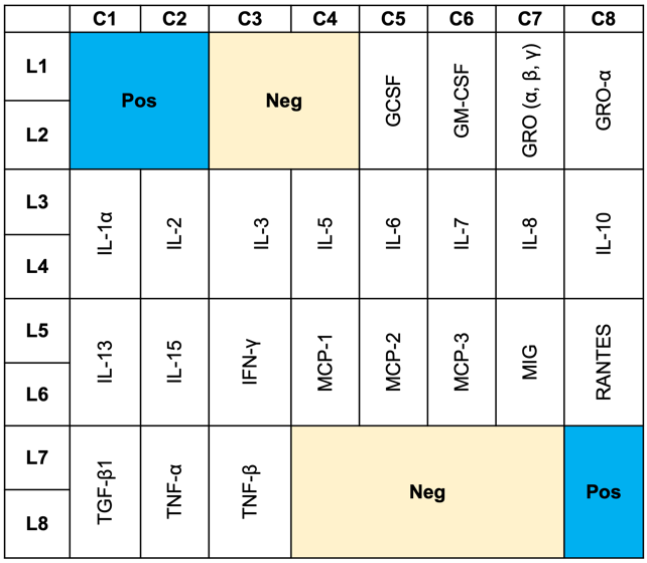

Figure 4.13: Human cytokine antibody array template. The array consisting of nitrocellulose-membrane allows the measurement of the relative abundance of 23 different targets, including cytokines and chemokines in duplicates. The membrane contains positive (pos) and negative (neg) internal controls to normalize the densitometry signals and know the array orientation.

To exclude the possibility that the anti-inflammatory effect of Mdivi-1 found in these cells was due to an increase in cell death, the release of LDH from both THP-1 monocytes and THP-1 macrophages was evaluated under all the studied conditions. As reported before (Genin, Clement, Fattaccioli, Raes, & Michiels, 2015), the treatment to induce cell polarization towards an M1-like phenotype showed an increase in LDH levels in these cells (**Figure 4.16A,B**), however, not significant differences were found between the group treated with LPS+IFN-γ alone and the treated Mdivi-1 under same inflammatory conditions (**Figure 4.16A,B**).

All these data provide evidence that Mdivi-1 reduces both expression and secretion of the inflammatory-cytokines and adhesion molecules involved in the inflammatory process of atherosclerosis development.

4.4 Mdivi-1 treatment decreased oxidative metabolism in monocytes/ macrophages.

As metabolic remodeling plays a key role in cell polarization, the next step was to determine whether Mdivi-1 could modulate monocyte and macrophage oxidative metabolism and impact on the cell polarization status towards the M1-like or M2-like phenotypes. The determination of bioenergetics parameters was accomplished by the sequential use of mitochondrial complex modulators (Divakaruni et al., 2014).

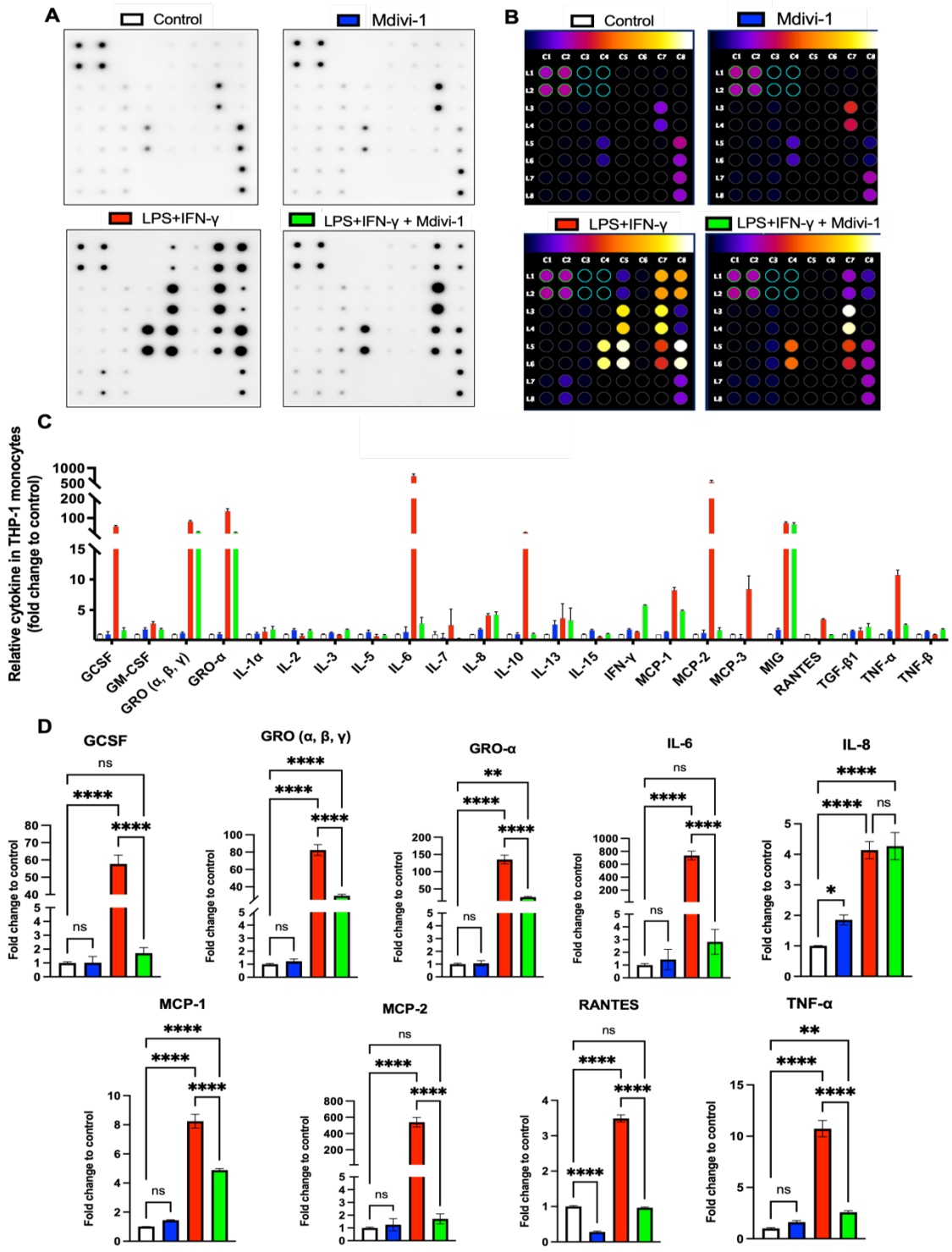

Figure 4.14: Mdivi-1 treatment reduced pro-inflammatory cytokines and chemokines in THP-1 monocytes. THP-1 monocytes were treated with LPS (100ng/mL) and IFN-γ (20ng/mL) and the relative abundance of 23 cytokines was analysed with a human cytokine antibody array. Representative membranes probed with supernatant from untreated (control) and LPS+IFN-γ treated THP-1 monocytes with or without Mdivi-1 are shown (A). Representative readouts of the protein Array Analyzer tool from ImageJ used for quantification, background correction and normalization of membrane signals (B). Quantitative signal intensity of all 23 targets (C) and some specific cytokines with statical significance (D) are documented and changes in cytokine levels are expressed as relative fold-change of the respective untreated control group (mean ± SD from three independent experiments). *P* values *P<0.05, **P<0.01, ***P<0.001, ****P<0.0001.

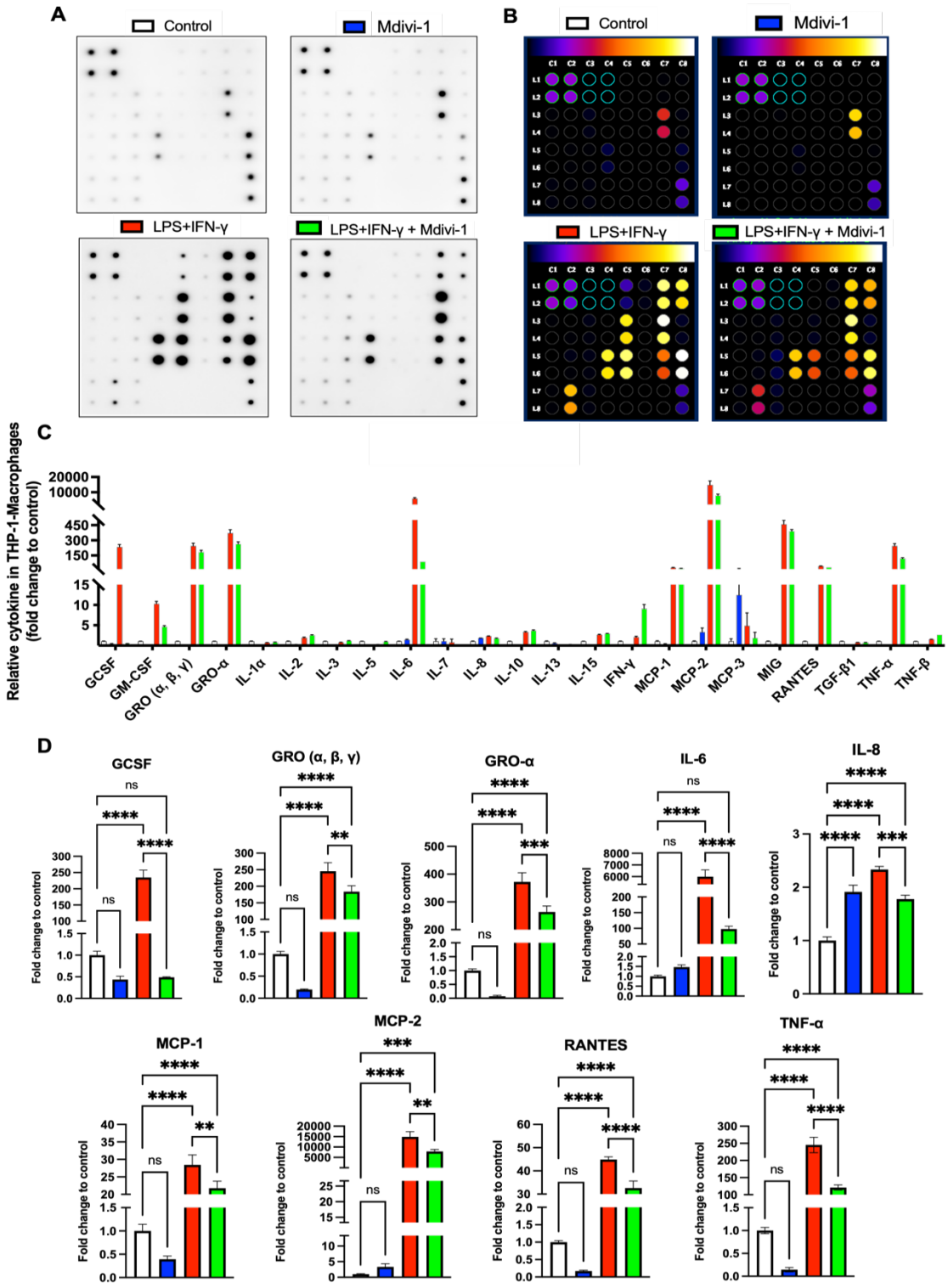

Figure 4.15: Mdivi-1 treatment reduced pro-inflammatory cytokines and chemokines in THP-1-derived macrophages. THP-1-derived macrophages were treated with LPS (100ng/mL) and IFN-γ (20ng/mL) and the relative abundance of 23 cytokines was analysed with a human cytokine antibody array. Representative membranes probed with supernatant from untreated (control) and LPS+IFN-γ treated THP-1 monocytes with or without Mdivi-1 are shown (A). Representative readouts of the protein Array Analyzer tool from ImageJ used for quantification, background correction and normalization of membrane signals (B). Quantitative signal intensity of all 23 targets (C) and some specific cytokines with statical significance (D) are documented and changes in cytokine levels are expressed as relative fold-change of the respective untreated control group (mean ± SD from three independent experiments). *P* values *P<0.05, **P<0.01, ***P<0.001, ****P<0.0001.

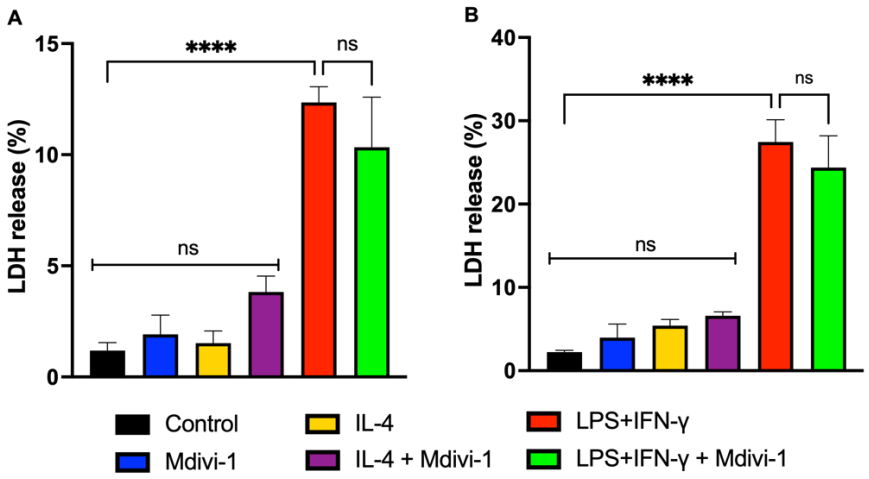

Figure 4.16: Cell death determination in THP-1 monocytes and THP-1 Macrophages. Release of LDH from THP-1 monocytes (A) and THP-1 derived macrophages (B) alone or after stimulating the cells for 24h, towards M1-like and M2-like phenotype in the presence or absence of Mdivi-1. Values represent mean ± SD from three independent experiments in triplicates. *P* values *P<0.05, **P<0.01, ***P<0.001, ****P<0.0001, ns=not significant.

First, the conditions to assess metabolic parameters were established by testing two different cell densities, and three different concentrations of the mitochondrial agents used to modulate the oxygen consumption on the seahorse assay (**Figure 4.17**). The recommended cell confluence in the cell microplate is 80 to 90% (Gu, Ma, Liu, & Wan, 2021) in a monolayer form.

No differences were seen when using 100,000 or 200,000 cells/well, however, by visual assessment, the density of 200,000 cells/well matched the recommended confluency (**Figure 4.17).** Additionally, the basal OCR was between the recommended range (20 and 200 pmol/O_2/min) (Underwood, Redell, Zhao, Moore, & Dash, 2020), ensuring that the OCR measures obtained are reliable and in this way minimize any potential floor and ceiling effect after drug injection.

When testing the mitochondrial modulators Oligomycin (**Figure 4.17A**), FCCP (**Figure 4.17B**) and rotenone/antimycin A (**Figure 4.17C**), at three different concentrations (1, 2.5 and 5 µM), no significant changes in OCR were seen. Therefore, the concentration of 1 µM was used for all these agents when testing the effect of Mdivi-1 in THP-1 cells under M1-like and M2-like polarization status.

After stablishing the conditions, the protocol consisted of one injection of Oligomycin after basal OCR measurement, followed by FCCP injection, and a final injection consisting of a combination of rotenone and antimycin A as previously described (Brand & Nicholls, 2011).

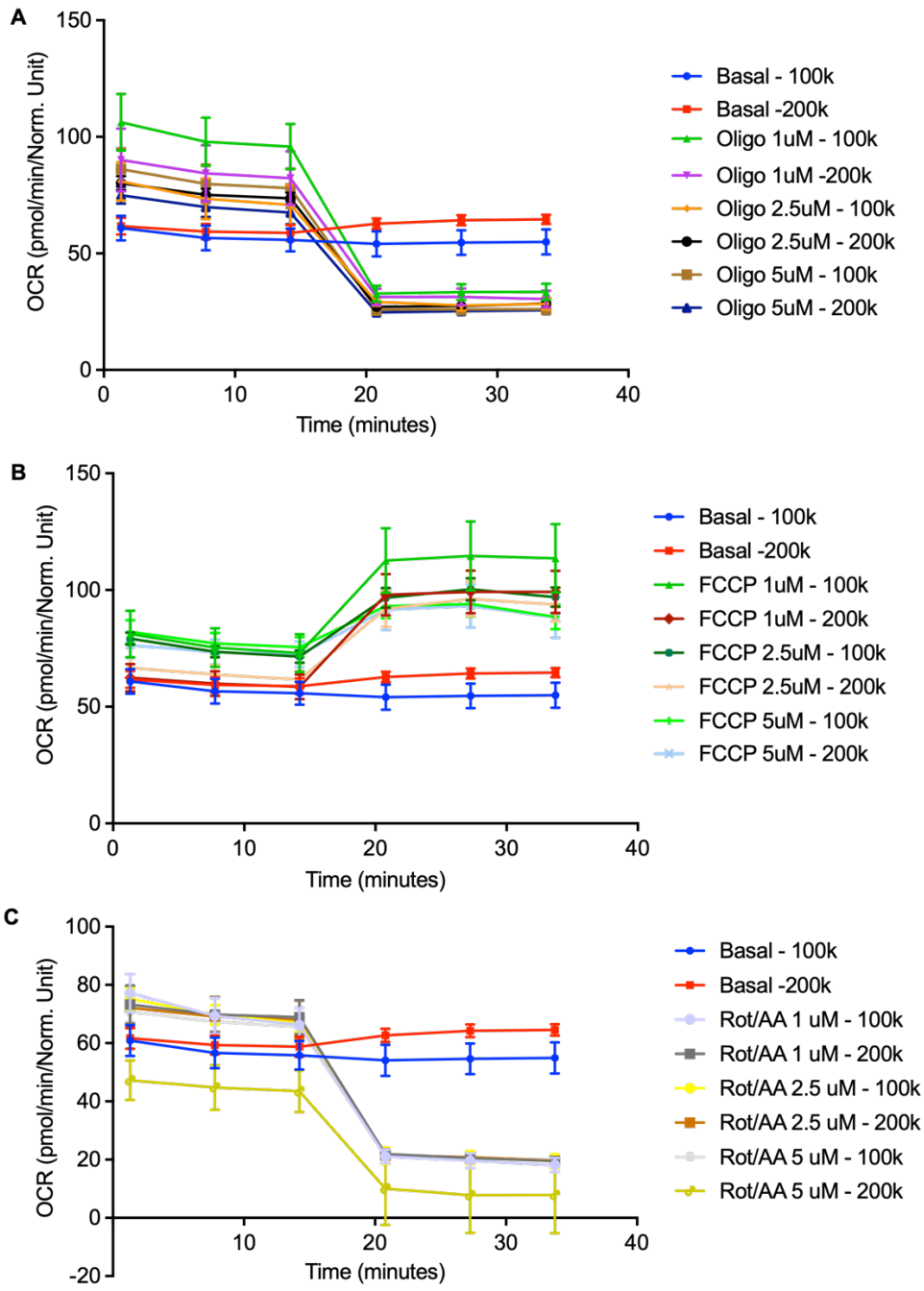

Figure 4.17: Seahorse Mito Stress assay optimization. Two different cells densities of THP-1 monocytes were seeded in the microplate seahorse assay. After basal OCR measure, cells were subjected to an injection of 3 different concentrations of oligomycin (A), FCCP (B) and antimycin A / rotenone (C), and changes in the oxygen consumption rate were monitored by the Seahorse XFe96 metabolic analyser. The optimal concentration for all the tested agents was 1µM. Results are presented as mean ± SD from three independent experiments performed in replicates of 15-20.

Both, M1-like (monocytes and macrophages) and M2-like (monocytes) polarized cells exhibited a higher basal OCR than unstimulated cells (DMSO), and this effect was abolished in the presence of Mdivi-1 (**Figure 4.18A,B; Figure 4.19.A,B**).

Moreover, maximal respiratory capacity (MRC) in LPS+IFN-γ (monocytes and macrophages) and IL-4 (macrophages)-treated cells was increased compared to unstimulated cells, but treatment with Mdivi-1 obliterated this response (**Figure 4.18C; Figure 4.19C**).

Similar findings were observed in M1-like (monocytes/macrophages) and M2-like cells (monocytes) treated with Mdivi-1 when assessing ATP-linked respiration (**Figure 4.18D; Figure 4.19D**).

Both, the reserve capacity (RC) and non-mitochondrial respiration (NMR) were increased in monocytes and macrophages treated with LPS+IFN-γ and such effects were inhibited by Mdivi-1 treatment. A similar observation was made in IL-4-treated macrophages in the presence of Mdivi-1 for both parameters (RC and NMR), and only a reduced OCR was seen on the IL-4-treated monocytes when assessing NMR but no changes in RC (**Figure 4.18E,F; Figure 4.19E,F**). Lastly, both M1-like and M2-like monocytes had a superior proton leak than unstimulated cells (DMSO), and this effect was abolished in the presence of Mdivi-1 (**Figure 4.18G**). No changes in proton leak were seen in macrophages (**Figure 4.19G**).

Taken together, these findings indicate that Mdivi-1 treatment reduced metabolic activity and oxidative capacity in both monocytes and macrophages.

4.5 Mdivi-1 reduced oxidative metabolism in THP-1 cells independent of Drp-1.

To investigate the role of mitochondrial dynamics in the observed metabolic effects of Mdivi-1, mitochondrial morphology assessment was performed in THP-1 monocytes under basal conditions and following treatment with LPS+IFN-γ / IL-4 in the presence or absence of Mdivi-1 (50 μM). Results showed not significant differences in mitochondrial morphology following treatment with Mdivi-1 in any of the studied groups when compared to control (**Figure 4.20A,B**).

To further confirm the observations seen on the mitochondria morphometric analysis, western blot analysis was performed in THP-1 cells, assessing the levels of total Drp1, as well as the phosphorylation levels of this protein at the two main sites, Ser616 and Ser637. No significant changes were seen in LPS+IFN-γ-treated monocytes in the presence or absence of Mdivi-1 (**Figure 4.21A,B**).

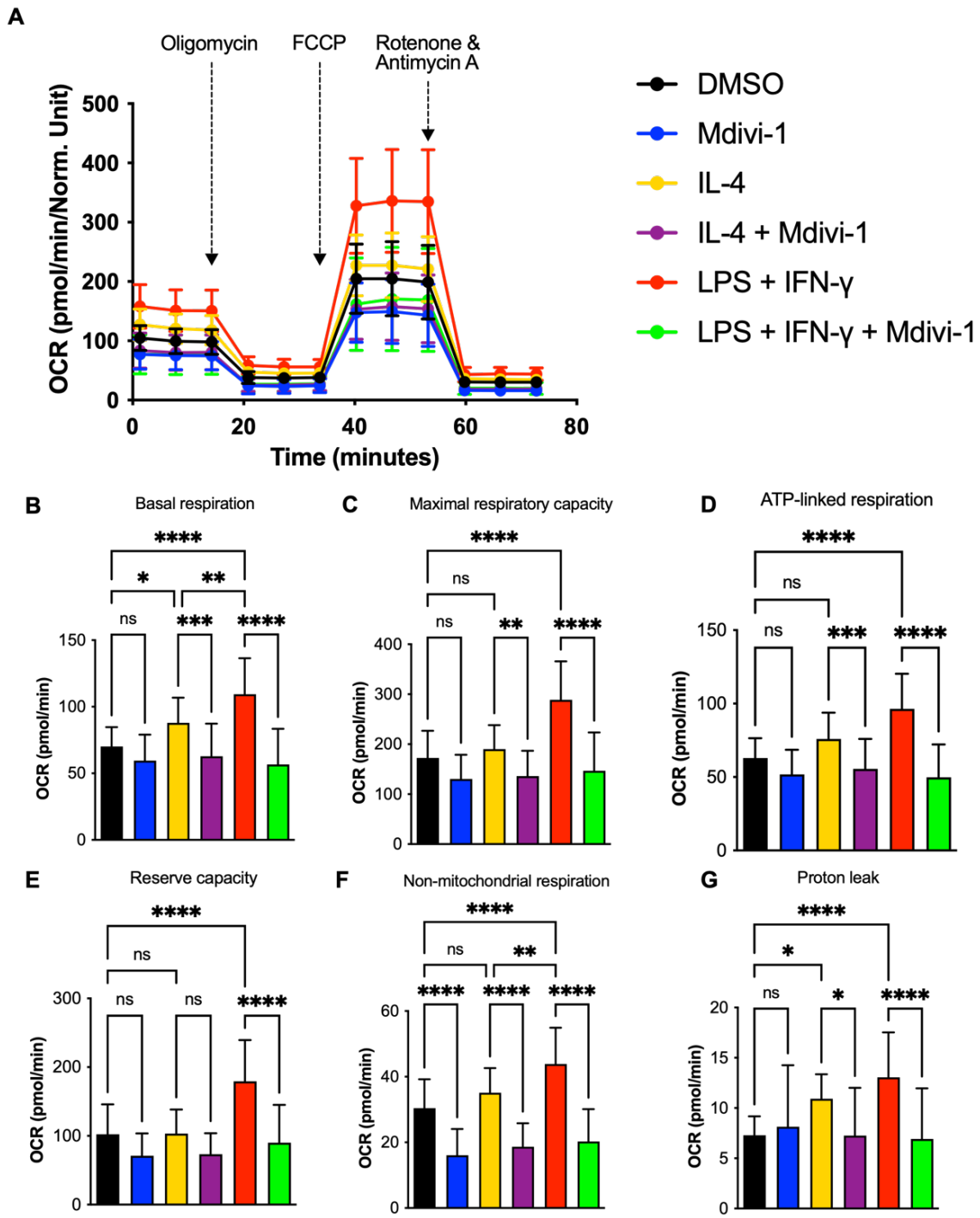

Figure 4.18: Mdivi-1 treatment inhibited oxygen consumption rates in THP-1 monocytes. THP-1 monocytes polarized to M1-like (LPS+IFN-γ) or M2-like (IL-4) phenotype and untreated (control) cells, in the presence or absence of Mdivi-1 were subjected to serial injections of oligomycin (ATP production), FCCP (Maximal respiration) and antimycin A / rotenone, and changes in the oxygen consumption rate (OCR) were monitored by the Seahorse XFe96 metabolic analyser (A). Metabolic parameters were determined as described in the methods: Basal respiration (B), Maximal respiratory capacity (C), ATP-linked respiration (D), Reserve capacity (E), non-mitochondrial respiration (F) and proton leak (G). Results are presented as mean ± SD from three independent experiments performed in replicates of 16; *P< 0.05; ** P< 0.01; *** p <0.001; ****P<0.0001 were used for comparisons. ns: not significant.

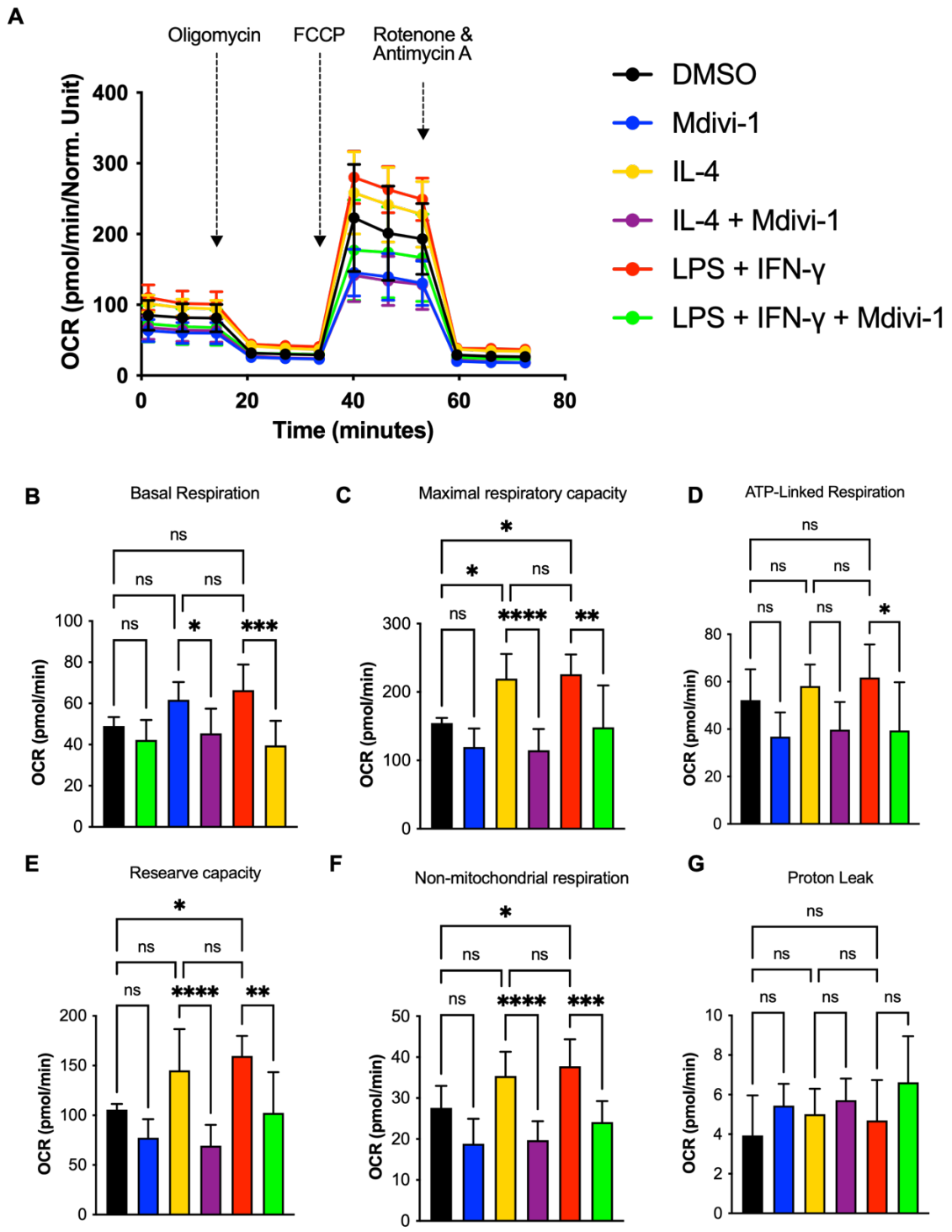

Figure 4.19: Mdivi-1 treatment inhibited oxygen consumption rates in THP-1 derived macrophages. THP-1 macrophages polarized to M1-like (LPS+IFN-γ) or M2-like (IL-4) phenotype and untreated (control) cells, in the presence or absence of Mdivi-1 were subjected to serial injections of oligomycin (ATP production), FCCP (Maximal respiration) and antimycin A / rotenone, and changes in the oxygen consumption rate (OCR) were monitored by the Seahorse XFe96 metabolic analyser (A). Metabolic parameters were determined as described in the methods: Basal respiration (B), Maximal respiratory capacity (C), ATP-linked respiration (D), Reserve capacity (E), non-mitochondrial respiration (F) and proton leak (G). Results are presented as mean ± SD from three independent experiments performed in replicates of 16; *P< 0.05; ** P< 0.01; *** p <0.001; ****P<0.0001 were used for comparisons. ns: not significant.

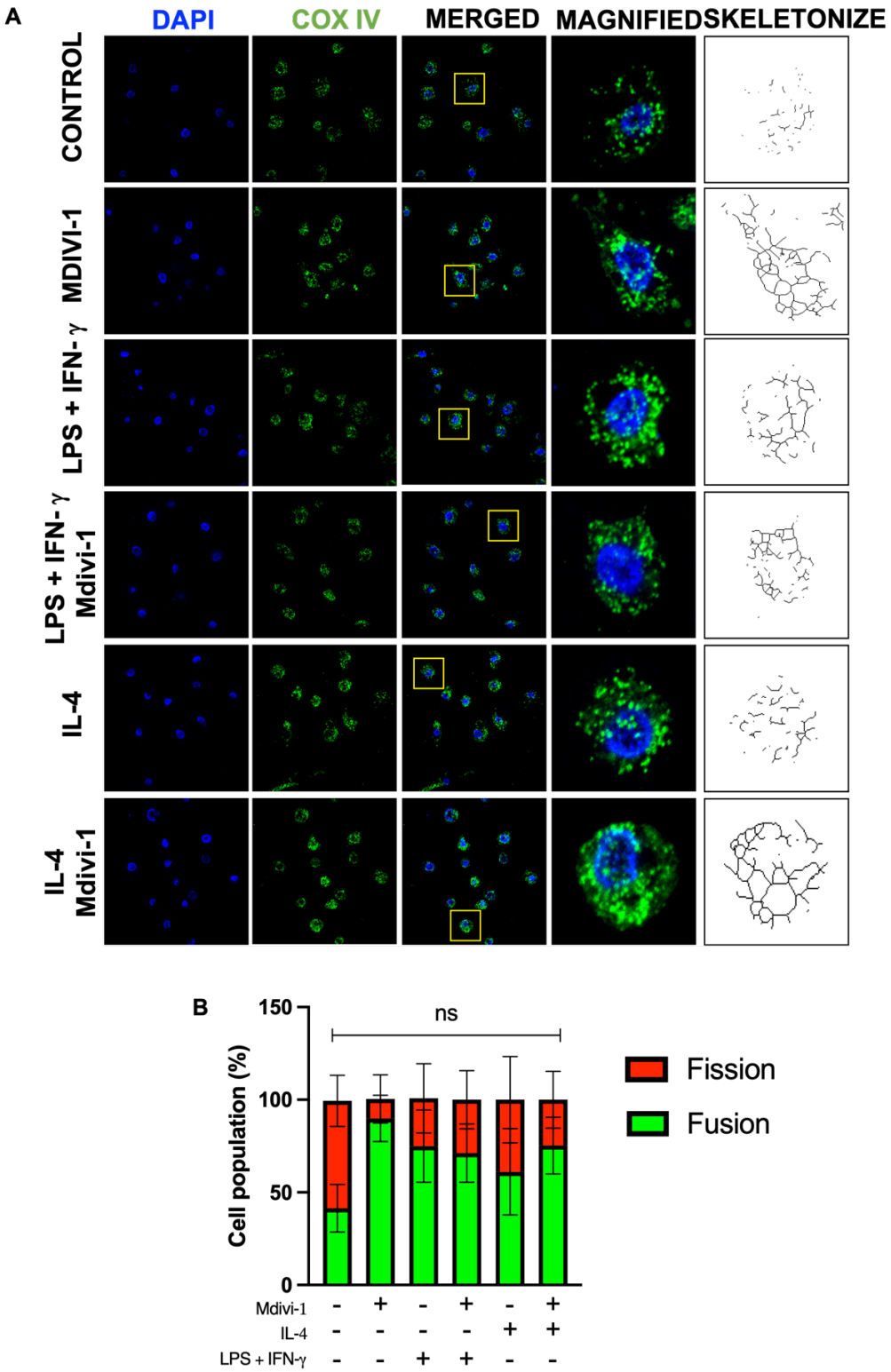

Figure 4.20: Mdivi-1 treatment did not affect mitochondrial morphology or Drp1 phosphorylation status in THP-1 monocytes. THP-1 monocytes polarized to M1-like (LPS+IFN-γ) or M2-like (IL-4) phenotype and untreated (control) cells, in the presence or absence of Mdivi-1, were evaluated under confocal microscopy. Cells were stained for DAPI (nuclei) and mitochondrial morphology (COX IV) was assessed after processing images under Image J as described in methods (A) 10 – 15 cells from 3 independent experiments (mean ± SD). Scoring percent of mitochondrial network morphology (Fused or Fissed) of M1-like or M2-like THP-1 monocytes with or without Mdivi-1 (B). *P< 0.05; ** P< 0.01; *** p <0.001; ****P<0.0001 were used for comparisons. ns: not significant.

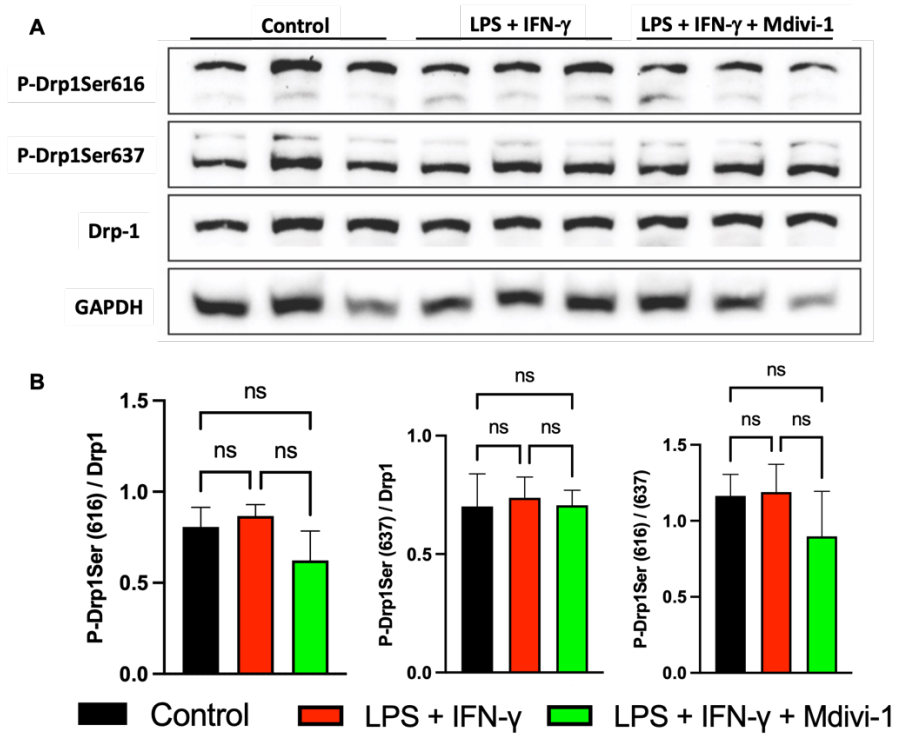

Figure 4.21: Mdivi-1 treatment did not affect mitochondrial morphology or Drp1 phosphorylation status in THP-1 monocytes. THP-1 monocytes polarized to M1-like (LPS+IFN-γ) phenotype and untreated (control) cells, in the presence or absence of Mdivi-1, were subjected to western blot analysis to assess levels of total and phosphorylated (Ser616 and Ser637) (A). Graphs show densitometry values of Drp-1. Signals were normalized using GAPDH as a loading control (B). *P< 0.05; ** P< 0.01; *** p <0.001; ****P<0.0001 were used for comparisons. ns: not significant.

These data indicate that the observed effects of Mdivi-1 on bioenergetics in human monocytes appear to be independent of changes in mitochondrial morphology and Drp-1 phosphorylation and it may be having off-targets effects as previously described (Bordt et al., 2017).

4.6 Mdivi-1 treatment reduced apoptosis in a preclinical wire-induced vascular injury model

Mitochondria are known to be a key source of ROS as they consume the majority of oxygen in the cell through the electron transport chain (Turrens, 2003). Therefore, it was anticipated that after the enhanced OXPHOS seen in pro-inflammatory monocytes and macrophages, high levels of mitochondrial ROS were being produced with the consequent increase of ROS-mediated apoptosis.

As Mdivi-1 was able to decrease OXPHOS, the next step was to evaluate his efficacy in preventing apoptosis *in vivo* after vascular injury. As expected, high levels of TUNEL positive cells were seen in the control group (**Figure 4.22**), denoting an increased level of

apoptosis taking place in plaque. However, in the Mdivi-1-treated group, a reduced number of TUNEL positive cells were found. Together, these data document the anti-apoptotic effect of Mdivi-1 during neointimal hyperplasia after vascular injury, which could be partially explained by the reduced OXPHOS seen in the M1-like cells which leads to a reduced ROS production.

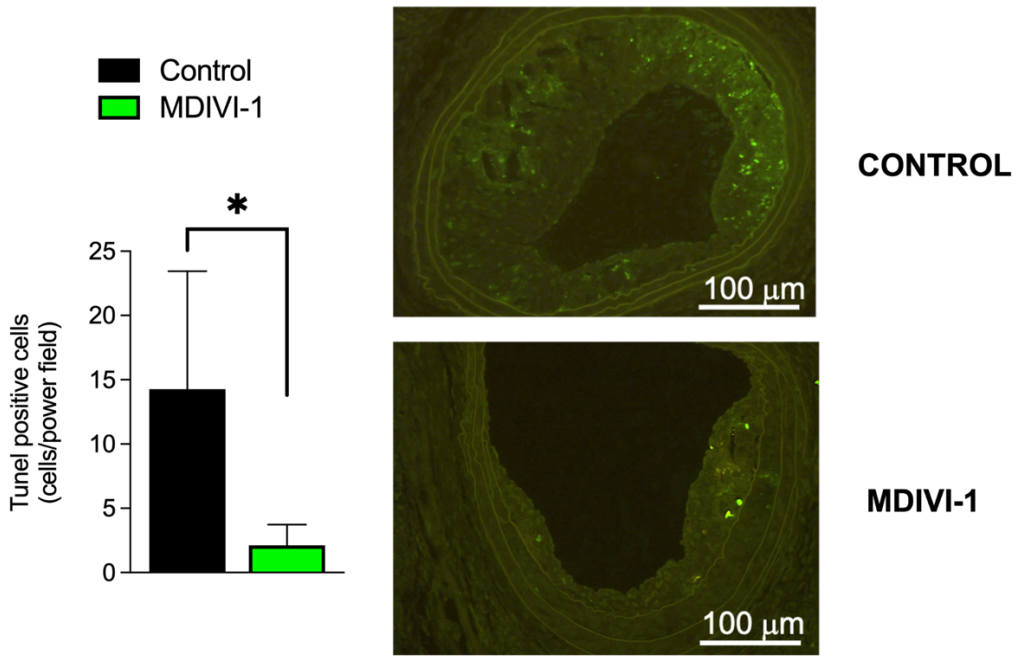

Figure 4.22: Mdivi-1 treatment reduced apoptosis in a wire-induced vascular injury model. Male *Apoe-/-* mice were fed a high-fat diet, treated with vehicle (DMSO) or Mdivi-1 and subjected to wire-induced injury of the common carotid artery. Compared to control, treatment with Mdivi-1 decreased levels of positive cells for TdT-mediated dUTP nick end labelling (TUNEL). Groups are abbreviated as Apoe−/− mice (Control); Apoe−/− mice treated with Mdivi-1 (Mdivi-1). Values represent mean±SEM (n=6 per group). *P* values (*P* values *P<0.05) were assessed using Student *t* tests.

5. Discussion

The present study shows for the first time that *in vivo* administration of Mdivi-1 significantly reduced neointimal hyperplasia, decreased monocyte recruitment into the plaque, and reduced vascular inflammation after carotid wire injury in HFD-fed *Apoe-/-* mice. These findings were accompanied by metabolic changes in monocytes and macrophages including decreased oxidative metabolism.

The anti-atherosclerotic activity of Mdivi-1 *in vivo*. The carotid wire-induced endothelial denudation mouse model is a widely used experimental procedure to induce tunica intimal hyperplasia and recapitulates the restenosis process seen in CAD and PAD patients that undergo angioplasty and stent procedures (Curaj, Zhoujun, Staudt, & Liehn, 2020). As expected, our HFD-fed *Apoe-/-* mice subjected to endothelial denudation, showed marked neointimal hyperplasia after two weeks of injury (Curaj et al., 2020; Schumacher et al., 2021) that was accompanied by an increase in cellularity in the vascular lesion. Following *in vivo* administration of Mdivi-1, a beneficial outcome was found on injury-related plaque remodelling after vascular injury, including reduced neointimal proliferation and significantly decreased vessel wall thickness; findings that were associated with reduced plaque complexity due to lower cell infiltration. Mdivi-1 treatment also lowered the number of macrophages and VSMCs recruited into the plaque area. These results are in agreement with previous data showing that expression of the dominant-negative Drp1 mutant, deficient in GTP hydrolysis (K38A), decreased intimal hyperplasia in mice subjected to femoral artery injury (L. Wang et al., 2015). In this situation, the PDGF-induced phosphorylation of Drp1 at serine 616 decreased, leading to a reduction of VMSC migration with inhibition of mitochondrial fission (L. Wang et al., 2015). However, the authors did neither implement any pharmacological approach to target mitochondrial fission nor assessed the number of macrophages present in the plaque.

In this regard, our *in vivo* data correlate with a recent study showing that genetic deletion of Drp1 in macrophages in mice significantly reduced intimal thickening and macrophage infiltration during femoral injury-induced vascular remodelling (Umezu et al., 2020), although mice used in this study contained functional ApoE and were not administered an atherogenic diet as in our experimental mice. Furthermore, the Cre recombinase system used to induce the genetic ablation of Drp1 in macrophages also targeted the neutrophil population, and it is therefore expected that the inflammatory response after vascular injury in these mice

was less severe when compared to our *in vivo* model of carotid-wire injury. All these findings reveal a favourable effect of Mdivi-1 administration on vascular remodelling following wire-induced endothelial injury that was accompanied by a significant reduction of VSMC and macrophage infiltration in the plaque.

Anti-inflammatory functions of Mdivi-1 *in vitro* and *in vivo* After endothelial denudation it has been reported that increased levels of the chemoattractant protein MCP-1 and M-CSF are released at the site of vascular injury, mediating the recruitment of monocytes from the circulation and their later differentiation into macrophages (Asare et al., 2020; Egashira et al., 2002; Georgakis, Bernhagen, Heitman, Weber, & Dichgans, 2022; Shiba et al., 2007) which is known to be a strong determinant for the extension of the neointimal formation(Schober & Weber, 2005; Shiba et al., 2007). Our *in vitro* data showed that Mdivi-1 reduced monocyte chemotaxis and transmigration in response to both, MCP-1 and M-CSF. In line with these findings, recent data have shown that Mdivi-1 could downregulate the expression of the MCP-1 receptor (CCR2) in murine macrophages (Umezu et al., 2020), and also our semi-quantitative protein determination showed a decreased production of MCP-1 and MCP-2 in LPS/IFN-γ-treated monocytes and macrophages, indicating that Mdivi-1 may be preventing cell migration via modulation of the MCP-1/CCR2 pathway. These data correlate very well with the reduction in macrophage content found in the plaques of mice treated with Mdivi-1 when compared to the control.

Macrophages have been classically identified as the source of TNF-α after vascular injury (Zimmerman et al., 2002). Consistent with this observation, the analysis revealed an anti-inflammatory response following Mdivi-1 treatment *in vivo*, with lowered levels of TNF-α and reduced expression of the adhesion molecule ICAM-1 in the vascular lesion. Adhesion molecules such as ICAM-1, V-CAM-1, and P-selectin are highly expressed after mechanical denudation of the vessel and are involved in the severity of the neointimal hyperplasia (D. Manka, Collins, Ley, Beaudet, & Sarembock, 2001; D. R. Manka et al., 1999; Oguchi et al., 2000) due to their roles in mediating inflammatory cell recruitment to the site of injury (Couffinhal, Duplaa, Moreau, Lamaziere, & Bonnet, 1994; Meerschaert & Furie, 1995; Rao, Yang, Garcia-Cardena, & Luscinskas, 2007). Consistent with this picture, our control mice (DMSO-treated) expressed the atherogenic adhesion molecule ICAM-1 in the vasculature after denudation. It has been reported that ICAM-1 is transcriptionally regulated by TNF-α in the endothelium in a NFκB-dependent manner (Clark, Manes, Pober, & Kluger, 2007; Hubbard &

Giardina, 2000; Kesanakurti, Chetty, Rajasekhar Maddirela, Gujrati, & Rao, 2013) and that TNF-α production is post-transcriptionally regulated by Drp-1 in macrophages (F. Gao et al., 2020). Hence, we hypothesize that Mdivi-1 may be modulating this regulatory mechanism which could explain the decreased levels of TNF-α and ICAM-1 seen in the carotid arteries after endothelial denudation. Together, these findings underline the properties of Mdivi-1 as an anti-inflammatory drug under conditions of vascular injury *in vivo*.

Mdivi-1 and immune cell polarization. Inflammation-related factors released by monocytes and macrophages, including cytokines and chemokines, are implicated in the initiation and progression of neointimal hyperplasia after vascular injury (Rectenwald, Moldawer, Huber, Seeger, & Ozaki, 2000; Zernecke & Weber, 2010). Here, *in vitro* evidence is provided in human THP-1 monocytes and THP-1-derived macrophages, showing that Mdivi-1 reduced the expression and production of several cytokines and chemokines following polarization to a M1-like phenotype using LPS/IFN-γ. Hence Mdivi-1 is promoting an M2-like phenotype that was evidenced by the upregulation of the M2-like marker CD206. As expected, levels of both TNF-α and IL-6 were higher in the macrophage population when compared to monocytes after stimulation with LPS+IFN-γ. This effect has been associated with a more susceptible response to pro-inflammatory stimuli of THP-1 cells after PMA treatment which induced the macrophage-like phenotype in these cells (Dreskin, Thomas, Dale, & Heasley, 2001; Smokelin, Mizzoni, Erndt-Marino, Kaplan, & Georgakoudi, 2020; Zarember & Godowski, 2002). In agreement with our findings, the anti-inflammatory effect of Mdivi-1 has been reported in different cell types, such as epithelial cells, T cells, endothelial cells, microglia, and murine macrophages (Forrester et al., 2020; Y. H. Li et al., 2019; R. Liu et al., 2020; X. Liu et al., 2021). Despite the overall anti-inflammatory function mediated by Mdivi-1 in these cells, THP-1 cells showed a constitutive production of IL-8, which has been previously reported in leukemic myelocytic cells as well (Baqui, Meiller, & Falkler, 1999; Tobler et al., 1993), and Mdivi-1 seemed to enhance this basal production. However, in THP-1 cells under inflammatory conditions (LPS/IFN-γ) this behaviour was not seen in the presence of Mdivi-1. Since this cytokine (IL-8) has been identified as an autocrine/paracrine growth factor for human hematopoietic progenitors, leading to growth and differentiation of cells of monocytic lineage (Corre, Pineau, & Hermouet, 1999), it is proposed that Mdivi-1 treatment potentiates these effects on THP-1 cells under basal conditions, but not after pro-inflammatory stimulation.

Influence of Mdivi-1 on cellular metabolism. As it is well known that changes in mitochondrial function may contribute to alterations in the immune response (Angajala et al., 2018), it was evaluated whether changes in mitochondrial function and metabolism could be associated with the observed anti-inflammatory effects of Mdivi-1. Recent studies have reported that metabolic changes in macrophages may be used to assess the polarization status of these cells. Typically, M1-like macrophages display enhanced glycolytic metabolism and reduced mitochondrial activity, while anti-inflammatory M2-like macrophages show high mitochondrial oxidative phosphorylation and are characterized by an enhanced spare respiratory capacity (SRC) (Nelson & O'Connell, 2020; Van den Bossche et al., 2015; Viola et al., 2019). In contrast to this consideration, the present results reveal that maximal oxidative metabolism is highly stimulated in M1-like monocytes and macrophages, while Mdivi-1 suppressed this response.

The metabolic reprogramming of mitochondria after an inflammatory stimulus has been studied in cells from myeloid linage, classifying them as early (0-6 h), sustained (up to 24 h), or tolerant (24 h stimulation followed by another 10-24 h) response (Zuo & Wan, 2019). The obtained data indeed displayed the phenotype of an early response. In line with this, monocytes and macrophages isolated from patients with atherosclerotic-CAD showed higher mitochondria activity after stimulation (3 h) with LPS/IFN-γ, presenting significantly higher OCR when compared to control. Also, the glycolytic flux in the same cells was markedly elevated as reflected by increased ECAR values (Shirai et al., 2016). Another study showed enhanced basal OCR and SRC in human monocytes after LPS treatment (4 h) (Lachmandas et al., 2016): The mechanism behind this finding was recently described by Langston et al. (Langston et al., 2019), who showed an increased oxidative metabolism and high glucose oxidation during acute LPS exposure of bone marrow-derived macrophages. This response was due to an enhanced activity of the mitochondrial glycerol 3-phosphate dehydrogenase (GPD2), a component of the glycerol phosphate shuttle (GPD), which drives forward electron transport (FET) in the electron transport chain and fuels the production of acetyl coenzyme A, thereby enhancing acetylation of histones and inflammatory gene induction in these cells. Therefore, a physiological interpretation of the increased of OXPHOS after M1-like polarization could be defined as early response of the cells to match the increased demand of ATP. Nonetheless, under sustained pro-inflammatory stimulus, it appears favourable to shift from mitochondrial respiration to aerobic glycolysis (Warburg effect) to promote faster ATP production, synthesis of inflammatory mediators and ROS (B. Kelly & O'Neill, 2015). This opens the possibility that

the reduced oxidative metabolism seen in the presence of Mdivi-1 in both monocytes and macrophages may be due to modulation of this adaptive mechanism of the mitochondria.

Contrary to the results from this study, Umezu et al. reported in murine macrophages neither an increase nor a decrease in mitochondrial respiration after exposure to LPS/IFN-γ alone or with and without Mdivi-1 (Umezu et al., 2020). Other studies in cancer cells have reported both, a reduction (Courtois et al., 2021; Dai et al., 2020) and an elevation (Cheng et al., 2016) of oxidative metabolism after Mdivi-1 treatment. Additionally, human smooth muscle cells (Hong et al., 2013) and mouse neuroblasts (Manczak, Kandimalla, Yin, & Reddy, 2019) presented increased OCR in the presence of Mdivi-1. The discordant findings may be due to the difference in cell type, culture conditions, Mdivi-1 concentration and treatment duration, or the metabolic assay used to assess mitochondrial respiration.

The present data also provide evidence for the capability of Mdivi-1 to modulate mitochondrial respiration in THP-1 cells. Yet, this effect has been associated with both, the inhibition of Drp1 as well as changes mediated by Drp1-independent mechanism, such as Mdivi-1 acting as a reversible inhibitor of the mitochondria complex I of the electron transport chain (Bordt et al., 2017). Since THP-1 cells after inflammatory stimulation provide both, increased mitochondrial respiration and elevated protein levels of the inner mitochondrial membrane OXPHOS complexes I and IV (Widdrington et al., 2018), it could be possible that the complex I inhibitory property attributed to Mdivi-1 may be involved in the reduced oxygen consumption rate seen in THP-1 cells.

Mdivi-1 and mitochondrial morphology. Alterations in mitochondrial function have been associated with changes in mitochondrial morphology, and it is well accepted that enhanced fission activity leads to mitochondrial fragmentation and impaired OXPHOS, whereas increased fusion activity leads to an enhanced oxidative metabolism (Picard, Shirihai, Gentil, & Burelle, 2013). As such, it was investigated whether the observed metabolic effects of Mdivi-1 were associated with changes in mitochondrial morphology in THP-1 monocytes. Unexpectedly, treatment with Mdivi-1 did neither evoke any significant changes in mitochondrial morphology, nor was the phosphorylation status of Drp1 on Ser616 and Ser637 altered, implying that the observed metabolic effects of Mdivi-1 were independent of changes in mitochondrial morphology or the Drp1 phosphorylation status. High levels of mitochondria fragmentation were displayed in THP-1 cells under basal conditions, which may be due to a constitutive IL-8 production found in THP-1 cells, since this interleukin has been reported to increase mitochondrial fragmentation in *in vitro* cultured cells (Buoncervello et al., 2019). In

contrast, other studies have reported an increase in mitochondrial fragmentation with enhanced phosphorylation of Drp1-Ser616 in murine macrophages after LPS stimulation, and such changes were reversed by treatment with Mdivi-1 alone (Umezu et al., 2020) or in combination with another fusion promoter molecule (Kapetanovic et al., 2020).

On the other hand, morphometric analysis of mitochondria in primary human monocytes and THP-1-macrophages subjected to pro-inflammatory stimulation (LPS/IFN-γ) displayed elongated fused mitochondria (Duroux-Richard et al., 2016; Lachmandas et al., 2016). The latter findings are consistent with our results in which LPS/IFN-γ treated THP-1 monocytes had a trend to increase mitochondrial fusion, even though the data was not statistically significant. Additionally, on T-memory cells, efficient OXPHOS and fatty acid oxidation with tight mitochondrial crista have been linked to elongated mitochondria, whereas in T-effector cells fragmented mitochondria have been associated with loose mitochondria cristae leading to a less effective transport of electrons through the ETC, stimulating glycolysis (Buck et al., 2016). This phenotype is not in consonance with the results seen after treatment with Mdivi-1 alone, in which cells displayed a trend to increase mitochondria fusion compared to control, but metabolically a reduced OXPHOS was seen as discussed above.

Taking together, this data indicates that the anti-inflammatory effect linked to reduced mitochondria respiration seen in THP-1 cells after Mdivi-1 treatment may be related to its inhibitory action on mitochondria complex I and the reduced production of reactive oxygen species (Bordt et al., 2017), instead of its pointed role as a Drp1 inhibitor.

Mdivi-1 and mitochondrial ROS production. The hypothesis that Mdivi-1 is mediating its effect via modulation of mitochondrial complex I, is supported by experimental evidence showing the role of ROS during neointimal hyperplasia after vascular injury, promoting cell proliferation, migration, and apoptosis (Azevedo et al., 2000; Gomez et al., 2015; Hirschberg et al., 2010; Perlman, Maillard, Krasinski, & Walsh, 1997; Zhou et al., 2016). Indeed, studies in rats have shown that at 14 days after vascular injury, there is an increase in apoptotic indexes of medial SMCs (Jagadeesha et al., 2005; Walsh, Smith, & Kim, 2000) and such elevation is correlated with the degree of the intimal hyperplasia (Bochaton-Piallat, Gabbiani, Redard, Desmouliere, & Gabbiani, 1995; D. K. Han et al., 1995). In line with this, the control mice showed increased levels of TdT-mediated dUTP nick end labelling (TUNEL), an indicator of apoptosis, and such elevation was reduced by Mdivi-1 treatment. Since Mdivi-1 has been reported to reduce apoptosis in cultured VSMC isolated from rats (W. R. Chen et al., 2020), it

is hypothesized that the reduction of TUNEL positive cells found in the plaque after wire-injury is due decrease apoptosis in the SMC population.

One can hypothesize that the reduced mitochondrial respiration after Mdivi-1 administration may lower the production of ROS via inhibition of mitochondria complex I, protecting it from ROS-mediated apoptosis. That statement is held by experimental evidence showing that pro-inflammatory stimulation of macrophages, dendritic cells, and microglia leads to an accumulation of succinate (Nair et al., 2019; Williams & O'Neill, 2018), which drives reverse electron transport, generating excessive mitochondrial ROS production (Chouchani et al., 2014; Niatsetskaya et al., 2012). In the case of microglia, the study showed that Mdivi-1 was able to prevent this link between the accumulation of succinate and ROS production (Nair et al., 2019). Moreover, the proposed ROS-mediated mechanism is also supported by a recent study showing that pharmacological inhibition of mitochondria complex I could attenuate neointimal hyperplasia after vascular injury via modulation of cell proliferation and migration, possibly by reducing ROS production (Yin et al., 2019). However, further studies are needed to elucidate the mechanisms by which Mdivi-1 potentially modulates ROS-induced neointimal hyperplasia.

Study limitations. There are some limitations of this study: First, the wire-induced injury was performed in a healthy blood vessel that lacks established atherogenic pathology, which differs from the clinical setting in which angioplasty or stenting is performed in a diseased vasculature. Second, while most of the experiments *in vitro* were performed on THP-1 cells, there are well-known differences between these immortalized cells and the primary human monocytes (Bosshart & Heinzelmann, 2016), and therefore, additional validation is needed using blood-derived monocytes to draw more definite conclusions. Third, the focus of the study was on the monocyte/ macrophage population, while more exploration to elucidate the protective effect of Mdivi-1 on VSMCs during vascular injury is needed. Lastly, due to the off-target effects of Mdivi-1, new studies are required using agents that target Drp1 in a specific manner, such as the recently developed Drpitor1 or Drpitor1a (Wu et al., 2020) to better understand the role of this mitochondrial fission protein during vascular restenosis. Nevertheless, despite these limitations, the present studies provide new insights into the interplay between mitochondrial function and modulation of the inflammatory response during vascular injury *in vivo* and *in vitro*.

Future directions and potential clinical implications. The microenvironment influences monocyte/macrophage functional characteristics via mitochondria and metabolic pathways, including oxygen and the metabolite availability. In the context of atherosclerosis, there is currently some evidence that inducing and maintaining substantial M2-like polarization has a long-lasting effect on the disease. This investigation has added key findings of how metabolic changes and mitochondrial functions may affect monocyte/macrophage phenotypic reversal in lesions, offering a new class of therapeutic targets by establishing molecular connections between mitochondrial responses and monocyte/macrophage functional change during vascular restenosis. Targeting cellular metabolism could inspire future research to investigate molecular mechanisms tying mitochondria and immune cell function in a number of disorders, given the extensive implications of innate immunity in human diseases.

In conclusion, this study describes for the first time that Mdivi-1 strongly protects against neointimal hyperplasia following endothelial wire-injury where it has beneficial effects on vascular remodeling by modulating mitochondrial oxidative metabolisms potentially through Drp1-independent mechanisms (**Figure 5.1**). Metabolic modulation of monocyte and macrophage polarization using Mdivi-1 may thereby provide a new therapeutic option for treating atherosclerosis and restenosis in patients with CAD and PAD.

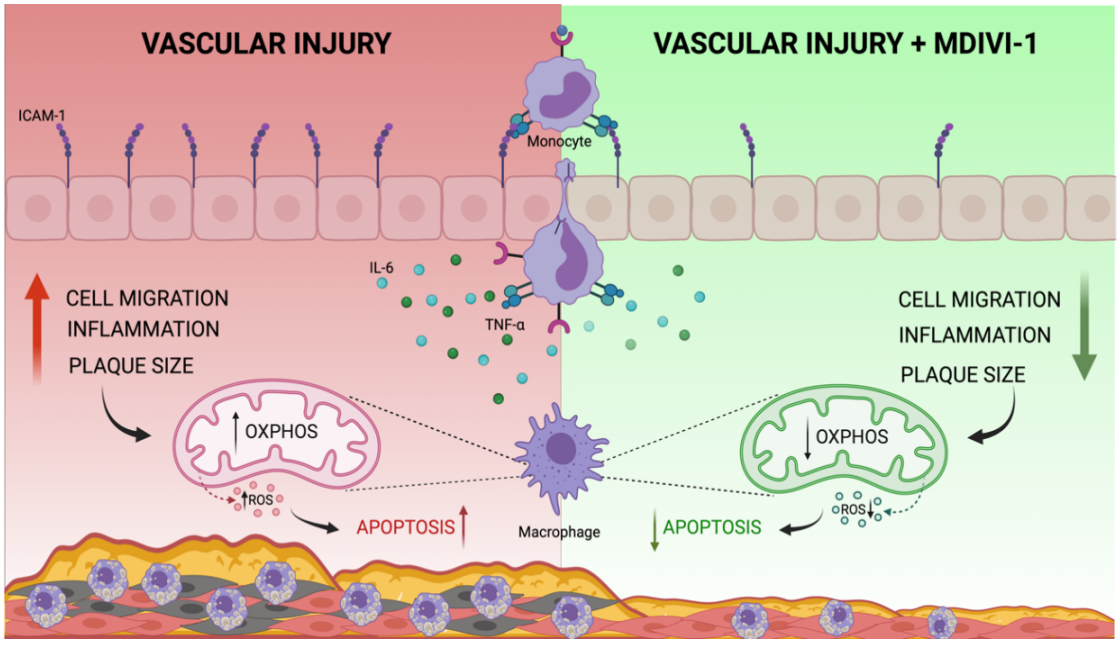

Figure 5.1: Schematic summary of findings. The left panel illustrates the events taking place after vascular injury, including the increment of plaque size, cell migration, secretion of inflammatory cytokines, expression of adhesion molecules, and oxidative phosphorylation. The right panel illustrates the effect of Mitochondrial division inhibitor 1 (Mdivi-1) after vascular injury: reduction of neointimal hyperplasia and inflammation via modulation of cell oxidative metabolism and migration**.**

6. References

Adamson, S., & Leitinger, N. (2011). Phenotypic modulation of macrophages in response to plaque lipids. *Curr Opin Lipidol, 22*(5), 335-342. doi:10.1097/MOL.0b013e32834a97e4

Adaniya, S. M., J, O. U., Cypress, M. W., Kusakari, Y., & Jhun, B. S. (2019). Posttranslational modifications of mitochondrial fission and fusion proteins in cardiac physiology and pathophysiology. *Am J Physiol Cell Physiol, 316*(5), C583-C604. doi:10.1152/ajpcell.00523.2018

Ait-Oufella, H., Taleb, S., Mallat, Z., & Tedgui, A. (2011). Recent advances on the role of cytokines in atherosclerosis. *Arterioscler Thromb Vasc Biol, 31*(5), 969-979. doi:10.1161/ATVBAHA.110.207415

Aleo, J. J., & Padh, H. (1985). Inhibition of ascorbic acid uptake by endotoxin: evidence of mediation by serum factor(s). *Proc Soc Exp Biol Med, 179*(1), 128-131. doi:10.3181/00379727-179-1-rc1

Angajala, A., Lim, S., Phillips, J. B., Kim, J. H., Yates, C., You, Z., & Tan, M. (2018). Diverse Roles of Mitochondria in Immune Responses: Novel Insights Into Immuno-Metabolism. *Front Immunol, 9*, 1605. doi:10.3389/fimmu.2018.01605

Arnheim, N., & Erlich, H. (1992). Polymerase chain reaction strategy. *Annu Rev Biochem, 61*, 131-156. doi:10.1146/annurev.bi.61.070192.001023

Asai, A., Nakamura, K., Kobayashi, M., Herndon, D. N., & Suzuki, F. (2012). CCL1 released from M2b macrophages is essentially required for the maintenance of their properties. *J Leukoc Biol, 92*(4), 859-867. doi:10.1189/jlb.0212107

Asare, Y., Koehncke, J., Selle, J., Simsekyilmaz, S., Jankowski, J., Shagdarsuren, G., . . . Shagdarsuren, E. (2020). Differential Role for Activating FcgammaRIII in Neointima Formation After Arterial Injury and Diet-Induced Chronic Atherosclerosis in Apolipoprotein E-Deficient Mice. *Front Physiol, 11*, 673. doi:10.3389/fphys.2020.00673

Auwerx, J. (1991). The human leukemia cell line, THP-1: a multifacetted model for the study of monocyte-macrophage differentiation. *Experientia, 47*(1), 22-31. doi:10.1007/BF02041244

Azevedo, L. C., Pedro, M. A., Souza, L. C., de Souza, H. P., Janiszewski, M., da Luz, P. L., & Laurindo, F. R. (2000). Oxidative stress as a signaling mechanism of the vascular response to injury: the redox hypothesis of restenosis. *Cardiovasc Res, 47*(3), 436-445. doi:10.1016/s0008-6363(00)00091-2

Baqui, A. A., Meiller, T. F., & Falkler, W. A. (1999). Enhanced interleukin-8 production in THP-1 human monocytic cells by lipopolysaccharide from oral microorganisms and granulocyte-macrophage colony-stimulating factor. *Oral Microbiol Immunol, 14*(5), 275-280. doi:10.1034/j.1399-302x.1999.140502.x

Barrett, T. J. (2020). Macrophages in Atherosclerosis Regression. *Arterioscler Thromb Vasc Biol, 40*(1), 20-33. doi:10.1161/ATVBAHA.119.312802

Bernhagen, J., Krohn, R., Lue, H., Gregory, J. L., Zernecke, A., Koenen, R. R., . . . Weber, C. (2007). MIF is a noncognate ligand of CXC chemokine receptors in inflammatory and atherogenic cell recruitment. *Nat Med, 13*(5), 587-596. doi:10.1038/nm1567

Bochaton-Piallat, M. L., Gabbiani, F., Redard, M., Desmouliere, A., & Gabbiani, G. (1995). Apoptosis participates in cellularity regulation during rat aortic intimal thickening. *Am J Pathol, 146*(5), 1059-1064. Retrieved from https://www.ncbi.nlm.nih.gov/pubmed/7747800

Bordt, E. A., Clerc, P., Roelofs, B. A., Saladino, A. J., Tretter, L., Adam-Vizi, V., . . . Polster, B. M. (2017). The Putative Drp1 Inhibitor mdivi-1 Is a Reversible Mitochondrial

Complex I Inhibitor that Modulates Reactive Oxygen Species. *Dev Cell, 40*(6), 583-594 e586. doi:10.1016/j.devcel.2017.02.020

Bosshart, H., & Heinzelmann, M. (2016). THP-1 cells as a model for human monocytes. *Ann Transl Med, 4*(21), 438. doi:10.21037/atm.2016.08.53

Brand, M. D., & Nicholls, D. G. (2011). Assessing mitochondrial dysfunction in cells. *Biochem J, 435*(2), 297-312. doi:10.1042/BJ20110162

Buck, M. D., O'Sullivan, D., Klein Geltink, R. I., Curtis, J. D., Chang, C. H., Sanin, D. E., . . . Pearce, E. L. (2016). Mitochondrial Dynamics Controls T Cell Fate through Metabolic Programming. *Cell, 166*(1), 63-76. doi:10.1016/j.cell.2016.05.035

Buoncervello, M., Maccari, S., Ascione, B., Gambardella, L., Marconi, M., Spada, M., . . . Gabriele, L. (2019). Inflammatory cytokines associated with cancer growth induce mitochondria and cytoskeleton alterations in cardiomyocytes. *J Cell Physiol, 234*(11), 20453-20468. doi:10.1002/jcp.28647

Bustin, S. A., & Mueller, R. (2005). Real-time reverse transcription PCR (qRT-PCR) and its potential use in clinical diagnosis. *Clin Sci (Lond), 109*(4), 365-379. doi:10.1042/CS20050086

Bzymek, R., Horsthemke, M., Isfort, K., Mohr, S., Tjaden, K., Muller-Tidow, C., . . . Hanley, P. J. (2016). Real-time two- and three-dimensional imaging of monocyte motility and navigation on planar surfaces and in collagen matrices: roles of Rho. *Sci Rep, 6*, 25016. doi:10.1038/srep25016

Calles, K., Svensson, I., Lindskog, E., & Haggstrom, L. (2006). Effects of conditioned medium factors and passage number on Sf9 cell physiology and productivity. *Biotechnol Prog, 22*(2), 394-400. doi:10.1021/bp050297a

Camici, P. G., Rimoldi, O. E., Gaemperli, O., & Libby, P. (2012). Non-invasive anatomic and functional imaging of vascular inflammation and unstable plaque. *Eur Heart J, 33*(11), 1309-1317. doi:10.1093/eurheartj/ehs067

Campello, S., Lacalle, R. A., Bettella, M., Manes, S., Scorrano, L., & Viola, A. (2006). Orchestration of lymphocyte chemotaxis by mitochondrial dynamics. *J Exp Med, 203*(13), 2879-2886. doi:10.1084/jem.20061877

Cao, Y. L., Meng, S., Chen, Y., Feng, J. X., Gu, D. D., Yu, B., . . . Gao, S. (2017). MFN1 structures reveal nucleotide-triggered dimerization critical for mitochondrial fusion. *Nature, 542*(7641), 372-376. doi:10.1038/nature21077

Chamie, D., Wang, Z., Bezerra, H., Rollins, A. M., & Costa, M. A. (2011). Optical Coherence Tomography and Fibrous Cap Characterization. *Curr Cardiovasc Imaging Rep, 4*(4), 276-283. doi:10.1007/s12410-011-9090-8

Chang, C. R., & Blackstone, C. (2007). Cyclic AMP-dependent protein kinase phosphorylation of Drp1 regulates its GTPase activity and mitochondrial morphology. *J Biol Chem, 282*(30), 21583-21587. doi:10.1074/jbc.C700083200

Chanput, W., Mes, J. J., Savelkoul, H. F., & Wichers, H. J. (2013). Characterization of polarized THP-1 macrophages and polarizing ability of LPS and food compounds. *Food Funct, 4*(2), 266-276. doi:10.1039/c2fo30156c

Chanput, W., Mes, J. J., & Wichers, H. J. (2014). THP-1 cell line: an in vitro cell model for immune modulation approach. *Int Immunopharmacol, 23*(1), 37-45. doi:10.1016/j.intimp.2014.08.002

Chen, H., Chomyn, A., & Chan, D. C. (2005). Disruption of fusion results in mitochondrial heterogeneity and dysfunction. *J Biol Chem, 280*(28), 26185-26192. doi:10.1074/jbc.M503062200

Chen, W. R., Zhou, Y. J., Sha, Y., Wu, X. P., Yang, J. Q., & Liu, F. (2020). Melatonin attenuates vascular calcification by inhibiting mitochondria fission via an AMPK/Drp1 signalling pathway. *J Cell Mol Med, 24*(11), 6043-6054. doi:10.1111/jcmm.15157

Cheng, C. T., Kuo, C. Y., Ouyang, C., Li, C. F., Chung, Y., Chan, D. C., . . . Ann, D. K. (2016). Metabolic Stress-Induced Phosphorylation of KAP1 Ser473 Blocks Mitochondrial Fusion in Breast Cancer Cells. *Cancer Res, 76*(17), 5006-5018. doi:10.1158/0008-5472.CAN-15-2921

Chouchani, E. T., Pell, V. R., Gaude, E., Aksentijevic, D., Sundier, S. Y., Robb, E. L., . . . Murphy, M. P. (2014). Ischaemic accumulation of succinate controls reperfusion injury through mitochondrial ROS. *Nature, 515*(7527), 431-435. doi:10.1038/nature13909

Chuang, Y., Hung, M. E., Cangelose, B. K., & Leonard, J. N. (2016). Regulation of the IL-10-driven macrophage phenotype under incoherent stimuli. *Innate Immun, 22*(8), 647-657. doi:10.1177/1753425916668243

Clark, P. R., Manes, T. D., Pober, J. S., & Kluger, M. S. (2007). Increased ICAM-1 expression causes endothelial cell leakiness, cytoskeletal reorganization and junctional alterations. *J Invest Dermatol, 127*(4), 762-774. doi:10.1038/sj.jid.5700670

Corre, I., Pineau, D., & Hermouet, S. (1999). Interleukin-8: an autocrine/paracrine growth factor for human hematopoietic progenitors acting in synergy with colony stimulating factor-1 to promote monocyte-macrophage growth and differentiation. *Exp Hematol, 27*(1), 28-36. doi:10.1016/s0301-472x(98)00032-0

Costantini, A., Viola, N., Berretta, A., Galeazzi, R., Matacchione, G., Sabbatinelli, J., . . . Bonafe, M. (2018). Age-related M1/M2 phenotype changes in circulating monocytes from healthy/unhealthy individuals. *Aging (Albany NY), 10*(6), 1268-1280. doi:10.18632/aging.101465

Couffinhal, T., Duplaa, C., Moreau, C., Lamaziere, J. M., & Bonnet, J. (1994). Regulation of vascular cell adhesion molecule-1 and intercellular adhesion molecule-1 in human vascular smooth muscle cells. *Circ Res, 74*(2), 225-234. doi:10.1161/01.res.74.2.225

Courtois, S., de Luxan-Delgado, B., Penin-Peyta, L., Royo-Garcia, A., Parejo-Alonso, B., Jagust, P., . . . Sancho, P. (2021). Inhibition of Mitochondrial Dynamics Preferentially Targets Pancreatic Cancer Cells with Enhanced Tumorigenic and Invasive Potential. *Cancers (Basel), 13*(4). doi:10.3390/cancers13040698

Curaj, A., Zhoujun, W., Staudt, M., & Liehn, E. A. (2020). Induction of Accelerated Atherosclerosis in Mice: The "Wire-Injury" Model. *J Vis Exp*(162). doi:10.3791/54571

Dai, W., Wang, G., Chwa, J., Oh, M. E., Abeywardana, T., Yang, Y., . . . Jiang, L. (2020). Mitochondrial division inhibitor (mdivi-1) decreases oxidative metabolism in cancer. *Br J Cancer, 122*(9), 1288-1297. doi:10.1038/s41416-020-0778-x

Daigneault, M., Preston, J. A., Marriott, H. M., Whyte, M. K., & Dockrell, D. H. (2010). The identification of markers of macrophage differentiation in PMA-stimulated THP-1 cells and monocyte-derived macrophages. *PLoS One, 5*(1), e8668. doi:10.1371/journal.pone.0008668

Deng, X., Yang, Q., Wang, Y., Yang, Y., Pei, G., Zhu, H., . . . Zeng, R. (2019). Association of plasma macrophage colony-stimulating factor with cardiovascular morbidity and all-cause mortality in chronic hemodialysis patients. *BMC Nephrol, 20*(1), 321. doi:10.1186/s12882-019-1510-z

Divakaruni, A. S., Paradyse, A., Ferrick, D. A., Murphy, A. N., & Jastroch, M. (2014). Analysis and interpretation of microplate-based oxygen consumption and pH data. *Methods Enzymol, 547*, 309-354. doi:10.1016/B978-0-12-801415-8.00016-3

Dreskin, S. C., Thomas, G. W., Dale, S. N., & Heasley, L. E. (2001). Isoforms of Jun kinase are differentially expressed and activated in human monocyte/macrophage (THP-1) cells. *J Immunol, 166*(9), 5646-5653. doi:10.4049/jimmunol.166.9.5646

Duroux-Richard, I., Roubert, C., Ammari, M., Presumey, J., Grun, J. R., Haupl, T., . . . Apparailly, F. (2016). miR-125b controls monocyte adaptation to inflammation

through mitochondrial metabolism and dynamics. *Blood, 128*(26), 3125-3136. doi:10.1182/blood-2016-02-697003

Egashira, K., Zhao, Q., Kataoka, C., Ohtani, K., Usui, M., Charo, I. F., . . . Takeshita, A. (2002). Importance of monocyte chemoattractant protein-1 pathway in neointimal hyperplasia after periarterial injury in mice and monkeys. *Circ Res, 90*(11), 1167-1172. doi:10.1161/01.res.0000020561.03244.7e

Elgass, K., Pakay, J., Ryan, M. T., & Palmer, C. S. (2013). Recent advances into the understanding of mitochondrial fission. *Biochim Biophys Acta, 1833*(1), 150-161. doi:10.1016/j.bbamcr.2012.05.002

Ernst, O., Glucksam-Galnoy, Y., Bhatta, B., Athamna, M., Ben-Dror, I., Glick, Y., . . . Zor, T. (2019). Exclusive Temporal Stimulation of IL-10 Expression in LPS-Stimulated Mouse Macrophages by cAMP Inducers and Type I Interferons. *Front Immunol, 10*, 1788. doi:10.3389/fimmu.2019.01788

Favero, G., Paganelli, C., Buffoli, B., Rodella, L. F., & Rezzani, R. (2014). Endothelium and its alterations in cardiovascular diseases: life style intervention. *Biomed Res Int, 2014*, 801896. doi:10.1155/2014/801896

Filadi, R., Pendin, D., & Pizzo, P. (2018). Mitofusin 2: from functions to disease. *Cell Death Dis, 9*(3), 330. doi:10.1038/s41419-017-0023-6

Finn, A. V., Nakano, M., Narula, J., Kolodgie, F. D., & Virmani, R. (2010). Concept of vulnerable/unstable plaque. *Arterioscler Thromb Vasc Biol, 30*(7), 1282-1292. doi:10.1161/ATVBAHA.108.179739

Fok, P. W. (2012). Growth of necrotic cores in atherosclerotic plaque. *Math Med Biol, 29*(4), 301-327. doi:10.1093/imammb/dqr012

Forrester, S. J., Preston, K. J., Cooper, H. A., Boyer, M. J., Escoto, K. M., Poltronetti, A. J., . . . Eguchi, S. (2020). Mitochondrial Fission Mediates Endothelial Inflammation. *Hypertension, 76*(1), 267-276. doi:10.1161/HYPERTENSIONAHA.120.14686

Forte, M., Schirone, L., Ameri, P., Basso, C., Catalucci, D., Modica, J., . . . Molecular Biology of the, H. (2021). The role of mitochondrial dynamics in cardiovascular diseases. *Br J Pharmacol, 178*(10), 2060-2076. doi:10.1111/bph.15068

Frangogiannis, N. G., Mendoza, L. H., Ren, G., Akrivakis, S., Jackson, P. L., Michael, L. H., . . . Entman, M. L. (2003). MCSF expression is induced in healing myocardial infarcts and may regulate monocyte and endothelial cell phenotype. *Am J Physiol Heart Circ Physiol, 285*(2), H483-492. doi:10.1152/ajpheart.01016.2002

Frostegard, J. (2013). Immunity, atherosclerosis and cardiovascular disease. *BMC Med, 11*, 117. doi:10.1186/1741-7015-11-117

Gallagher, S. R. (2017). Quantitation of DNA and RNA with Absorption and Fluorescence Spectroscopy. *Curr Protoc Immunol, 116*, A 3L 1-A 3L 14. doi:10.1002/cpim.20

Gao, F., Reynolds, M. B., Passalacqua, K. D., Sexton, J. Z., Abuaita, B. H., & O'Riordan, M. X. D. (2020). The Mitochondrial Fission Regulator DRP1 Controls Post-Transcriptional Regulation of TNF-alpha. *Front Cell Infect Microbiol, 10*, 593805. doi:10.3389/fcimb.2020.593805

Gao, J., Shi, L., Gu, J., Zhang, D., Wang, W., Zhu, X., & Liu, J. (2021). Difference of immune cell infiltration between stable and unstable carotid artery atherosclerosis. *J Cell Mol Med, 25*(23), 10973-10979. doi:10.1111/jcmm.17018

Gasier, H. G., Dohl, J., Suliman, H. B., Piantadosi, C. A., & Yu, T. (2020). Skeletal muscle mitochondrial fragmentation and impaired bioenergetics from nutrient overload are prevented by carbon monoxide. *Am J Physiol Cell Physiol, 319*(4), C746-C756. doi:10.1152/ajpcell.00016.2020

Ge, Y., Shi, X., Boopathy, S., McDonald, J., Smith, A. W., & Chao, L. H. (2020). Two forms of Opa1 cooperate to complete fusion of the mitochondrial inner-membrane. *Elife, 9*. doi:10.7554/eLife.50973

Genin, M., Clement, F., Fattaccioli, A., Raes, M., & Michiels, C. (2015). M1 and M2 macrophages derived from THP-1 cells differentially modulate the response of cancer cells to etoposide. *BMC Cancer, 15*, 577. doi:10.1186/s12885-015-1546-9

Georgakis, M. K., Bernhagen, J., Heitman, L. H., Weber, C., & Dichgans, M. (2022). Targeting the CCL2-CCR2 axis for atheroprotection. *European heart journal, 43*(19), 1799-1808. doi:10.1093/eurheartj/ehac094

Gomez, C., Martinez, L., Mesa, A., Duque, J. C., Escobar, L. A., Pham, S. M., & Vazquez-Padron, R. I. (2015). Oxidative stress induces early-onset apoptosis of vascular smooth muscle cells and neointima formation in response to injury. *Biosci Rep, 35*(4). doi:10.1042/BSR20140122

Gomez Perdiguero, E., Klapproth, K., Schulz, C., Busch, K., Azzoni, E., Crozet, L., . . . Rodewald, H. R. (2015). Tissue-resident macrophages originate from yolk-sac-derived erythro-myeloid progenitors. *Nature, 518*(7540), 547-551. doi:10.1038/nature13989

Green, M. R., & Sambrook, J. (2019). Removing DNA Contamination from RNA Samples by Treatment with RNase-Free DNase I. *Cold Spring Harb Protoc, 2019*(10). doi:10.1101/pdb.prot101725

Gu, X., Ma, Y., Liu, Y., & Wan, Q. (2021). Measurement of mitochondrial respiration in adherent cells by Seahorse XF96 Cell Mito Stress Test. *STAR Protoc, 2*(1), 100245. doi:10.1016/j.xpro.2020.100245

Han, D. K., Haudenschild, C. C., Hong, M. K., Tinkle, B. T., Leon, M. B., & Liau, G. (1995). Evidence for apoptosis in human atherogenesis and in a rat vascular injury model. *Am J Pathol, 147*(2), 267-277. Retrieved from https://www.ncbi.nlm.nih.gov/pubmed/7639326

Han, S., Zhao, F., Hsia, J., Ma, X., Liu, Y., Torres, S., . . . Zhu, X. (2021). The role of Mfn2 in the structure and function of endoplasmic reticulum-mitochondrial tethering in vivo. *J Cell Sci, 134*(13). doi:10.1242/jcs.253443

Hansson, G. K., & Libby, P. (2006). The immune response in atherosclerosis: a double-edged sword. *Nat Rev Immunol, 6*(7), 508-519. doi:10.1038/nri1882

Hatch, A. L., Gurel, P. S., & Higgs, H. N. (2014). Novel roles for actin in mitochondrial fission. *J Cell Sci, 127*(Pt 21), 4549-4560. doi:10.1242/jcs.153791

Hay, R. J., Macy, M. L., & Chen, T. R. (1989). Mycoplasma infection of cultured cells. *Nature, 339*(6224), 487-488. doi:10.1038/339487a0

Hirosawa, N., Uchida, K., Kuniyoshi, K., Murakami, K., Inoue, G., Miyagi, M., . . . Ohtori, S. (2018). Vein wrapping promotes M2 macrophage polarization in a rat chronic constriction injury model. *J Orthop Res*. doi:10.1002/jor.23875

Hirschberg, K., Radovits, T., Korkmaz, S., Loganathan, S., Zollner, S., Seidel, B., . . . Szabo, G. (2010). Combined superoxide dismutase mimetic and peroxynitrite scavenger protects against neointima formation after endarterectomy in association with decreased proliferation and nitro-oxidative stress. *Eur J Vasc Endovasc Surg, 40*(2), 168-175. doi:10.1016/j.ejvs.2010.03.024

Hong, Z., Kutty, S., Toth, P. T., Marsboom, G., Hammel, J. M., Chamberlain, C., . . . Archer, S. L. (2013). Role of dynamin-related protein 1 (Drp1)-mediated mitochondrial fission in oxygen sensing and constriction of the ductus arteriosus. *Circ Res, 112*(5), 802-815. doi:10.1161/CIRCRESAHA.111.300285

Honold, L., & Nahrendorf, M. (2018). Resident and Monocyte-Derived Macrophages in Cardiovascular Disease. *Circ Res, 122*(1), 113-127. doi:10.1161/CIRCRESAHA.117.311071

Hu, C., Huang, Y., & Li, L. (2017). Drp1-Dependent Mitochondrial Fission Plays Critical Roles in Physiological and Pathological Progresses in Mammals. *Int J Mol Sci, 18*(1). doi:10.3390/ijms18010144

Huang, S. C., Everts, B., Ivanova, Y., O'Sullivan, D., Nascimento, M., Smith, A. M., . . . Pearce, E. J. (2014). Cell-intrinsic lysosomal lipolysis is essential for alternative activation of macrophages. *Nat Immunol, 15*(9), 846-855. doi:10.1038/ni.2956

Huang, S. C., Smith, A. M., Everts, B., Colonna, M., Pearce, E. L., Schilling, J. D., & Pearce, E. J. (2016). Metabolic Reprogramming Mediated by the mTORC2-IRF4 Signaling Axis Is Essential for Macrophage Alternative Activation. *Immunity, 45*(4), 817-830. doi:10.1016/j.immuni.2016.09.016

Hubbard, A. K., & Giardina, C. (2000). Regulation of ICAM-1 expression in mouse macrophages. *Inflammation, 24*(2), 115-125. doi:10.1023/a:1007029409521

Imbeaud, S., Graudens, E., Boulanger, V., Barlet, X., Zaborski, P., Eveno, E., . . . Auffray, C. (2005). Towards standardization of RNA quality assessment using user-independent classifiers of microcapillary electrophoresis traces. *Nucleic Acids Res, 33*(6), e56. doi:10.1093/nar/gni054

Jagadeesha, D. K., Lindley, T. E., Deleon, J., Sharma, R. V., Miller, F., & Bhalla, R. C. (2005). Tempol therapy attenuates medial smooth muscle cell apoptosis and neointima formation after balloon catheter injury in carotid artery of diabetic rats. *Am J Physiol Heart Circ Physiol, 289*(3), H1047-1053. doi:10.1152/ajpheart.01071.2004

Jakopin, Z., & Corsini, E. (2019). THP-1 Cells and Pro-inflammatory Cytokine Production: An in Vitro Tool for Functional Characterization of NOD1/NOD2 Antagonists. *Int J Mol Sci, 20*(17). doi:10.3390/ijms20174265

Jebari-Benslaiman, S., Galicia-Garcia, U., Larrea-Sebal, A., Olaetxea, J. R., Alloza, I., Vandenbroeck, K., . . . Martin, C. (2022). Pathophysiology of Atherosclerosis. *Int J Mol Sci, 23*(6). doi:10.3390/ijms23063346

Ji, W. K., Chakrabarti, R., Fan, X., Schoenfeld, L., Strack, S., & Higgs, H. N. (2017). Receptor-mediated Drp1 oligomerization on endoplasmic reticulum. *J Cell Biol, 216*(12), 4123-4139. doi:10.1083/jcb.201610057

Jin, J. Y., Wei, X. X., Zhi, X. L., Wang, X. H., & Meng, D. (2021). Drp1-dependent mitochondrial fission in cardiovascular disease. *Acta Pharmacol Sin, 42*(5), 655-664. doi:10.1038/s41401-020-00518-y

Kaandorp, T. A., Lamb, H. J., Bax, J. J., van der Wall, E. E., & de Roos, A. (2005). Magnetic resonance imaging of coronary arteries, the ischemic cascade, and myocardial infarction. *Am Heart J, 149*(2), 200-208. doi:10.1016/j.ahj.2004.07.033

Kalkhoran., S. B., Crespo-Avilan., G. E., Hernandez-Resendiz., S., Ramachandra., C. J. A., Ong., S.-G., & Hausenloy., D. J. (2020). Pharmacological modulators of mitochondrial dynamics as novel therapeutics for cardiovascular and neurological diseases. *Conditioning Medicine, 3*(3), 16. Retrieved from http://www.conditionmed.org/Assets/userfiles/sys_eb538c1c-65ff-4e82-8e6a-a1ef01127fed/files/CM-0014-20-REV%20144-159.pdf

Kapellos, T. S., Bonaguro, L., Gemund, I., Reusch, N., Saglam, A., Hinkley, E. R., & Schultze, J. L. (2019). Human Monocyte Subsets and Phenotypes in Major Chronic Inflammatory Diseases. *Front Immunol, 10*, 2035. doi:10.3389/fimmu.2019.02035

Kapetanovic, R., Afroz, S. F., Ramnath, D., Lawrence, G. M., Okada, T., Curson, J. E., . . . Sweet, M. J. (2020). Lipopolysaccharide promotes Drp1-dependent mitochondrial fission and associated inflammatory responses in macrophages. *Immunol Cell Biol, 98*(7), 528-539. doi:10.1111/imcb.12363

Kawai, T., & Akira, S. (2006). TLR signaling. *Cell Death Differ, 13*(5), 816-825. doi:10.1038/sj.cdd.4401850

Kelly, A., Grabiec, A. M., & Travis, M. A. (2018). Culture of Human Monocyte-Derived Macrophages. *Methods Mol Biol, 1784*, 1-11. doi:10.1007/978-1-4939-7837-3_1

Kelly, B., & O'Neill, L. A. (2015). Metabolic reprogramming in macrophages and dendritic cells in innate immunity. *Cell Res, 25*(7), 771-784. doi:10.1038/cr.2015.68

Kesanakurti, D., Chetty, C., Rajasekhar Maddirela, D., Gujrati, M., & Rao, J. S. (2013). Essential role of cooperative NF-kappaB and Stat3 recruitment to ICAM-1 intronic consensus elements in the regulation of radiation-induced invasion and migration in glioma. *Oncogene, 32*(43), 5144-5155. doi:10.1038/onc.2012.546

Keuper, M., Sachs, S., Walheim, E., Berti, L., Raedle, B., Tews, D., . . . Hofmann, S. M. (2017). Activated macrophages control human adipocyte mitochondrial bioenergetics via secreted factors. *Mol Metab, 6*(10), 1226-1239. doi:10.1016/j.molmet.2017.07.008

Kierdorf, K., Prinz, M., Geissmann, F., & Gomez Perdiguero, E. (2015). Development and function of tissue resident macrophages in mice. *Semin Immunol, 27*(6), 369-378. doi:10.1016/j.smim.2016.03.017

Kohro, T., Tanaka, T., Murakami, T., Wada, Y., Aburatani, H., Hamakubo, T., & Kodama, T. (2004). A comparison of differences in the gene expression profiles of phorbol 12-myristate 13-acetate differentiated THP-1 cells and human monocyte-derived macrophage. *J Atheroscler Thromb, 11*(2), 88-97. doi:10.5551/jat.11.88

Kraus, F., & Ryan, M. T. (2017). The constriction and scission machineries involved in mitochondrial fission. *J Cell Sci, 130*(18), 2953-2960. doi:10.1242/jcs.199562

Kubista, M., Andrade, J. M., Bengtsson, M., Forootan, A., Jonak, J., Lind, K., . . . Zoric, N. (2006). The real-time polymerase chain reaction. *Mol Aspects Med, 27*(2-3), 95-125. doi:10.1016/j.mam.2005.12.007

Kyriakoudi, S., Drousiotou, A., & Petrou, P. P. (2021). When the Balance Tips: Dysregulation of Mitochondrial Dynamics as a Culprit in Disease. *Int J Mol Sci, 22*(9). doi:10.3390/ijms22094617

Lachmandas, E., Boutens, L., Ratter, J. M., Hijmans, A., Hooiveld, G. J., Joosten, L. A., . . . Stienstra, R. (2016). Microbial stimulation of different Toll-like receptor signalling pathways induces diverse metabolic programmes in human monocytes. *Nat Microbiol, 2*, 16246. doi:10.1038/nmicrobiol.2016.246

Langston, P. K., Nambu, A., Jung, J., Shibata, M., Aksoylar, H. I., Lei, J., . . . Horng, T. (2019). Glycerol phosphate shuttle enzyme GPD2 regulates macrophage inflammatory responses. *Nat Immunol, 20*(9), 1186-1195. doi:10.1038/s41590-019-0453-7

Legros, F., Lombes, A., Frachon, P., & Rojo, M. (2002). Mitochondrial fusion in human cells is efficient, requires the inner membrane potential, and is mediated by mitofusins. *Mol Biol Cell, 13*(12), 4343-4354. doi:10.1091/mbc.e02-06-0330

Ley, K., Miller, Y. I., & Hedrick, C. C. (2011). Monocyte and macrophage dynamics during atherogenesis. *Arterioscler Thromb Vasc Biol, 31*(7), 1506-1516. doi:10.1161/ATVBAHA.110.221127

Li, Y. H., Xu, F., Thome, R., Guo, M. F., Sun, M. L., Song, G. B., . . . Zhang, G. X. (2019). Mdivi-1, a mitochondrial fission inhibitor, modulates T helper cells and suppresses the development of experimental autoimmune encephalomyelitis. *J Neuroinflammation, 16*(1), 149. doi:10.1186/s12974-019-1542-0

Li, Y. J., Cao, Y. L., Feng, J. X., Qi, Y., Meng, S., Yang, J. F., . . . Gao, S. (2019). Structural insights of human mitofusin-2 into mitochondrial fusion and CMT2A onset. *Nat Commun, 10*(1), 4914. doi:10.1038/s41467-019-12912-0

Liao, C., Ashley, N., Diot, A., Morten, K., Phadwal, K., Williams, A., . . . Poulton, J. (2017). Dysregulated mitophagy and mitochondrial organization in optic atrophy due to OPA1 mutations. *Neurology, 88*(2), 131-142. doi:10.1212/WNL.0000000000003491

Libby, P., Ridker, P. M., & Maseri, A. (2002). Inflammation and atherosclerosis. *Circulation, 105*(9), 1135-1143. doi:10.1161/hc0902.104353

Liongue, C., Sertori, R., & Ward, A. C. (2016). Evolution of Cytokine Receptor Signaling. *J Immunol, 197*(1), 11-18. doi:10.4049/jimmunol.1600372

Liu, L., Lu, Y., Martinez, J., Bi, Y., Lian, G., Wang, T., . . . Wang, R. (2016). Proinflammatory signal suppresses proliferation and shifts macrophage metabolism from Myc-dependent to HIF1alpha-dependent. *Proc Natl Acad Sci U S A, 113*(6), 1564-1569. doi:10.1073/pnas.1518000113

Liu, R., Wang, S. C., Li, M., Ma, X. H., Jia, X. N., Bu, Y., . . . Yu, K. J. (2020). An Inhibitor of DRP1 (Mdivi-1) Alleviates LPS-Induced Septic AKI by Inhibiting NLRP3 Inflammasome Activation. *Biomed Res Int, 2020*, 2398420. doi:10.1155/2020/2398420

Liu, X., Zhang, X., Niu, X., Zhang, P., Wang, Q., Xue, X., . . . Ma, C. (2021). Mdivi-1 Modulates Macrophage/Microglial Polarization in Mice with EAE via the Inhibition of the TLR2/4-GSK3beta-NF-kappaB Inflammatory Signaling Axis. *Mol Neurobiol*. doi:10.1007/s12035-021-02552-1

Livak, K. J., & Schmittgen, T. D. (2001). Analysis of relative gene expression data using real-time quantitative PCR and the 2(-Delta Delta C(T)) Method. *Methods, 25*(4), 402-408. doi:10.1006/meth.2001.1262

Loeffler, H., Jonitz-Heincke, A., Peters, K., Mueller-Hilke, B., Fiedler, T., Bader, R., & Klinder, A. (2020). Comparison of Inflammatory Effects in THP-1 Monocytes and Macrophages after Exposure to Metal Ions. *Materials (Basel), 13*(5). doi:10.3390/ma13051150

Lopez, M. L., Bruges, G., Crespo, G., Salazar, V., Deglesne, P. A., Schneider, H., . . . Preissner, K. T. (2014). Thrombin selectively induces transcription of genes in human monocytes involved in inflammation and wound healing. *Thromb Haemost, 112*(5), 992-1001. doi:10.1160/TH14-01-0034

Lopez-Zambrano, M., Rodriguez-Montesinos, J., Crespo-Avilan, G. E., Munoz-Vega, M., & Preissner, K. T. (2020). Thrombin Promotes Macrophage Polarization into M1-Like Phenotype to Induce Inflammatory Responses. *Thromb Haemost, 120*(4), 658-670. doi:10.1055/s-0040-1703007

Luong, V. H., Chino, T., Oyama, N., Matsushita, T., Sasaki, Y., Ogura, D., . . . Hasegawa, M. (2018). Blockade of TGF-beta/Smad signaling by the small compound HPH-15 ameliorates experimental skin fibrosis. *Arthritis Res Ther, 20*(1), 46. doi:10.1186/s13075-018-1534-y

Macdonald, P. J., Francy, C. A., Stepanyants, N., Lehman, L., Baglio, A., Mears, J. A., . . . Ramachandran, R. (2016). Distinct Splice Variants of Dynamin-related Protein 1 Differentially Utilize Mitochondrial Fission Factor as an Effector of Cooperative GTPase Activity. *J Biol Chem, 291*(1), 493-507. doi:10.1074/jbc.M115.680181

Madamanchi, N. R., & Runge, M. S. (2007). Mitochondrial dysfunction in atherosclerosis. *Circ Res, 100*(4), 460-473. doi:10.1161/01.RES.0000258450.44413.96

Malekmohammad, K., Bezsonov, E. E., & Rafieian-Kopaei, M. (2021). Role of Lipid Accumulation and Inflammation in Atherosclerosis: Focus on Molecular and Cellular Mechanisms. *Front Cardiovasc Med, 8*, 707529. doi:10.3389/fcvm.2021.707529

Malka, F., Guillery, O., Cifuentes-Diaz, C., Guillou, E., Belenguer, P., Lombes, A., & Rojo, M. (2005). Separate fusion of outer and inner mitochondrial membranes. *EMBO Rep, 6*(9), 853-859. doi:10.1038/sj.embor.7400488

Manczak, M., Kandimalla, R., Yin, X., & Reddy, P. H. (2019). Mitochondrial division inhibitor 1 reduces dynamin-related protein 1 and mitochondrial fission activity. *Hum Mol Genet, 28*(2), 177-199. doi:10.1093/hmg/ddy335

Maneechote, C., Palee, S., Chattipakorn, S. C., & Chattipakorn, N. (2017). Roles of mitochondrial dynamics modulators in cardiac ischaemia/reperfusion injury. *J Cell Mol Med, 21*(11), 2643-2653. doi:10.1111/jcmm.13330

Maneechote, C., Palee, S., Kerdphoo, S., Jaiwongkam, T., Chattipakorn, S. C., & Chattipakorn, N. (2021). Modulating mitochondrial dynamics attenuates cardiac ischemia-reperfusion injury in prediabetic rats. *Acta Pharmacol Sin*. doi:10.1038/s41401-021-00626-3

Manka, D., Collins, R. G., Ley, K., Beaudet, A. L., & Sarembock, I. J. (2001). Absence of p-selectin, but not intercellular adhesion molecule-1, attenuates neointimal growth after arterial injury in apolipoprotein e-deficient mice. *Circulation, 103*(7), 1000-1005. Retrieved from http://www.ncbi.nlm.nih.gov/entrez/query.fcgi?cmd=Retrieve&db=PubMed&dopt=Citation&list_uids=11181476

Manka, D. R., Wiegman, P., Din, S., Sanders, J. M., Green, S. A., Gimple, L. W., . . . Sarembock, I. J. (1999). Arterial injury increases expression of inflammatory adhesion molecules in the carotid arteries of apolipoprotein-E-deficient mice. *J Vasc Res, 36*(5), 372-378. doi:10.1159/000025676

Martinez, F. O., Sica, A., Mantovani, A., & Locati, M. (2008). Macrophage activation and polarization. *Front Biosci, 13*, 453-461. doi:10.2741/2692

McBride, H. M., Neuspiel, M., & Wasiak, S. (2006). Mitochondria: more than just a powerhouse. *Curr Biol, 16*(14), R551-560. doi:10.1016/j.cub.2006.06.054

McGarrity, G. J., Vanaman, V., & Sarama, J. (1984). Cytogenetic effects of mycoplasmal infection of cell cultures: a review. *In Vitro, 20*(1), 1-18. doi:10.1007/BF02633326

Meerschaert, J., & Furie, M. B. (1995). The adhesion molecules used by monocytes for migration across endothelium include CD11a/CD18, CD11b/CD18, and VLA-4 on monocytes and ICAM-1, VCAM-1, and other ligands on endothelium. *J Immunol, 154*(8), 4099-4112. Retrieved from https://www.ncbi.nlm.nih.gov/pubmed/7535821

Meijer, K., Weening, D., de Vries, M. P., Priebe, M. G., Vonk, R. J., & Roelofsen, H. (2015). Quantitative proteomics analyses of activation states of human THP-1 macrophages. *J Proteomics, 128*, 164-172. doi:10.1016/j.jprot.2015.07.013

Movsisyan, N. K., Vinciguerra, M., Medina-Inojosa, J. R., & Lopez-Jimenez, F. (2020). Cardiovascular Diseases in Central and Eastern Europe: A Call for More Surveillance and Evidence-Based Health Promotion. *Ann Glob Health, 86*(1), 21. doi:10.5334/aogh.2713

Nair, S., Sobotka, K. S., Joshi, P., Gressens, P., Fleiss, B., Thornton, C., . . . Hagberg, H. (2019). Lipopolysaccharide-induced alteration of mitochondrial morphology induces a metabolic shift in microglia modulating the inflammatory response in vitro and in vivo. *Glia, 67*(6), 1047-1061. doi:10.1002/glia.23587

Nelson, M. C., & O'Connell, R. M. (2020). MicroRNAs: At the Interface of Metabolic Pathways and Inflammatory Responses by Macrophages. *Front Immunol, 11*, 1797. doi:10.3389/fimmu.2020.01797

Newton, K., & Dixit, V. M. (2012). Signaling in innate immunity and inflammation. *Cold Spring Harb Perspect Biol, 4*(3). doi:10.1101/cshperspect.a006049

Niatsetskaya, Z. V., Sosunov, S. A., Matsiukevich, D., Utkina-Sosunova, I. V., Ratner, V. I., Starkov, A. A., & Ten, V. S. (2012). The oxygen free radicals originating from mitochondrial complex I contribute to oxidative brain injury following hypoxia-ischemia in neonatal mice. *J Neurosci, 32*(9), 3235-3244. doi:10.1523/JNEUROSCI.6303-11.2012

Noe, J. T., & Mitchell, R. A. (2019). Tricarboxylic acid cycle metabolites in the control of macrophage activation and effector phenotypes. *J Leukoc Biol, 106*(2), 359-367. doi:10.1002/JLB.3RU1218-496R

O'Neill, L. A., Kishton, R. J., & Rathmell, J. (2016). A guide to immunometabolism for immunologists. *Nat Rev Immunol, 16*(9), 553-565. doi:10.1038/nri.2016.70

O'Neill, L. A., & Pearce, E. J. (2016). Immunometabolism governs dendritic cell and macrophage function. *J Exp Med, 213*(1), 15-23. doi:10.1084/jem.20151570

Oguchi, S., Dimayuga, P., Zhu, J., Chyu, K. Y., Yano, J., Shah, P. K., . . . Cercek, B. (2000). Monoclonal antibody against vascular cell adhesion molecule-1 inhibits neointimal formation after periadventitial carotid artery injury in genetically hypercholesterolemic mice. *Arterioscler Thromb Vasc Biol, 20*(7), 1729-1736. doi:10.1161/01.atv.20.7.1729

Olingy, C. E., San Emeterio, C. L., Ogle, M. E., Krieger, J. R., Bruce, A. C., Pfau, D. D., . . . Botchwey, E. A. (2017). Non-classical monocytes are biased progenitors of wound healing macrophages during soft tissue injury. *Sci Rep, 7*(1), 447. doi:10.1038/s41598-017-00477-1

Olvera Lopez, E., Ballard, B. D., & Jan, A. (2022). Cardiovascular Disease. In *StatPearls*. Treasure Island (FL).

Ong, S. B., Subrayan, S., Lim, S. Y., Yellon, D. M., Davidson, S. M., & Hausenloy, D. J. (2010). Inhibiting mitochondrial fission protects the heart against ischemia/reperfusion injury. *Circulation, 121*(18), 2012-2022. doi:10.1161/CIRCULATIONAHA.109.906610

Orekhov, A. N., Sukhorukov, V. N., Nikiforov, N. G., Kubekina, M. V., Sobenin, I. A., Foxx, K. K., . . . Oishi, Y. (2020). Signaling Pathways Potentially Responsible for Foam Cell Formation: Cholesterol Accumulation or Inflammatory Response-What is First? *Int J Mol Sci, 21*(8). doi:10.3390/ijms21082716

Papac-Milicevic, N., Busch, C. J., & Binder, C. J. (2016). Malondialdehyde Epitopes as Targets of Immunity and the Implications for Atherosclerosis. *Adv Immunol, 131*, 1-59. doi:10.1016/bs.ai.2016.02.001

Papadopulos, F., Spinelli, M., Valente, S., Foroni, L., Orrico, C., Alviano, F., & Pasquinelli, G. (2007). Common tasks in microscopic and ultrastructural image analysis using ImageJ. *Ultrastruct Pathol, 31*(6), 401-407. doi:10.1080/01913120701719189

Park, E. K., Jung, H. S., Yang, H. I., Yoo, M. C., Kim, C., & Kim, K. S. (2007). Optimized THP-1 differentiation is required for the detection of responses to weak stimuli. *Inflamm Res, 56*(1), 45-50. doi:10.1007/s00011-007-6115-5

Park, J., Choi, H., Min, J. S., Park, S. J., Kim, J. H., Park, H. J., . . . Lee, D. S. (2013). Mitochondrial dynamics modulate the expression of pro-inflammatory mediators in microglial cells. *J Neurochem, 127*(2), 221-232. doi:10.1111/jnc.12361

Peng, W., Cai, G., Xia, Y., Chen, J., Wu, P., Wang, Z., . . . Wei, D. (2019). Mitochondrial Dysfunction in Atherosclerosis. *DNA Cell Biol, 38*(7), 597-606. doi:10.1089/dna.2018.4552

Perlman, H., Maillard, L., Krasinski, K., & Walsh, K. (1997). Evidence for the rapid onset of apoptosis in medial smooth muscle cells after balloon injury. *Circulation, 95*(4), 981-987. doi:10.1161/01.cir.95.4.981

Picard, M., Shirihai, O. S., Gentil, B. J., & Burelle, Y. (2013). Mitochondrial morphology transitions and functions: implications for retrograde signaling? *Am J Physiol Regul Integr Comp Physiol, 304*(6), R393-406. doi:10.1152/ajpregu.00584.2012

Pinto, F. J., Pineiro, D., Banerjee, A., Perel, P., Pervan, B., & Eisele, J. L. (2021). World Heart Day 2021: COVID-19, digital health, and tackling cardiovascular disease. *Lancet, 398*(10310), 1467-1468. doi:10.1016/S0140-6736(21)02144-9

Pinyopummintr, T., & Bavister, B. D. (1994). Development of bovine embryos in a cell-free culture medium: Effects of type of serum, timing of its inclusion and heat inactivation. *Theriogenology, 41*(6), 1241-1249. doi:10.1016/0093-691x(94)90481-w

Postea, O., Vasina, E. M., Cauwenberghs, S., Projahn, D., Liehn, E. A., Lievens, D., . . . Koenen, R. R. (2012). Contribution of platelet CX(3)CR1 to platelet-monocyte complex formation and vascular recruitment during hyperlipidemia. *Arterioscler Thromb Vasc Biol, 32*(5), 1186-1193. doi:10.1161/ATVBAHA.111.243485

Rao, R. M., Yang, L., Garcia-Cardena, G., & Luscinskas, F. W. (2007). Endothelial-dependent mechanisms of leukocyte recruitment to the vascular wall. *Circ Res, 101*(3), 234-247. doi:10.1161/CIRCRESAHA.107.151860b

Rectenwald, J. E., Moldawer, L. L., Huber, T. S., Seeger, J. M., & Ozaki, C. K. (2000). Direct evidence for cytokine involvement in neointimal hyperplasia. *Circulation, 102*(14), 1697-1702. doi:10.1161/01.cir.102.14.1697

Rogers, M. A., Hutcheson, J. D., Okui, T., Goettsch, C., Singh, S. A., Halu, A., . . . Aikawa, E. (2021). Dynamin-related protein 1 inhibition reduces hepatic PCSK9 secretion. *Cardiovasc Res, 117*(11), 2340-2353. doi:10.1093/cvr/cvab034

Rogers, M. A., Maldonado, N., Hutcheson, J. D., Goettsch, C., Goto, S., Yamada, I., . . . Aikawa, E. (2017). Dynamin-Related Protein 1 Inhibition Attenuates Cardiovascular Calcification in the Presence of Oxidative Stress. *Circ Res, 121*(3), 220-233. doi:10.1161/CIRCRESAHA.116.310293

Ross, R. (1999). Atherosclerosis--an inflammatory disease. *N Engl J Med, 340*(2), 115-126. doi:10.1056/NEJM199901143400207

Rottem, S., & Yogev, D. (2000). Mycoplasma interaction with eukaryotic cells. *Subcell Biochem, 33*, 199-227. doi:10.1007/978-1-4757-4580-1_9

Roy, M., Reddy, P. H., Iijima, M., & Sesaki, H. (2015). Mitochondrial division and fusion in metabolism. *Curr Opin Cell Biol, 33*, 111-118. doi:10.1016/j.ceb.2015.02.001

Ruiz, A., Alberdi, E., & Matute, C. (2018). Mitochondrial Division Inhibitor 1 (mdivi-1) Protects Neurons against Excitotoxicity through the Modulation of Mitochondrial Function and Intracellular Ca(2+) Signaling. *Front Mol Neurosci, 11*, 3. doi:10.3389/fnmol.2018.00003

Ruiz-Villalba, A., van Pelt-Verkuil, E., Gunst, Q. D., Ruijter, J. M., & van den Hoff, M. J. (2017). Amplification of nonspecific products in quantitative polymerase chain reactions (qPCR). *Biomol Detect Quantif, 14*, 7-18. doi:10.1016/j.bdq.2017.10.001

Sag, D., Carling, D., Stout, R. D., & Suttles, J. (2008). Adenosine 5'-monophosphate-activated protein kinase promotes macrophage polarization to an anti-inflammatory functional phenotype. *J Immunol, 181*(12), 8633-8641. doi:10.4049/jimmunol.181.12.8633

Salminen, A. T., Allahyari, Z., Gholizadeh, S., McCloskey, M. C., Ajalik, R., Cottle, R. N., . . . McGrath, J. L. (2020). In vitro Studies of Transendothelial Migration for Biological and Drug Discovery. *Front Med Technol, 2*, 600616. doi:10.3389/fmedt.2020.600616

Samangouei, P., Crespo-Avilan, G. E., Cabrera-Fuentes, H., Hernandez-Resendiz, S., Ismail, N. I., Katwadi, K. B., . . . Hausenloy, D. J. (2018). MiD49 and MiD51: New mediators of mitochondrial fission and novel targets for cardioprotection. *Cond Med, 1*(5), 239-246. Retrieved from https://www.ncbi.nlm.nih.gov/pubmed/30338314

Schober, A., & Weber, C. (2005). Mechanisms of monocyte recruitment in vascular repair after injury. *Antioxid Redox Signal, 7*(9-10), 1249-1257. doi:10.1089/ars.2005.7.1249

Schumacher, D., Liehn, E. A., Nilcham, P., Mayan, D. C., Rattanasopa, C., Anand, K., . . . Hausenloy, D. J. (2021). A neutralizing IL-11 antibody reduces vessel hyperplasia in a mouse carotid artery wire injury model. *Sci Rep, 11*(1), 20674. doi:10.1038/s41598-021-99880-y

Serasinghe, M. N., & Chipuk, J. E. (2017). Mitochondrial Fission in Human Diseases. *Handb Exp Pharmacol, 240*, 159-188. doi:10.1007/164_2016_38

Shagdarsuren, E., Bidzhekov, K., Djalali-Talab, Y., Liehn, E. A., Hristov, M., Matthijsen, R. A., . . . Weber, C. (2008). C1-esterase inhibitor protects against neointima formation after arterial injury in atherosclerosis-prone mice. *Circulation, 117*(1), 70-78. doi:10.1161/CIRCULATIONAHA.107.715649

Shagdarsuren, E., Djalali-Talab, Y., Aurrand-Lions, M., Bidzhekov, K., Liehn, E. A., Imhof, B. A., . . . Zernecke, A. (2009). Importance of junctional adhesion molecule-C for neointimal hyperplasia and monocyte recruitment in atherosclerosis-prone mice-brief report. *Arterioscler Thromb Vasc Biol, 29*(8), 1161-1163. doi:10.1161/ATVBAHA.109.187898

Shemiakova, T., Ivanova, E., Grechko, A. V., Gerasimova, E. V., Sobenin, I. A., & Orekhov, A. N. (2020). Mitochondrial Dysfunction and DNA Damage in the Context of Pathogenesis of Atherosclerosis. *Biomedicines, 8*(6). doi:10.3390/biomedicines8060166

Shemiakova, T., Ivanova, E., Wu, W. K., Kirichenko, T. V., Starodubova, A. V., & Orekhov, A. N. (2021). Atherosclerosis as Mitochondriopathy: Repositioning the Disease to Help Finding New Therapies. *Front Cardiovasc Med, 8*, 660473. doi:10.3389/fcvm.2021.660473

Shen, Q., Yamano, K., Head, B. P., Kawajiri, S., Cheung, J. T., Wang, C., . . . van der Bliek, A. M. (2014). Mutations in Fis1 disrupt orderly disposal of defective mitochondria. *Mol Biol Cell, 25*(1), 145-159. doi:10.1091/mbc.E13-09-0525

Shen, Y. L., Shi, Y. Z., Chen, G. G., Wang, L. L., Zheng, M. Z., Jin, H. F., & Chen, Y. Y. (2018). TNF-alpha induces Drp1-mediated mitochondrial fragmentation during inflammatory cardiomyocyte injury. *Int J Mol Med, 41*(4), 2317-2327. doi:10.3892/ijmm.2018.3385

Shiba, Y., Takahashi, M., Yoshioka, T., Yajima, N., Morimoto, H., Izawa, A., . . . Ikeda, U. (2007). M-CSF accelerates neointimal formation in the early phase after vascular injury in mice: the critical role of the SDF-1-CXCR4 system. *Arterioscler Thromb Vasc Biol, 27*(2), 283-289. doi:10.1161/01.ATV.0000250606.70669.14

Shirai, T., Nazarewicz, R. R., Wallis, B. B., Yanes, R. E., Watanabe, R., Hilhorst, M., . . . Weyand, C. M. (2016). The glycolytic enzyme PKM2 bridges metabolic and inflammatory dysfunction in coronary artery disease. *J Exp Med, 213*(3), 337-354. doi:10.1084/jem.20150900

Shyy, Y. J., Wickham, L. L., Hagan, J. P., Hsieh, H. J., Hu, Y. L., Telian, S. H., . . . Chien, S. (1993). Human monocyte colony-stimulating factor stimulates the gene expression of monocyte chemotactic protein-1 and increases the adhesion of monocytes to endothelial monolayers. *J Clin Invest, 92*(4), 1745-1751. doi:10.1172/JCI116762

Silva Ramos, E., Larsson, N. G., & Mourier, A. (2016). Bioenergetic roles of mitochondrial fusion. *Biochim Biophys Acta, 1857*(8), 1277-1283. doi:10.1016/j.bbabio.2016.04.002

Singh, S., Anshita, D., & Ravichandiran, V. (2021). MCP-1: Function, regulation, and involvement in disease. *Int Immunopharmacol, 101*(Pt B), 107598. doi:10.1016/j.intimp.2021.107598

Smith, G., & Gallo, G. (2017). To mdivi-1 or not to mdivi-1: Is that the question? *Dev Neurobiol, 77*(11), 1260-1268. doi:10.1002/dneu.22519

Smokelin, I., Mizzoni, C., Erndt-Marino, J., Kaplan, D., & Georgakoudi, I. (2020). Optical changes in THP-1 macrophage metabolism in response to pro- and anti-inflammatory stimuli reported by label-free two-photon imaging. *J Biomed Opt, 25*(1), 1-14. doi:10.1117/1.JBO.25.1.014512

Suhalim, J. L., Chung, C. Y., Lilledahl, M. B., Lim, R. S., Levi, M., Tromberg, B. J., & Potma, E. O. (2012). Characterization of cholesterol crystals in atherosclerotic plaques using stimulated Raman scattering and second-harmonic generation microscopy. *Biophys J, 102*(8), 1988-1995. doi:10.1016/j.bpj.2012.03.016

Tabas, I., & Bornfeldt, K. E. (2016). Macrophage Phenotype and Function in Different Stages of Atherosclerosis. *Circ Res, 118*(4), 653-667. doi:10.1161/CIRCRESAHA.115.306256

Taylor, S. C., & Mrkusich, E. M. (2014). The state of RT-quantitative PCR: firsthand observations of implementation of minimum information for the publication of quantitative real-time PCR experiments (MIQE). *J Mol Microbiol Biotechnol, 24*(1), 46-52. doi:10.1159/000356189

Tobler, A., Moser, B., Dewald, B., Geiser, T., Studer, H., Baggiolini, M., & Fey, M. F. (1993). Constitutive expression of interleukin-8 and its receptor in human myeloid and lymphoid leukemia. *Blood, 82*(8), 2517-2525. Retrieved from http://www.ncbi.nlm.nih.gov/entrez/query.fcgi?cmd=Retrieve&db=PubMed&dopt=Citation&list_uids=8400299

Tondera, D., Grandemange, S., Jourdain, A., Karbowski, M., Mattenberger, Y., Herzig, S., . . . Martinou, J. C. (2009). SLP-2 is required for stress-induced mitochondrial hyperfusion. *EMBO J, 28*(11), 1589-1600. doi:10.1038/emboj.2009.89

Traaseth, N., Elfering, S., Solien, J., Haynes, V., & Giulivi, C. (2004). Role of calcium signaling in the activation of mitochondrial nitric oxide synthase and citric acid cycle. *Biochim Biophys Acta, 1658*(1-2), 64-71. doi:10.1016/j.bbabio.2004.04.015

Triglia, R. P., & Linscott, W. D. (1980). Titers of nine complement components, conglutinin and C3b-inactivator in adult and fetal bovine sera. *Mol Immunol, 17*(6), 741-748. doi:10.1016/0161-5890(80)90144-3

Tsuchiya, S., Yamabe, M., Yamaguchi, Y., Kobayashi, Y., Konno, T., & Tada, K. (1980). Establishment and characterization of a human acute monocytic leukemia cell line (THP-1). *Int J Cancer, 26*(2), 171-176. doi:10.1002/ijc.2910260208

Turrens, J. F. (2003). Mitochondrial formation of reactive oxygen species. *J Physiol, 552*(Pt 2), 335-344. doi:10.1113/jphysiol.2003.049478

Umezu, R., Koga, J. I., Matoba, T., Katsuki, S., Wang, L., Hasuzawa, N., . . . Egashira, K. (2020). Macrophage (Drp1) Dynamin-Related Protein 1 Accelerates Intimal Thickening After Vascular Injury. *Arterioscler Thromb Vasc Biol, 40*(7), e214-e226. doi:10.1161/ATVBAHA.120.314383

Underwood, E., Redell, J. B., Zhao, J., Moore, A. N., & Dash, P. K. (2020). A method for assessing tissue respiration in anatomically defined brain regions. *Sci Rep, 10*(1), 13179. doi:10.1038/s41598-020-69867-2

Valente, A. J., Maddalena, L. A., Robb, E. L., Moradi, F., & Stuart, J. A. (2017). A simple ImageJ macro tool for analyzing mitochondrial network morphology in mammalian cell culture. *Acta Histochem, 119*(3), 315-326. doi:10.1016/j.acthis.2017.03.001

Van den Bossche, J., Baardman, J., & de Winther, M. P. (2015). Metabolic Characterization of Polarized M1 and M2 Bone Marrow-derived Macrophages Using Real-time Extracellular Flux Analysis. *J Vis Exp*(105). doi:10.3791/53424

Varanita, T., Soriano, M. E., Romanello, V., Zaglia, T., Quintana-Cabrera, R., Semenzato, M., . . . Scorrano, L. (2015). The OPA1-dependent mitochondrial cristae remodeling pathway controls atrophic, apoptotic, and ischemic tissue damage. *Cell Metab, 21*(6), 834-844. doi:10.1016/j.cmet.2015.05.007

Verma, S., Buchanan, M. R., & Anderson, T. J. (2003). Endothelial function testing as a biomarker of vascular disease. *Circulation, 108*(17), 2054-2059. doi:10.1161/01.CIR.0000089191.72957.ED

Viola, A., Munari, F., Sanchez-Rodriguez, R., Scolaro, T., & Castegna, A. (2019). The Metabolic Signature of Macrophage Responses. *Front Immunol, 10*, 1462. doi:10.3389/fimmu.2019.01462

von Ehr, A., Bode, C., & Hilgendorf, I. (2022). Macrophages in Atheromatous Plaque Developmental Stages. *Front Cardiovasc Med, 9*, 865367. doi:10.3389/fcvm.2022.865367

Walsh, K., Smith, R. C., & Kim, H. S. (2000). Vascular cell apoptosis in remodeling, restenosis, and plaque rupture. *Circ Res, 87*(3), 184-188. doi:10.1161/01.res.87.3.184

Wang, L., Yu, T., Lee, H., O'Brien, D. K., Sesaki, H., & Yoon, Y. (2015). Decreasing mitochondrial fission diminishes vascular smooth muscle cell migration and ameliorates intimal hyperplasia. *Cardiovasc Res, 106*(2), 272-283. doi:10.1093/cvr/cvv005

Wang, N., Liang, H., & Zen, K. (2014). Molecular mechanisms that influence the macrophage m1-m2 polarization balance. *Front Immunol, 5*, 614. doi:10.3389/fimmu.2014.00614

Wang, Q., Zhang, M., Torres, G., Wu, S., Ouyang, C., Xie, Z., & Zou, M. H. (2017). Metformin Suppresses Diabetes-Accelerated Atherosclerosis via the Inhibition of Drp1-Mediated Mitochondrial Fission. *Diabetes, 66*(1), 193-205. doi:10.2337/db16-0915

Wang, W., Wang, Y., Long, J., Wang, J., Haudek, S. B., Overbeek, P., . . . Danesh, F. R. (2012). Mitochondrial fission triggered by hyperglycemia is mediated by ROCK1 activation in podocytes and endothelial cells. *Cell Metab, 15*(2), 186-200. doi:10.1016/j.cmet.2012.01.009

Wang, Y., Wang, G. Z., Rabinovitch, P. S., & Tabas, I. (2014). Macrophage mitochondrial oxidative stress promotes atherosclerosis and nuclear factor-kappaB-mediated inflammation in macrophages. *Circ Res, 114*(3), 421-433. doi:10.1161/CIRCRESAHA.114.302153

Waterham, H. R., Koster, J., van Roermund, C. W., Mooyer, P. A., Wanders, R. J., & Leonard, J. V. (2007). A lethal defect of mitochondrial and peroxisomal fission. *N Engl J Med, 356*(17), 1736-1741. doi:10.1056/NEJMoa064436

Weber, C., Zernecke, A., & Libby, P. (2008). The multifaceted contributions of leukocyte subsets to atherosclerosis: lessons from mouse models. *Nat Rev Immunol, 8*(10), 802-815. doi:10.1038/nri2415

Westermann, B. (2012). Bioenergetic role of mitochondrial fusion and fission. *Biochim Biophys Acta, 1817*(10), 1833-1838. doi:10.1016/j.bbabio.2012.02.033

Widdrington, J. D., Gomez-Duran, A., Pyle, A., Ruchaud-Sparagano, M. H., Scott, J., Baudouin, S. V., . . . Simpson, A. J. (2018). Exposure of Monocytic Cells to Lipopolysaccharide Induces Coordinated Endotoxin Tolerance, Mitochondrial Biogenesis, Mitophagy, and Antioxidant Defenses. *Front Immunol, 9*, 2217. doi:10.3389/fimmu.2018.02217

Williams, N. C., & O'Neill, L. A. J. (2018). A Role for the Krebs Cycle Intermediate Citrate in Metabolic Reprogramming in Innate Immunity and Inflammation. *Front Immunol, 9*, 141. doi:10.3389/fimmu.2018.00141

Wu, D., Dasgupta, A., Chen, K. H., Neuber-Hess, M., Patel, J., Hurst, T. E., . . . Archer, S. L. (2020). Identification of novel dynamin-related protein 1 (Drp1) GTPase inhibitors: Therapeutic potential of Drpitor1 and Drpitor1a in cancer and cardiac ischemia-reperfusion injury. *FASEB J, 34*(1), 1447-1464. doi:10.1096/fj.201901467R

Xu, F., Armstrong, R., Urrego, D., Qazzaz, M., Pehar, M., Armstrong, J. N., . . . Syed, N. (2016). The mitochondrial division inhibitor Mdivi-1 rescues mammalian neurons from anesthetic-induced cytotoxicity. *Mol Brain, 9*, 35. doi:10.1186/s13041-016-0210-x

Xu, S., Ilyas, I., Little, P. J., Li, H., Kamato, D., Zheng, X., . . . Weng, J. (2021). Endothelial Dysfunction in Atherosclerotic Cardiovascular Diseases and Beyond: From

Mechanism to Pharmacotherapies. *Pharmacol Rev, 73*(3), 924-967. doi:10.1124/pharmrev.120.000096

Yakala, G. K., Cabrera-Fuentes, H. A., Crespo-Avilan, G. E., Rattanasopa, C., Burlacu, A., George, B. L., . . . Singaraja, R. R. (2019). FURIN Inhibition Reduces Vascular Remodeling and Atherosclerotic Lesion Progression in Mice. *Arterioscler Thromb Vasc Biol, 39*(3), 387-401. doi:10.1161/ATVBAHA.118.311903

Yang, T. C., Chen, Y. J., Chang, S. F., Chen, C. H., Chang, P. Y., & Lu, S. C. (2014). Malondialdehyde mediates oxidized LDL-induced coronary toxicity through the Akt-FGF2 pathway via DNA methylation. *J Biomed Sci, 21*, 11. doi:10.1186/1423-0127-21-11

Yao, C. H., Wang, R., Wang, Y., Kung, C. P., Weber, J. D., & Patti, G. J. (2019). Mitochondrial fusion supports increased oxidative phosphorylation during cell proliferation. *Elife, 8*. doi:10.7554/eLife.41351

Yeh, H. L., Kuo, L. T., Sung, F. C., & Yeh, C. C. (2018). Association between Polymorphisms of Antioxidant Gene (MnSOD, CAT, and GPx1) and Risk of Coronary Artery Disease. *Biomed Res Int, 2018*, 5086869. doi:10.1155/2018/5086869

Yin, J., Xia, W., Wu, M., Zhang, Y., Huang, S., Zhang, A., & Jia, Z. (2019). Inhibition of mitochondrial complex I activity attenuates neointimal hyperplasia by inhibiting smooth muscle cell proliferation and migration. *Chem Biol Interact, 304*, 73-82. doi:10.1016/j.cbi.2019.03.002

Youle, R. J., & van der Bliek, A. M. (2012). Mitochondrial fission, fusion, and stress. *Science, 337*(6098), 1062-1065. doi:10.1126/science.1219855

Yu, E. P. K., Reinhold, J., Yu, H., Starks, L., Uryga, A. K., Foote, K., . . . Bennett, M. (2017). Mitochondrial Respiration Is Reduced in Atherosclerosis, Promoting Necrotic Core Formation and Reducing Relative Fibrous Cap Thickness. *Arterioscler Thromb Vasc Biol, 37*(12), 2322-2332. doi:10.1161/ATVBAHA.117.310042

Yu, R., Lendahl, U., Nister, M., & Zhao, J. (2020). Regulation of Mammalian Mitochondrial Dynamics: Opportunities and Challenges. *Front Endocrinol (Lausanne), 11*, 374. doi:10.3389/fendo.2020.00374

Yu, R., Liu, T., Jin, S. B., Ning, C., Lendahl, U., Nister, M., & Zhao, J. (2017). MIEF1/2 function as adaptors to recruit Drp1 to mitochondria and regulate the association of Drp1 with Mff. *Sci Rep, 7*(1), 880. doi:10.1038/s41598-017-00853-x

Yu, X., Jia, L., Yu, W., & Du, H. (2019). Dephosphorylation by calcineurin regulates translocation of dynamin-related protein 1 to mitochondria in hepatic ischemia reperfusion induced hippocampus injury in young mice. *Brain Res, 1711*, 68-76. doi:10.1016/j.brainres.2019.01.018

Yu, X. H., Zheng, X. L., & Tang, C. K. (2015). Nuclear Factor-kappaB Activation as a Pathological Mechanism of Lipid Metabolism and Atherosclerosis. *Adv Clin Chem, 70*, 1-30. doi:10.1016/bs.acc.2015.03.004

Yurdagul, A., Jr., Finney, A. C., Woolard, M. D., & Orr, A. W. (2016). The arterial microenvironment: the where and why of atherosclerosis. *Biochem J, 473*(10), 1281-1295. doi:10.1042/BJ20150844

Yusuf-Makagiansar, H., Anderson, M. E., Yakovleva, T. V., Murray, J. S., & Siahaan, T. J. (2002). Inhibition of LFA-1/ICAM-1 and VLA-4/VCAM-1 as a therapeutic approach to inflammation and autoimmune diseases. *Med Res Rev, 22*(2), 146-167. doi:10.1002/med.10001

Yvan-Charvet, L., Ranalletta, M., Wang, N., Han, S., Terasaka, N., Li, R., . . . Tall, A. R. (2007). Combined deficiency of ABCA1 and ABCG1 promotes foam cell accumulation and accelerates atherosclerosis in mice. *J Clin Invest, 117*(12), 3900-3908. doi:10.1172/JCI33372

Zarember, K. A., & Godowski, P. J. (2002). Tissue expression of human Toll-like receptors and differential regulation of Toll-like receptor mRNAs in leukocytes in response to microbes, their products, and cytokines. *J Immunol, 168*(2), 554-561. doi:10.4049/jimmunol.168.2.554

Zengel, P., Nguyen-Hoang, A., Schildhammer, C., Zantl, R., Kahl, V., & Horn, E. (2011). mu-Slide Chemotaxis: a new chamber for long-term chemotaxis studies. *BMC Cell Biol, 12*, 21. doi:10.1186/1471-2121-12-21

Zernecke, A., & Weber, C. (2010). Chemokines in the vascular inflammatory response of atherosclerosis. *Cardiovasc Res, 86*(2), 192-201. doi:10.1093/cvr/cvp391

Zhou, Y., Que, K. T., Zhang, Z., Yi, Z. J., Zhao, P. X., You, Y., . . . Liu, Z. J. (2018). Iron overloaded polarizes macrophage to proinflammation phenotype through ROS/acetyl-p53 pathway. *Cancer Med, 7*(8), 4012-4022. doi:10.1002/cam4.1670

Zhou, Y., Zhang, M. J., Li, B. H., Chen, L., Pi, Y., Yin, Y. W., . . . Zhang, L. L. (2016). PPARgamma Inhibits VSMC Proliferation and Migration via Attenuating Oxidative Stress through Upregulating UCP2. *PLoS One, 11*(5), e0154720. doi:10.1371/journal.pone.0154720

Zimmerman, M. A., Selzman, C. H., Reznikov, L. L., Miller, S. A., Raeburn, C. D., Emmick, J., . . . Harken, A. H. (2002). Lack of TNF-alpha attenuates intimal hyperplasia after mouse carotid artery injury. *Am J Physiol Regul Integr Comp Physiol, 283*(2), R505-512. doi:10.1152/ajpregu.00033.2002

Zuo, H., & Wan, Y. (2019). Metabolic Reprogramming in Mitochondria of Myeloid Cells. *Cells, 9*(1). doi:10.3390/cells9010005

7. Declaration

Hiermit erkläre ich, dass ich die vorliegende Arbeit selbständig und ohne unzulässige Hilfe oder Benutzung anderer als der angegebenen Hilfsmittel angefertigt habe. Alle Textstellen, die wörtlich oder sinngemäß aus veröffentlichten oder nichtveröffentlichten Schriften entnommen sind, und alle Angaben, die auf mündlichen Auskünften beruhen, sind als solche kenntlich gemacht. Bei den von mir durchgeführten und in der Dissertation erwähnten Untersuchungen habe ich die Grundsätze guter wissenschaftlicher Praxis, wie sie in der „Satzung der Justus-Liebig-Universität Gießen zur Sicherung guter wissenschaftlicher Praxis“ niedergelegt sind, eingehalten sowie ethische, datenschutzrechtliche und tierschutzrechtliche Grundsätze befolgt. Ich versichere, dass Dritte von mir weder unmittelbar noch mittelbar geldwerte Leistungen für Arbeiten erhalten haben, die im Zusammenhang mit dem Inhalt der vorgelegten Dissertation stehen, und dass die vorgelegte Arbeit weder im Inland noch im Ausland in gleicher oder ähnlicher Form einer anderen Prüfungsbehörde zum Zweck einer Promotion oder eines anderen Prüfungsverfahrens vorgelegt wurde. Alles aus anderen Quellen und von anderen Personen übernommene Material, das in der Arbeit verwendet wurde oder auf das direkt Bezug genommen wird, wurde als solches kenntlich gemacht. Insbesondere wurden alle Personen genannt, die direkt und indirekt an der Entstehung der vorliegenden Arbeit beteiligt waren. Mit der Überprüfung meiner Arbeit durch eine Plagiatserkennungssoftware bzw. ein internetbasiertes Softwareprogramm erkläre ich mich einverstanden.

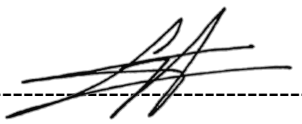

Gustavo Enrique Crespo-Avilan

8. Acknowledgement

I extend my profound thanks to my esteemed PhD supervisors, Prof. Derek Hausenloy and Prof. Klaus T. Preissner, whose guidance and mentorship have not only fostered my academic achievements but also contributed significantly to my professional growth.

Dr. Sauri Hernandez Resendiz, your academic support and genuine friendship have been indispensable throughout this journey. Your attentive listening, encouraging words, and motivational guidance have been the driving force behind my progress. Thank you, a thousand times.

Prof. Elisa Liehn and Asst. Prof. Chrishan Ramachandra, I'm sincerely thankful for your academic support and collaborative spirit, which have been central to my success. Your invaluable knowledge and surgical skills have played a vital role in shaping my academic journey.

Dr. Mercedes Lopez Zambrano, your role in igniting my passion for science and pushing me beyond my comfort zone is deeply appreciated. Your unwavering support and assistance during administrative processes have been invaluable.

I'm deeply thankful to Justus Liebig University, DUKE-NUS, and the National Heart Centre of Singapore, as well as all the dedicated lab members, with special acknowledgment to Dr. Lu, Dr. Ying-hsi, Dr. Cabrera, Mr. Julian Rodriguez, and Ms. Yap Ping. Their collaborative projects have played a pivotal role in my career development.

To my family—my parents, Fernando Crespo Carrasquero, and Maira Avilan, and my brother, Luis Fernando Crespo Avilan—I extend my heartfelt thanks for your unwavering support throughout these challenging years.

Lastly, I want to express my appreciation to my PhD committee, PD Dr. Erkapic, Prof. Dr. Knipper, and Prof. Dr. Gräf, for their valuable feedback, which has enriched this dissertation and for their recognition of my academic work and achievements.